IDAHO TRANSPORTATION DEPARTMENT

RESEARCH REPORT

Your Safety • Your Mobility
Your Economic Opportunity

RP 273

Field Performance of HES Class 50AF Concrete with Fibers as Field-Cast Connection between Deck Bulb-T Girders in ABC Applications

By

PIs: Arya Ebrahimpour and Mustafa Mashal

Graduate Students: Christopher Clauson, and Ali Shokrgozar

Prepared for

Idaho Transportation Department

Research Program, Contracting Services

Division of Construction and Operations

http://itd.idaho.gov/highways/research/

May 2020

Standard Disclaimer

This document is disseminated under the sponsorship of the Idaho Transportation Department and the United States Department of Transportation in the interest of information exchange. The State of Idaho and the United States Government assume no liability of its contents or use thereof.

The contents of this report reflect the view of the authors, who are responsible for the facts and accuracy of the data presented herein. The contents do not necessarily reflect the official policies of the Idaho Transportation Department or the United States Department of Transportation.

The State of Idaho and the United States Government do not endorse products or manufacturers. Trademarks or manufacturers' names appear herein only because they are considered essential to the object of this document.

This report does not constitute a standard, specification or regulation.

1. Report No. FHWA-ID-19-273	2. Government Accession No.	3. Recipient's Catalog No.
4. Title and Subtitle Field Performance of HES Class 50AF Concrete with Fibers as Field-Cast Connection between Deck Bulb-T Girders in ABC Applications		5. Report Date May 2020 6. Performing Organization Code
7. Author(s) Arya Ebrahimpour, Mustafa Mashal, Christopher Clauson, and Ali Shokrgozar		8. Performing Organization Report No.
9. Performing Organization Name and Address Department of Civil and Environmental Engineering Idaho State University Pocatello, Idaho 83209		10. Work Unit No. (TRAIS) 11. Contract or Grant No. ISU-18-02
12. Sponsoring Agency Name and Address Idaho Transportation Department (SPR) Division of Construction and Operations, Contracting Services, Research Program PO Box 7129 Boise, ID 83707-7129		13. Type of Report and Period Covered Final Report 3/15/2018 -- 2/28/2020 14. Sponsoring Agency Code RP 273
15. Supplementary Notes Project performed in cooperation with the Idaho Transportation Department and the Federal Highway Administration.		

16. Abstract

Accelerated Bridge Construction (ABC) technologies are being adopted by the state departments of transportation. ABC increases public's and worker's safety by lowering exposure to construction activities and also increases mobility and economic opportunities by reducing traffic interruptions and delays. As an alternative to Ultra-High Performance Concrete (UHPC), Idaho Transportation Department (ITD) is interested in the suitability of High-Early Strength (HES) concrete Class 50AF with Polypropylene fibers in closure pours between bridge Deck Bulb-T Girders. The advantages of this alternate material are the reduction in costs and construction time. In the first phase of the project, an optimum concrete mix with good material properties was identified through a series of standard laboratory experiments and tests on larger specimens. In this phase, field performance of a closure pour mix similar to the optimum mix found in Phase 1 is examined by placing the material in the closure pours between Deck Bulb-T Girders in the SH-36 Bridge over Bear River near Preston, Idaho. Despite some deviations from the standard construction practices, the strain data in seven out of eight sets of gages (four sets of concrete and four sets of steel gages) shows low strains. The finite element computer model of the bridge shows that, if properly installed, the HES Class 50AF concrete with Polypropylene fibers in the ITD's 10-in. closure pours performs well under the AASHTO design truck loading.

17. Key Words Bridge, deck, high-early strength concrete, connection, precast elements, field performance, accelerated bridge construction		18. Distribution Statement Copies available online at http://itd.idaho.gov/highways/research/	
19. Security Classification (of this report) Unclassified	20. Security Classification (of this page) Unclassified	21. No. of Pages 96	22. Price None

FHWA Form F 1700.7

METRIC (SI*) CONVERSION FACTORS

APPROXIMATE CONVERSIONS TO SI UNITS

Symbol	When You Know	Multiply By	To Find	Symbol
		LENGTH		
in	inches	25.4	millimeters	mm
ft	feet	0.3048	meters	m
yd	yards	0.914	meters	m
mi	Miles (statute)	1.61	kilometers	km
		AREA		
in^2	square inches	645.2	millimeters squared	cm^2
ft^2	square feet	0.0929	meters squared	m^2
yd^2	square yards	0.836	meters squared	m^2
mi^2	square miles	2.59	kilometers squared	km^2
ac	acres	0.4046	hectares	ha
		MASS (weight)		
oz	Ounces (avdp)	28.35	grams	g
lb	Pounds (avdp)	0.454	kilograms	kg
T	Short tons (2000 lb)	0.907	megagrams	mg
		VOLUME		
fl oz	fluid ounces (US)	29.57	milliliters	mL
gal	Gallons (liq)	3.785	liters	liters
ft^3	cubic feet	0.0283	meters cubed	m^3
yd^3	cubic yards	0.765	meters cubed	m^3
		TEMPERATURE (exact)		
°F	Fahrenheit temperature	5/9 (°F-32)	Celsius temperature	°C
		ILLUMINATION		
fc	Foot-candles	10.76	lux	lx
fl	foot-lamberts	3.426	candela/m^2	cd/cm^2
		FORCE and PRESSURE or STRESS		
lbf	pound-force	4.45	newtons	N
psi	pound-force per square inch	6.89	kilopascals	kPa

Note: Volumes greater than 1000 L shall be shown in m^3

APPROXIMATE CONVERSIONS FROM SI UNITS

Symbol	When You Know	Multiply By	To Find	Symbol
		LENGTH		
mm	millimeters	0.039	inches	in
m	meters	3.28	feet	ft
m	meters	1.09	yards	yd
km	kilometers	0.621	Miles (statute)	mi
		AREA		
mm^2	millimeters squared	0.0016	square inches	in^2
m^2	meters squared	10.764	square feet	ft^2
km^2	kilometers squared	0.39	square miles	mi^2
ha	hectares (10,000 m^2)	2.471	acres	ac
		MASS (weight)		
g	grams	0.0353	Ounces (avdp)	oz
kg	kilograms	2.205	Pounds (avdp)	lb
mg	megagrams (1000 kg)	1.103	short tons	T
		VOLUME		
mL	milliliters	0.034	fluid ounces (US)	fl oz
liters	0.264	Gallons (liq)	gal	m^3
	meters cubed	35.315	cubic feet	ft^3
m^3	meters cubed	1.308	cubic yards	yd^3
		TEMPERATURE (exact)		
°C	Celsius temperature	9/5 °C+32	Fahrenheit temperature	°F
		ILLUMINATION		
lx	lux	0.0929	foot-candles	fc
cd/cm	candela/m^2	0.2919	foot-lamberts	fl
		FORCE and PRESSURE or STRESS		
N	newtons	0.225	pound-force	lbf
kPa	kilopascals	0.145	pound-force per square inch	psi

Acknowledgements

The authors would like to thank the Idaho Transportation Department for supporting this research project. We would like to thank the members of the Technical Advisory Committee, Matt Farrar, Dan Gorley, Leonard Ruminski, Ned Parish, and Ed Miltner for their support and valuable input. Leonard Ruminski developed the project and provided extensive input in several key parts of this project. Dr. Bijan Khaleghi of the Washington Department of Transportation served as the peer reviewer for this project. This project provided experience in laboratory and field experimental research, data acquisition, data analysis, and structural computer modeling for two graduate students (Christopher Clauson and Ali Shokrgozar) and one undergraduate student (Rhiannon Lord) at Idaho State University. Financial support for the undergraduate student from the Idaho State Board of Education is greatly appreciated.

Technical Advisory Committee

Each research project is overseen by a technical advisory committee (TAC), which is led by an ITD project sponsor and project manager. The Technical Advisory Committee (TAC) is responsible for monitoring project progress, reviewing deliverables, ensuring that study objectives are met, and facilitating implementation of research recommendations, as appropriate. ITD's Research Program Manager appreciates the work of the following TAC members in guiding this research study.

Project Sponsor – Matt Farrar, P.E.

Project Manager – Dan Gorley, P.E.

TAC Members
Leonard Ruminski, P.E.
Ned Parrish

FHWA-Idaho Advisor – Ed Miltner, P.E.

Table of Contents

List of Tables

List of Figures

List of Acronyms

ABC	Accelerated Bridge Construction
ACI	American Concrete Institute
AASHTO	American Association of State Highway and Transportation Officials
ASD	Allowable Stress Design
ASTM	American Society for Testing and Materials
DAQ	Data Acquisition System
FE	Finite Element
FHWA	Federal Highway Administration
HES	High-Early Strength
ISU	Idaho State University
ITD	Idaho Transportation Department
LRFD	Load and Resistance Factor Design
LVDT	Linear Variable Differential Transformer
TAC	Technical Advisory Committee
UBIT	Under the Bridge Inspection Truck
UHPC	Ultra-High Performance Concrete

Executive Summary

Introduction

Accelerated Bridge Construction (ABC) technologies are being adopted by state departments of transportation. ABC increases public's and worker's safety by lowering exposure to construction activities and increases mobility and economic opportunities by reducing traffic interruptions and delays. ABC requires that bridge precast concrete components be effectively connected to one another in the field.

As an alternative to Ultra-High Performance Concrete (UHPC), Idaho Transportation Department (ITD) is interested in the suitability of High-Early Strength (HES) concrete Class 50AF with Polypropylene fibers in 10-inch closure pours between bridge Deck Bulb-T Girders. The advantages of this alternate material are the reduction in costs and construction time. In the first phase of the project, an optimum concrete mix with good material properties was identified through a series of standard laboratory experiments and tests on larger specimens. In this phase, field performance of a closure pour mix similar to the optimum mix found in Phase 1 is examined by placing the material in the closure pours between Deck Bulb-T Girders in the SH-36 Bridge over Bear River near Preston, Idaho.

Project Objectives and Tasks

The project objectives are to: (1) assess the performance of a closure pour mix similar to the ISU's optimum closure pour mix in the field; and (2) improve the bridge Finite Element (FE) model and refine it based on the observed field data. To carry out these objectives, the following tasks were assigned.

- Task 1: Bridge girder headed bar instrumentation.
- Task 2: Bridge deck instrumentation.
- Task 3: Strain data measurement under known truck loads.
- Task 4: Strain data measurement under commercial truck loading.
- Task 5: Data analysis and experimental results.
- Task 6: Refine and calibrate the FE model of the bridge and determine closure pour stresses under the AASHTO design truck loading.
- Task 7: Prepare and give a final presentation to the ITD Bridge Section staff.
- Task 8: Submit the final project report.

This report focuses on Tasks 1 to 6. Chapter 1 provides an introduction. Chapter 2 presents a literature review. Chapters 3-5 present instrumentation, types of loading, and data collection which address Tasks 1-4. Chapter 6 summarizes Task 5. Finally, Chapter 7 addresses Task 6.

Literature Review

In order to gain insight in the research by others, the literature review included four areas; these are: (1) instrumentation of bridges to measure response to traffic or environmental loads, (2) static and dynamic

loading on bridges, (3) data acquisition system, and (4) finite element modeling of the bridges. The following important considerations were identified: (1) properly attaching and protecting the instrumentation, (2) sampling rate and noise reduction, and (3) developing a computer model of the bridge with correct boundary conditions and refining it using the collected field data. In addition, the strain gage material in the technical data sheets by Micro-Measurements was very useful.

Instrumentation, Loading, and Data Acquisition

The SH-36 Bridge over Bear River was instrumented with 94 strain gages. The instrumentation is located along a section approximately 20 ft from the west end of the bridge. Each of the four closure pours were instrumented with 16 rebar gages and six concrete gages under the deck. In addition, six gages were installed on the bulbs of the interior three girders; data from these gages were to be used in refining the FE model of the bridge. In collaboration with ITD Technical Advisory Committee (TAC), both static and dynamic load tests were developed. The static loading involved the known Under the Bridge Inspection Truck (UBIT) loads provided by ITD and the dynamic loading was imposed by both UBITs and truck traffic. Two types of static load cases were used: (1) Load Case 1 had one UBIT front wheel directly over a closure pour (six tests); and (2) Load Case 2 had the UBIT at ¼, ½, and ¾ span on both sides of the bridge centerline (also six tests). Load Case 2 was used for calibrating the FE model. Both the small UBIT (31 kips total weight with front axle of 11.62 kips) and the large UBIT (65.5 kips total weight with front axle of 19.85 kips) were used for loading. Figure ES1 shows a typical Load Case 1 loading. In all tests, the data acquisition sampling rate of 33 Hz was adequate to capture the data without having too much information for data processing.

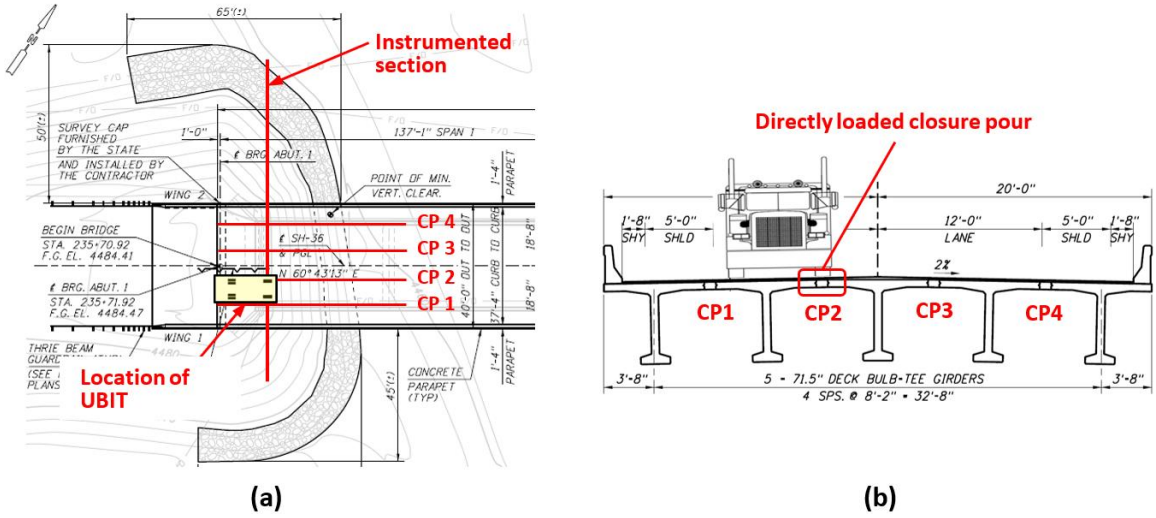

Figure ES1. (a) UBIT front wheel on instrumented section, (b) Closure Pour 2 directly loaded.

Experimental Results

Table ES1 shows the Load Case 1 strain data for small and large UBITs. It can be observed that concrete strain in Closure Pour 2 is much larger than the strain in the other closure pours. In most cases the

maximum strain occurred at the interface of precast concrete and closure pour concrete. Concrete strains in Closure Pour 2 exceeded the Phase 1 laboratory-measured concrete strain at the interface bond strength of 120 microstrain. All steel strain values are significantly lower than the steel yield strain (i.e., 2,069 microstrain).

Table ES1. Small and large UBIT maximum measured strain values under Load Case 1 tests.

Load Test	Small UBIT					Large UBIT				
	Max. concrete strain, $\mu\varepsilon$				Max. rebar strain, $\mu\varepsilon$	Max. concrete strain, $\mu\varepsilon$				Max. rebar strain, $\mu\varepsilon$
	CP1	CP2	CP3	CP4		CP1	CP2	CP3	CP4	
1.1	13	**62**	-	-	19	27	**138**	-	-	38
1.2	11	**71**	-	-	22	10	**200**	-	-	60
1.3	-	**104**	7	-	36	-	**180**	24	-	50
1.4	-	**60**	14	-	17	-	**225**	60	-	68
1.5	-	-	7	19	14	-	-	35	9	20
1.6	-	-	7	18	16	-	-	9	26	22

Figures ES2 and ES3 show the concrete and steel strain due to commercial trucks with three or more axles for Closure Pours 1 and 2. Closure Pours 1, 3, and 4 had similar behavior with lower maximum strains compared to those of Closure Pour 2. As shown in Figure ES3(a), again the maximum concrete strain in Closure Pour 2 exceeded the strain at the interface bond strength. During the construction, the research team observed that the precast exposed aggregate surfaces were not wetted before placement of closure pour concrete. In addition, three of the closure pours, including Closure Pour 2, were placed in November 2018 without the use of any heaters. When the bridge deck overlay was poured later in November, heaters were used underneath the bridge to provide warmth to cure the concrete properly.

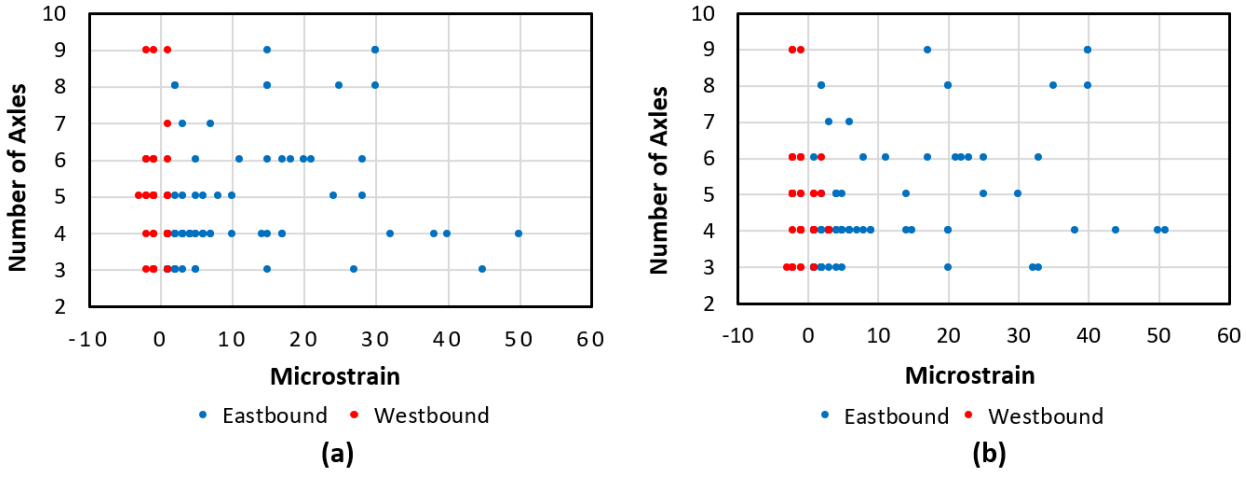

Figure ES2. (a) Maximum concrete and (b) maximum rebar strains in Closure Pour 1 vs. no. of axles.

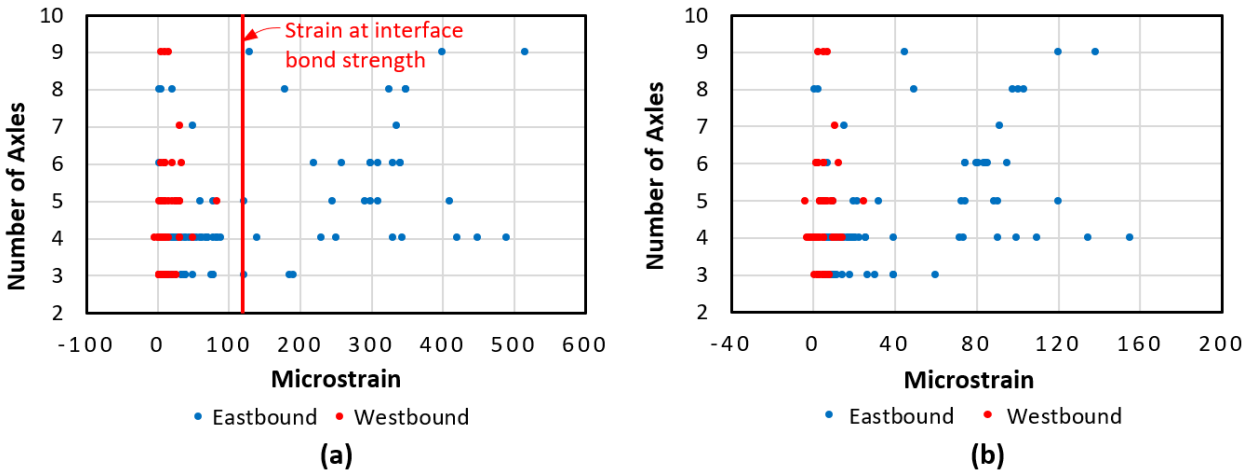

Figure ES3. (a) Maximum concrete and (b) maximum rebar strains in Closure Pour 2 vs. no. of axles.

Computer Modeling and Stress Analysis under AASHTO Design Truck

A finite element model of the bridge was developed in ANSYS FE modeling software consisting of both spans, the cap beam, and three columns at the center pier. Shell elements were used for the deck and beam elements were used for the remaining elements. Figure ES4 shows two views of the bridge model.

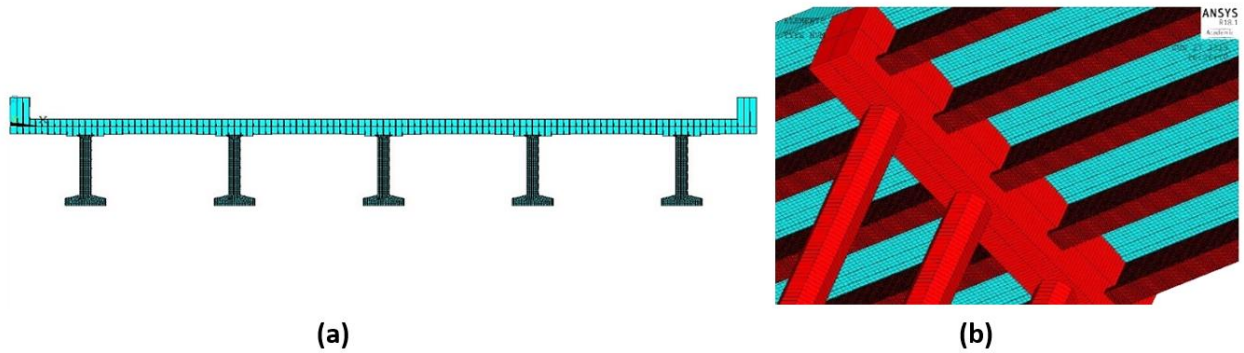

Figure ES4. (a) Cross section of deck and girders, and (b) view showing cap beam and columns.

In the FE model, the rotational stiffness of the two abutments was calibrated using the experimental UBIT loads at ¼, ½, and ¾ span locations over the instrumented bridge span. As shown in Table ES2, using the calibrated model, when comparing the FE and measured strains under the directly loaded closure pours (Load Case 1), as expected, the results did not match for Closure Pour 2. However, for the remaining closure pours, the FE estimated concrete strain values at the interface were close to the experimental results. On average, the FE strain values are about 10% lower than the experimental values.

Finally, the bridge model was analyzed under the AASHTO design truck. The concrete stresses at the interface of closure pour concrete and precast met the AASHTO Service I Limit State for controlling flexural cracking. The stresses in the headed bars were significantly lower than the bar yield stress.

Although not required by AASHTO LRFD Bridge Design Specifications, the stresses in the bars also met the Fatigue I Limit State for infinite load-induced fatigue life.

Table ES2. FE and experimental interface concrete strains at the directly-loaded closure pours.

Load Case	Small UBIT		Large UBIT	
	Experimental Average Strain (microstrain)	Numerical Average Strain for Optimum Abutment Stiffness (microstrain)	Experimental Average Strain (microstrain)	Numerical Average Strain for Optimum Abutment Stiffness (microstrain)
1.1	11.0	9.3	18.3	16.1
1.2	45.0	9.7	172.5	16.7
1.3	84.5	10.2	171.3	17.7
1.4	11.5	10.2	19.5	17.7
1.5	11.0	9.7	17.5	16.7
1.6	8.5	9.3	19.0	16.1

Conclusions and Future Work

The field-measured experimental strain data show that: (1) the concrete strain in Closure Pour 2 exceeds the strain corresponding to the interface bond strength (i.e., approximately 120 microstrain) for some of the static and dynamic loads, but the remaining closure pour concrete strains remains low; and (2) the maximum strain values in the rebars are significantly lower than the strain corresponding to the steel specified yield strength (i.e., 2,069 microstrain).

The FE computer model shows that, if properly installed, the High-Early Strength Class 50AF concrete with Polypropylene fibers in the ITD's 10-in. closure pours performs well under AASHTO design truck loading.

The third phase of this project has been approved. This phase involves the long-term monitoring of the performance of the closure pours under both UBIT loading and commercial truck traffic. The tasks in this phase are: (1) replacing/preparing concrete strain gages for long-term moisture protection, (2) periodic measurement of the bridge under UBIT loading, (3) more data under commercial traffic; and (4) periodic closure pour inspection.

Chapter 1
Introduction

Description of the Problem

Accelerated Bridge Construction (ABC) technologies are being adopted by state departments of transportation. Compared to the conventional methods, when ABC is implemented, bridge construction time is typically reduced by 30-70%. This in turn increases public's and worker's safety by lowering exposure to construction activities and also increases mobility and economic opportunities by reducing traffic interruptions and delays. ABC requires that bridge precast concrete components be effectively connected to one another in the field. Currently there is a trend of using Ultra-High Performance Concrete (UHPC) to connect precast bridge deck panels or girders in 6-in. wide closure pours between the precast elements. As an alternative, Idaho Transportation Department (ITD) has proposed to place High-Early Strength (HES) concrete with polypropylene fibers in 10-in. closure pours between girders. The advantages of HES concrete in closure pours are:

- HES concrete can be batched in the ready mix plant, brought to the field in the mixing truck, and placed similar to a conventional concrete.
- ITD allows removal of forms for HES concrete after one day and compressive strength of 3 ksi, while for UHPC a minimum curing time of four days and a compressive strength of 14 ksi is required.
- In Idaho, the installed cost of HES concrete ranges between $900 to $1000 per cubic yard, or about $200 per cubic yard more than for conventional concrete. The UHPC costs about $13,000 to $15,000 per cubic yard. The use of HES instead of UHPC results in about $100,000 cost savings per average 120 ft long span for a two-lane bridge.

This project is the second phase of the research project investigating suitability of HES concrete Class 50AF with fibers as an alternative to UHPC in closure pours between bridge Deck Bulb-T Girders. In the first phase of the project, an optimum concrete mix with good material properties was identified through a series of standard laboratory experiments and tests on larger specimens. Details of the optimum mix and its properties are documented in the first phase final report (Ebrahimpour, et al. 2018).[(1)]

The laboratory tests in the first phase were not designed to address the two-way behavior of an actual bridge deck with reinforcing steel bars in both directions. In this phase of the project, field performance of a closure pour mix similar to the optimum mix found in Phase 1 is examined. This material was used in the closure pour between Deck Bulb-T Girders in the SH-36 Bridge over Bear River near Preston, Idaho. The bridge was instrumented with strain gages to monitor strain data in the closure pour (headed steel bar and closure pour concrete) and the interface of closure pour and precast concrete under both known truck loads and commercial truck traffic.

Project Objectives

The project objectives are:

- Assess the performance of a closure pour mix similar to the ISU's optimum closure pour mix in the field.
- Improve the bridge FE model and refine it based on the observed field data.

Project Tasks

The project tasks are:

- Task 1: Bridge girder headed bar instrumentation – Strain gages are placed on the headed bars of five of the girders in the precast yard before they are transported to the bridge site. The strain gages are on the girders that bear on one side on the southwest abutment. Four headed bars are instrumented in each closure pour.

- Task 2: Bridge deck instrumentation – Strain gages are installed on the concrete surface below the bridge deck along the same section as the instrument headed bars. The concrete gages are placed on the closure pour, on the precast concrete, and at each of the two interfaces of closure pours.

- Task 3: Strain data measurement under known load – trucks with known axle loads are placed on the bridge to measure strain data.

- Task 4: Strain data measurement under commercial truck loading – several hours of strain data are collected with commercial trucks having three or more axles. During the strain measurements, photos are taken of the vehicle traveling across the bridge to determine the position of the tires in the lanes. Other information about the vehicles such as type of vehicle, number of axles, and comments are recorded.

- Task 5: Data analysis and experimental results – Both the measured static and dynamic strain responses are summarized in graphical and tabular format. The data are analyzed to see if strain and stress levels are within the acceptable range. The strain data is also used to refine the FE model (Task 6).

- Task 6: Refine the FE model – The FE model developed in Phase 1 is revised. Based on the strain data collected in the field, the model is further refined. In addition, closure pour stresses are calculated under the AASHTO design truck loading.

- Task 7: Make a presentation to the ITD Bridge Section staff describing the project and results.

- Task 8: Submit the final project report.

This report presents Tasks 1 to 6.

Report Overview

This report is divided into eight chapters.

- Chapter 1 presented an introduction to the research problem, the objectives, and project tasks.
- Chapter 2 presents the literature review.
- Chapter 3 presents the instrumentation used in the SH-36 Bridge over Bear River.
- Chapter 4 describes the bridge loading.
- Chapter 5 describes the data acquisition system.
- Chapter 6 presents the results of bridge response to static and dynamic truck loading.
- Chapter 7 describes the revised finite element model of the bridge and the calibration of the model using the experimental data. The second part of this chapter presents the closure pour stresses under the AASHTO design truck loading.
- Chapter 8 presents a summary, conclusions and future work.

Chapter 2
Literature Review

Introduction

The first step in any research project is to review previous literature to determine what the best approach is and review any issues encountered during similar projects. The literature review for this project consists of four main components. The first section deals with instrumentation of bridges and is focused on literature involving the instrumentation of any type of bridge under various loading conditions. In the second section prior research on static and dynamic loading of bridges is reviewed. This includes using large trucks of known weight to obtain experimental data for use in the process of refining a Finite Element (FE) model. The third section reviews and explains both manual and electronic data collection and analysis on earlier research. The data collection mainly focuses on strain and temperature in and around the bridge. The fourth section summarizes literature on FE modeling including modeling bridge elements and determining boundary conditions. The fourth section also reviews prior research on refining finite element models using updated material properties and the inclusion of non-structural components. Chapter 2 ends with a summary of the research reviewed within this chapter.

Instrumentation

The practice of instrumenting bridges has been an effective way to determine how bridges perform under static and dynamic loading. It is the most effective way to get real time data on how a bridge is functioning. Instrumentation can include the use of strain gages, potentiometers, Linear Variable Differential Transformers (LVDTs), anemometers, thermometers and much more. Strain gages are used in many bridge monitoring projects for their accuracy and small size. There are three main types of strain gages: vibrating wire, resistive, and fiber-optic. Hedegaard et al. (2013) used all three types of strain gages in the instrumentation of the new I-35W St. Anthony Falls Bridge after the collapse in 2007.[(2)] For the I-35 project, vibrating wire gages were used primarily for static measurements, resistive gages were used for dynamic measurements, and fiber-optic gages were used to determine the longitudinal curvature of a specific span of the bridge due to their long gage length (13 ft) (Hedegaard et al. 2013).[(2)] For this project, only resistive gages were used since they were long enough to capture true strain values and collect static and dynamic strain data. There are many important contributing factors when selecting and installing strain gages on steel and concrete surfaces. According to Micro-Measurements, strain gages which are to be installed on concrete should be long enough to cover multiple lengths of the largest aggregate to get an average strain and not the local variations in strain due to cement and aggregate contact (Micro-Measurements 2018).[(3)] For strain gage installation on reinforcing bar Micro-Measurements recommends using CEA-Series strain gages (Micro-Measurements 2015).[(4)] Both recommendations were followed during the selection of strain gages for this research project.

Strain gage installation is a delicate and time-consuming procedure to ensure the gages are installed properly. The Micro-Measurements tech tip document on strain gage installation for concrete structures provides instructions on how to properly prepare the surfaces of rebar and concrete for gage installation. This involves grinding down the ribs on the rebar and pre-filling the pores in the concrete with the proper adhesive (Micro-Measurements 2015).[4] These steps were followed as instructed in the tech tip and all recommendations on adhesive and gage selection were followed. Furthermore, proper surface cleaning procedures and placement of gage layout lines were done in accordance of the Micro-Measurement suggestions in the tech tip previously mentioned. One of the most challenging aspects of gage installation underneath the bridge on a flat surface, is clamping the gage while the adhesive cures. For this project, all the concrete strain gages had to be installed upside down. Micro-Measurement Tech Tip 610 provides strain gage clamping techniques and a version of one of the figures in the document was used to clamp the gages underneath the bridge. Figure 1 shows the clamping technique suggested by Micro-Measurements (Micro-Measurements 2015).[5] The actual clamping procedure used in this project will be discussed in subsequent chapters.

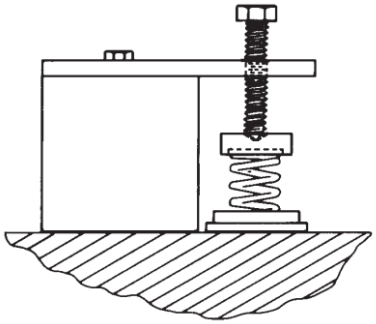

Figure 1. Clamping technique for flat surfaces.

For clamping on rebar, Micro-Measurements suggests using a clamping plate which matches the contour of the piece to be instrumented (Micro-Measurements 2015).[5] For this project polyvinyl chloride (PVC) pipe halves were used to obtain the curved contour shape of the rebar. Figure 2 shows an example of the clamping setup used in this project.

Figure 2. Rebar clamping procedure.

Protection of strain gages is important to ensure proper measurements and the longevity of the gages. Micro-Measurements suggests using M-Coat JA to protect the strain gages (Micro-Measurements

2015).[4] For this project a different gage protectant was used called M-Coat F. This decision was made since M-Coat F was used in a prior research project on the same topic outlined in Casanovas' thesis (Casanova 2018) and Micro-Measurements M-Coat F application instructions states M-Coat F is typically used in Bridge and rebar applications and on vertical or inverted surfaces (Micro-Measurements 2014).[6,7] The final step in protecting the instrumentation is to protect the lead wires attached to the gages. For the gages embedded in the concrete Micro-Measurements recommends placing the lead wires in a conduit to protect them from damage during placement and curing of the concrete (Micro-Measurements 2015).[4] For this project the lead wires for the rebar gages were protected using clear plastic tubing through the bottom of the bridge. Further protection of lead wires will be discussed later in this report.

Lead wires also need protection from electric and/or magnetic fields which can cause changes in low frequency analog signals (Campbell Scientific 2001).[8] According to Micro-Measurements, in an ideal instrumentation lead wires do not add or subtract anything from the measurement signal (Micro-Measurements 2010).[9] It is also indicated there are many ways to protect cables from electric and magnetic fields, but the most popular are twisted and shielded wires. The length of the wires greatly contributes to the amount of noise seen in the system. Micro-Measurements states wires 50 ft or more can have significant levels of noise introduced into the system (Micro-Measurements 2013).[10] For this project the maximum analog cable length is estimated to be 42 ft, so there should not be a need for noise protection in the system. More discussion on noise protection and cable will be discussed later in this report.

Bridge Loading

Bridges see many types of loads but the most significant is the vehicles which travel across it. Many projects have researched how the load is distributed between members in the bridge or how individual elements of the bridge behave under certain loads. Load testing of a bridge can be done both statically and dynamically to try and mimic the types of loading a bridge will see during its life cycle. The load can be placed on the bridge in such a way to induce maximum stresses at the instrumented locations or maximum stresses on the overall structure. Bridges are usually sectioned off by lanes and longitudinally by a predetermined length in order to obtain different arrangements of the load. Provines et al. sectioned the bridges into three lanes: centerline, upstream, and downstream (Provines et al. 2014).[11] Sanayei et al. also divided their bridge up transversely the same way for two lanes of traffic (Sanayei et al. 2012).[12] Many studies performed both static and dynamic tests with trucks of known load. Further, Chajes and Shenton explain each test should be repeated to make sure the data collected is reliable and repeatable (Chajes and Shenton 2006).[13] The same practices will be used in this project and will be discussed in further detail in future chapters.

The objective of the static load test is to obtain strain data from the bridge in order to calibrate the finite element model (FEM) by replicating the stresses observed in the bridge (Sanayei et al. 2012).[12] Static load tests are generally done with a truck of known axle weights parked in different arrangements. Hedegaard et al. used eight sand trucks of known weight in five different static loading scenarios to

examine longitudinal bending, load distribution, transverse bending, and load distribution due to torsional bending (Hedegaard et al. 2013).[2] Provines et al. (2014) parked unloaded trucks at mid-span of a railroad flatcar bridge and collected static strain data to determine if the loaded truck can be placed on the bridge.[11] If they determined the bridge could handle a fully loaded truck they performed the same tests with the loaded truck at mid-span to determine a load rating procedure for railroad flatcar bridges (Provines et al. 2014).[11] In another study Sanayei et al. performed static tests on 3 different travel lanes with a tri-axle dump truck of known axle weights traveling along the bridge and stopping at designated locations for ten seconds each to let the dynamic effect of the truck settle out of the bridge. Tests were repeated three times for reliability (Sanayei et al. 2012).[12]

Dynamic loading is done by having a load travel across the bridge at a predetermined speed. The dynamic test data includes vibration seen in normal travel across the bridge. One of the most widely used dynamic tests performed on bridges is the crawl test where a truck travels across the bridge at a low speed. The purpose of traveling across the bridge at such low speeds is to reduce the dynamic effect of the load (Barr et al. 2006).[14] Most crawl tests performed in this literature search were performed at speeds around 5 miles per hour (mph). Some projects involved faster dynamic loading tests in increments until the bridge speed limit was reached to determine the strain seen by the bridge under normal operating conditions.

Data Collection

The components of data collection are the sampling rate, data integrity, and type of data. In a dynamic test, it is important to have fast enough sampling rate in order not to miss any peaks in the data. It is also ideal not to have too much data so the right sampling rate can make data collection and processing much easier and more effective. The sampling rate for previous studies has ranged from 10-200 hertz (Hz), but only Sanayei et al. used a sample rate larger than 50 Hz (Sanayei et al. 2012).[12] In this project, the optimum sampling rate was determined based on a trial and error method. For the number of sensors used in this project (94 sensors), the maximum sampling rate the system can record is 50 Hz (50 samples per second). A decision was made that the sampling rate of 33 Hz can adequately capture the peak dynamic responses in this project.

Data integrity is a large concern in the use of data acquisition systems. If not addressed, data can become skewed and provide results not representative of the actual conditions at the gage locations. Sources of error can come from magnetic/electrical fields, temperature fluctuations, and long lead wires. Sources of magnetic/electrical fields at a bridge site would include utilities, generators, and vehicles. If these sources affect the data, the strain data will appear as if it is oscillating like in Figure 3. This oscillating effect is usually called electrical “noise”. This noisy data in Figure 3 came from a project where strain on steel truss bridges was measured under wind loading (Rutz et al. 2008).[15]

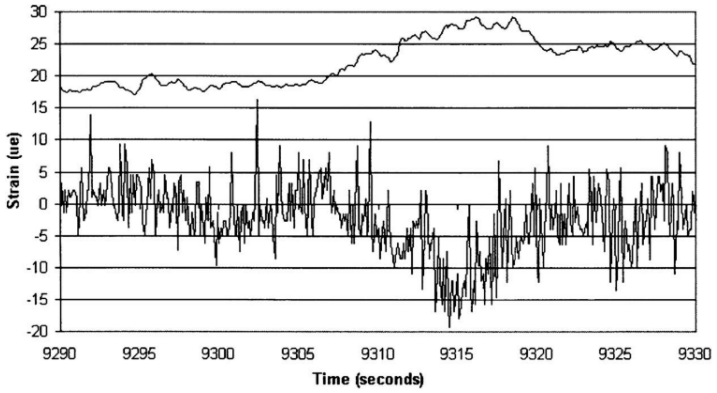

Figure 3. Noisy strain data.

There are a few methods to reduce the amount of electrical noise seen in data. One method is to use shielded cable. The shielding protects the cable inside from most of the outside sources of noise and the shield is connected to a ground to eliminate sources of noise. The next method is to use twisted pair of wires. The twisted pairs of wires offer protection from both electrical and magnetic fields (Campbell Scientific 2001).[8] Another method the Campbell Scientific data acquisition system uses to reduce electrical noise is integrating and averaging the signal to the measurement device. By doing this, certain frequencies can be targeted and removed from the data (Campbell Scientific 2001).[8] The data acquisition system used in this project is a Campbell Scientific system, so this method is used to help reduce noise in the data.

The next section of data integrity is temperature fluctuations. Temperature fluctuations can affect the resistance of the wires which can in turn affect the strain data. The best way to cancel out the effects of temperature fluctuations is to make sure all wires experience the same temperature fluctuations. For three wire strain gages, it is best to make sure lead wires are all of the same length and placed together (Campbell Scientific 2017).[16] This will ensure the wires have the same resistance and experience the same fluctuations in temperature.

Long lead wires are the third potential source of error in data acquisition. When lead wires become longer the wires resistance become more of a factor in the data. Campbell Scientific provides mathematical and shunt calibration methods to account for longer lead wires. Another error which can be encountered when long lead wires are present is a sensitivity reduction in the system. The methods used to correct this error are the same as previously mentioned with the increased resistance due to longer lead wires. These methods are outlined in the manual for Campbell Scientific's Terminal Input Modules (TIMs) (Campbell Scientific 2017).[16] For this project, experiments were conducted to determine the effects of the longer lead wires. It was determined with a maximum lead wire length of 42 feet, the strain data is unchanged so the methods outlined above will not need to be used to correct for longer lead wire. Micro-Measurements also notes that problems due to lead wire length start to occur when lead wires are 50 feet or more (Micro-Measurements 2013).[10]

The third part of data collection is the type of data being collected. Through research of previous literature there are many different types of data collected from bridges such as strain, deflection,

temperature, corrosion of reinforcing bars, acceleration, and tilt angles. Rutz et al. collected strain, wind speed, wind direction, and temperature data to analyze the stresses in historic truss bridges in Colorado (Rutz et al. 2008).[15] Jáuregui et al. used strain data from the I-40 Bridge over the Rio Grande River to evaluate the bridge and compared the data to the finite element model of the bridge in order to refine the model (Jáuregui and Barr 2004).[17] In another project Cardini and DeWolf used strain data to determine the live load distribution, peak strains, live load stresses, and neutral axis location of the bridge and its elements. A finite element model was then created to verify the results of the acquired data (Cardini and DeWolf 2008).[18] Hedegaard et al. collected strain, temperature, acceleration, and displacement data to determine the behavior of the bridge and refine their finite element model (Hedegaard et al. 2013).[2] For this project, strain data is collected to determine the behavior of the closure pour connections between bridge girders under different loading conditions.

Finite Element Modeling

Finite Element (FE) modeling is an important tool used to estimate the behavior of bridges before they are built. Most research dealing with bridges involves both physical measurements and computer modeling. There are three main steps in FE modeling which contribute to the accuracy of a model. The first step is modeling the bridge structure. Different elements are used to represent the girders, deck, columns, and reinforcing throughout the bridge. Secondly, the supports need to be modeled to correctly replicate the actual support conditions occurring at the bridge. The final step is to refine the computer model.

Modeling the bridge structure itself involves knowing all dimensions and properties of the materials used in the construction of the bridge. Different elements can be used to model various structural components of the bridge. The most widely used type of element in bridge modeling is the shell element. The shell element is used in applications where linear elastic analysis is assumed. Hedegaard et al. used shell elements to model the pre-stressed strands inside the box girder flanges. The shell elements were given no bending stiffness and the appropriate axial stiffness to properly represent the stiffness of the strands (Hedegaard et al. 2013).[2] Bell et al. modeled a bridge with a concrete deck placed on steel stringers and used shell elements to model the deck and the steel reinforcing in the deck (Bell et al. 2013).[19] Jáuregui and Barr also used shell elements to model the concrete deck of the I-40 Bridge over the Rio Grande River (Jáuregui and Barr 2004).[17] Frame elements are used to model steel girders in composite bridges. Also, solid elements are sometimes used to model bridge decks. Each element type has different properties allowing it to better represent the bridge being modeled. Choosing the element type to use in a model is determined on a case by case basis as it depends on how detailed the model needs to be and what properties are most important to represent accurately in the model.

Another important aspect of modeling the bridge is using elements that are sized properly. The size of the element determines how detailed the results will be. One should balance the element size to avoid long computational times but also still get reliable results. Hedegaard et al. used an element size of 24 in. by 24 in. This resulted in roughly 500 elements along the length of the bridge and anywhere from 8 to

15 elements throughout the depth of the girders (Hedegaard et al. 2013).[2] Jáuregui and Barr used elements sizes of 14.5 by 12 inches transversely and longitudinally respectively.[17] This was done to match the girder spacing. The girders were also modeled with 12 in. longitudinal elements to match the deck model for ease of modeling (Jáuregui and Barr 2004).[17] For this project, for the deck elements, an element size of 4 in. (in the transverse direction) by 6 in. (in the longitudinal direction) is used as it provides reliable results and save on time during the modeling process.

Correctly modeling the boundary conditions has a significant influence on the overall model behavior. The fixity of the supports is what is to be determined. This is usually altered to better match experimental results as there is no good way to determine how rigid the supports are at the bridge site. Bell et al. modeled the bridge deck and steel girders supporting the deck. Elastomeric bearing pads were used in between the steel girders and cap beam to support the bridge. The elastomeric pads were modeled using linear rotational springs with the proper stiffness values to represent the steel reinforced bearing pads used on the bridge (Bell et al. 2013).[19] Jáuregui and Barr considered three different support conditions in their finite element model.[17] The first condition used pin supports at the fixed bearing locations and roller supports at the expansion bearing locations. The first model did not consider the pier stiffness. The second model used frame elements to model the pier. The base of the pier was fixed and the connection between the columns and the girder was rigidly constrained. For the third model, the intermediate connections were completely fixed so as not to allow translation or rotation. This was done to represent the extreme upper limit of pier stiffness (Jáuregui and Barr 2004).[17] Hedegaard et al. modeled three out of the four spans of the I-35W St. Anthony Falls Bridge because there is an expansion joint between Spans 3 and 4 separating the forces acting on either side of the joint and keeps them from distributing across the joint.[2] The profile view of the bridge is shown in Figure 4. For their model, Piers 2 and 3 were assumed to be fixed at the base. Vertical constraints were used to model the bearing pads at Abutment 1 and Pier 4. Pin supports were used to model the connections at Piers 2 and 3 (Hedegaard et al. 2013).[2]

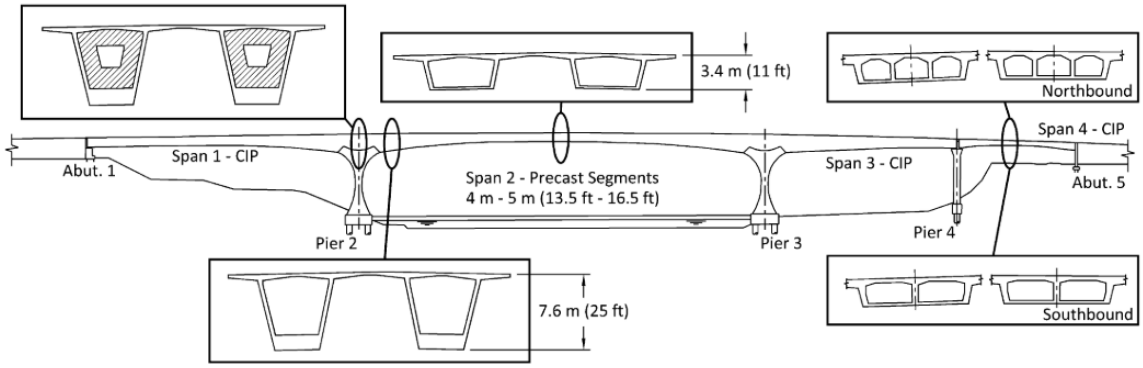

Figure 4. Profile view of I-35W St. Anthony Falls Bridge.

The final step taken after a finite element model is produced and analyzed is to refine the model to better represent the actual conditions at the bridge site. The usual method for determining if the steps taken to refine the model are working is to compare the results of the model to experimentally obtained

data using field instrumentation. There are multiple refinements which can be done to update a finite element model. The first and most common step is to update the concrete compression strength when the concrete from the project is tested in a laboratory. When concrete is produced at the plant it is made to be stronger than what the specifications ask for. This is to reduce any possibility of a batch of concrete not achieving the required strength. This step was taken by all researchers included in this literature review. It is important to include all elements of the bridge into the model as they will almost certainly affect the stiffness and weight of the overall bridge. Bell et al. modeled the safety curbs on the bridge since they observed the safety curb reinforcement was placed before the pour of the deck and would contribute to the overall stiffness of the bridge (Bell et al. 2013).[19]

Summary

Through research of existing literature dealing with the instrumentation and testing of bridges, many ideas were confirmed or realized which needed to be considered in this project. Properly attaching and protecting the instrumentation is important to ensure accurate reading and longevity of the devices. Recording data needs to be done with care as the sampling rate and noise associated with data collection is crucial to collecting quality data. Creating a computer model of bridge is another important part of this project and extensive research was done on existing literature to make sure all components are covered. Correctly modeling bridge elements and the boundary conditions were covered in the literature review. Refining a computer model was also reviewed to determine what steps could be taken initially to create an accurate model which closely estimates the behavior of the bridge in this project.

Chapter 3
Instrumentation

Introduction

The SH-36 bridge over Bear River was instrumented with 94 strain gages. All instrumentation is located along a section approximately twenty feet from the west end of the bridge. Lines representing the instrumented section and each of the four closure pour connections are shown in Figure 5. Closure Pours 1 to 4 are shown as CP 1 to CP 4. All strain gages, except for the six bulb strain gages (to be discussed later) are located at the four intersections of the red lines.

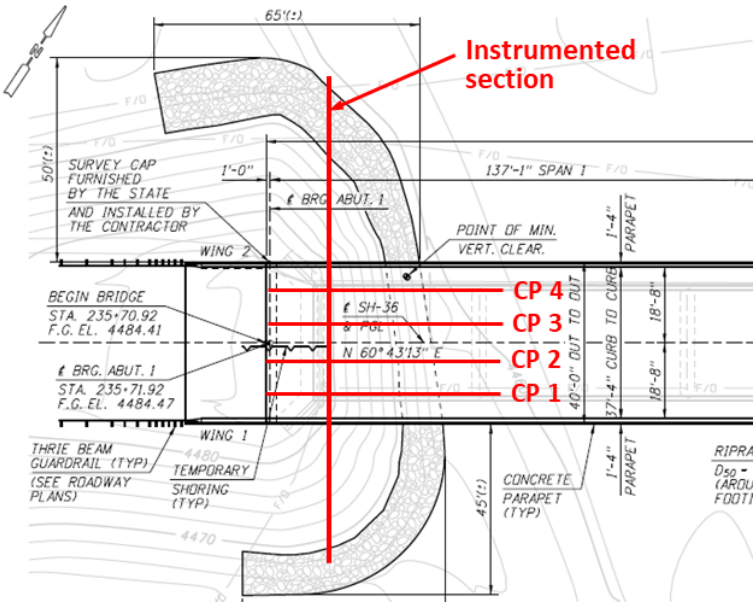

Figure 5. Line of instrumented cross section.

Rebar Gages

On May 7-8, 2018, 64 strain gages were installed at the Forterra Structural Precast plant in Caldwell, Idaho. Figure 6 shows the sequence of rebar surface preparation, strain gage installation, and protecting the gages from damage during transportation.

All the girders along the instrumented section on the southwestern span were instrumented with strain gages on the reinforcing steel protruding from the girders which became part of the closure pour connection. The strain gages used for instrumenting the rebar in this project were 0.25 in. long and have a resistance of 350 ohms. They were purchased from Micro-Measurements and came with 10 feet of pre-attached lead wire. Further information on the strain gages used in this project can be found in Appendix A of the thesis by Clauson, C. (2019).[20]

(a) Grinding headed bars **(b) Preparing for gage installation** **(c) Attaching strain gages**

(d) Installed bar strain gages **(e) Protective PVC pipes** **(f) Placing PVC pipes over bars**

Figure 6. Strain gage installation at Forterra Structural Precast plant in Caldwell, Idaho.

There were 16 strain gages installed in each connection. Four headed rebars, two from each girder being connected, were instrumented with the strain gages. Figure 7 shows a diagram of one headed rebar with strain gage locations. Two strain gages were placed on opposite sides of the rebar close to the interface between the girder and the closure pour concrete. Two more gages were installed on opposite sides of the rebar at a location close to the headed bars. Figure 8 shows one of the girders after all eight strain gages were installed on the reinforcing bars.

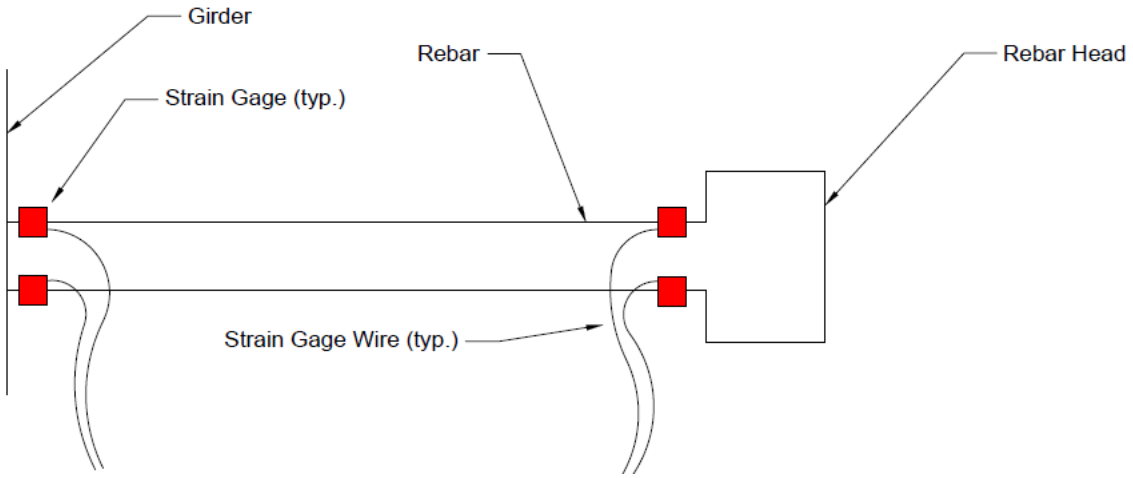

Figure 7. Rebar strain gage diagram.

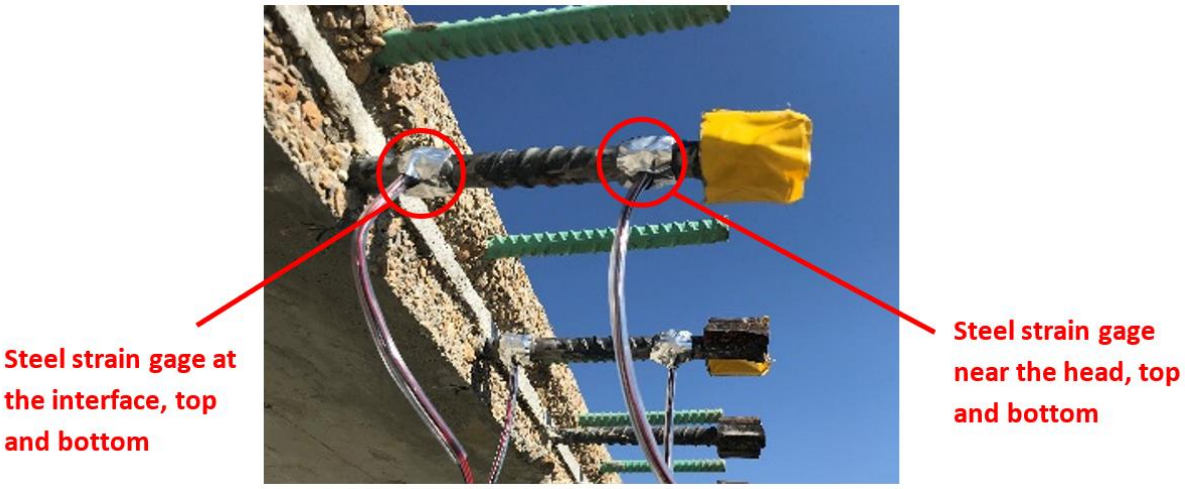

Figure 8. Instrumented rebars.

The first step in the instrumentation process was to determine which headed rebars would be instrumented. It was decided the rebars to be instrumented would be located approximately twenty feet from the end of the top flange of the prefabricated girders at the southwest abutment. A line showing the section of the bridge which was instrumented can be seen in Figure 5. The decision on the location of the strain gages (i.e., 20 ft from the end of the top flange) was made in order to safely install the concrete gages at the bridge site and still obtain transverse bending without any effects from the abutment to girder connection. Girders were measured and rebars which were selected for instrumentation were marked with yellow tape. The installation process followed the same procedure as was previously followed for first phase of the ITD research project. The ribs on the rebars were ground off with an electric grinder in order to prepare a smooth surface for gage installation and remove any imperfections on the steel surface. Figure 9 shows the rebar after the grinding process was complete.

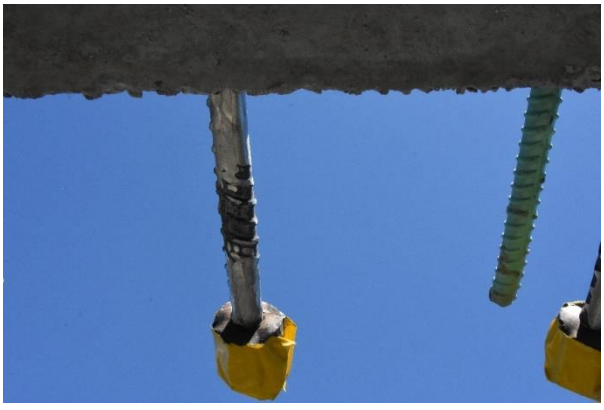

Figure 9. Rebar with ribs removed.

After the grinding process was complete, the surface was cleaned using the conditioner and neutralizer purchased from Micro-Measurements. The next step involved using a special gage installation tape from Micro-Measurements to tape the strain gages down to a clean piece of glass. This is done in order to place the strain gage on the rebar without touching the strain gage. Then the taped gages were transferred to the rebar. Once all gages were placed and ready for installation, a two-part epoxy (Micro-Measurements M-Bond AE-10) was prepared and placed underneath the gages and tape and were clamped for at least eight hours to ensure proper bonding. The data sheet for the epoxy used in this project can be found in Appendix A of the thesis by Clauson, C. (2019).[20] The clamping procedure is the same as the one tested in the lab and is demonstrated in Figure 10. The clamping mechanism consisted of rubber pads to distribute the clamping pressure uniformly over the strain gages. In addition, 1.5 in. PVC pipes were cut in half longitudinally to create two PVC pipe halves. The PVC pipe pieces were glued to a small piece of wood for the spring clamps to apply pressure without slipping off the pipe. This clamping technique was tested in the lab and the strain gages adhered to the rebar without any problems.

Figure 10. Rebar clamping technique.

Once the clamps were removed, the tape covering the gage was also removed and two coats of polyurethane were applied over the gages to protect them from any dust or moisture. After the polyurethane dried, a protection called M-Coat F was applied over the gage areas to protect from damage caused by placement and curing of concrete. This protection was recommended by and purchased from Micro-Measurements. The M-Coat F protection consisted of a layer of butyl rubber placed completely around the rebar at strain gage locations followed by a layer of aluminum tape. The lead-wires were run through a small plastic tube which protected the wires which were encased in the closure pour concrete. Large PVC pipe halves were then taped over the instrumented rebar to protect the gages during transportation and placement of the girders. Once the girders and formwork were in place the PVC halves were removed and the wires which were protected by means of small plastic tubing which was run down through the formwork. Figure 11 shows a closure pour fully prepared for placement of concrete. The process of placing the concrete is shown in Figure 12. The placement of concrete consisted of concrete trucks delivering the closure pour concrete to the bridge site where it

was then loaded into a pump truck at the end of the bridge and pumped through a large hose along the length of the closure pour for placement.

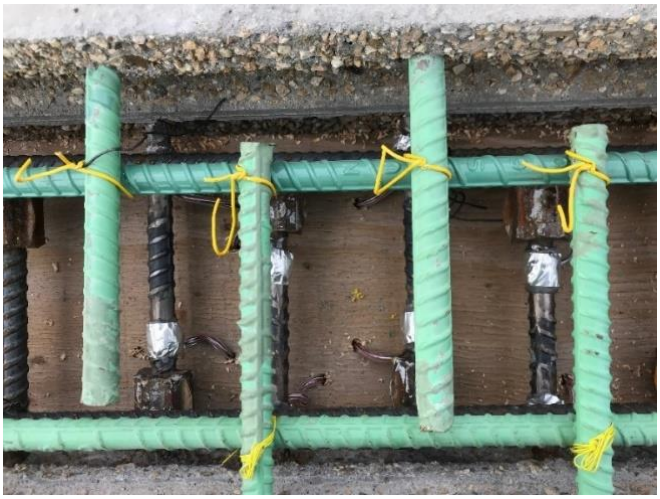

Figure 11. Closure pour prepared for concrete placement.

Figure 12. Placement of concrete in closure pour.

After the concrete cured, the forms underneath the bridge were removed and the gages were tested to make sure all gages measured 350 ohms of resistance. A picture from below the bridge after the forms were removed is shown in Figure 13. Complete surface preparation, gage installation, and protection instructions are provided in Appendix B of the thesis by Clauson, C. (2019).[20]

Figure 13. Closure pour with rebar gages installed.

Concrete Gages

Installation of concrete gages took place after the closure pour connections were poured, cured, and formwork was removed. The numbering system used in this project to identify closure pours is shown in Figure 14. The closure pour connection furthest downstream is labeled CP 1 and the remaining three were numbered in order. Closure Pour 1 was poured in August, Closure Pours 3 and 4 were poured in the first week of November and Closure Pour 2 was placed last sometime in November. The ISU team were present during the installation of Closure Pours 3 and 4.

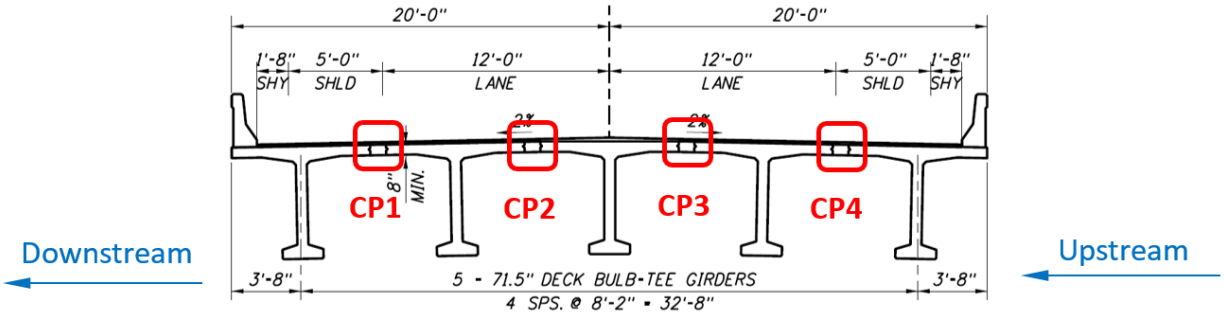

Figure 14. Closure pour numbering system.

Each closure pour was instrumented with 6 concrete strain gages in the orientation shown in Figure 15. One strain gage was placed over each interface between the girders and the closure pour concrete. Two more gages were placed on each side of one of the interfaces to observe if similar strains are occurring through the location of the interface. Two more gages were also placed at the center of the closure pour to observe the transverse and longitudinal strains occurring in the closure pour material.

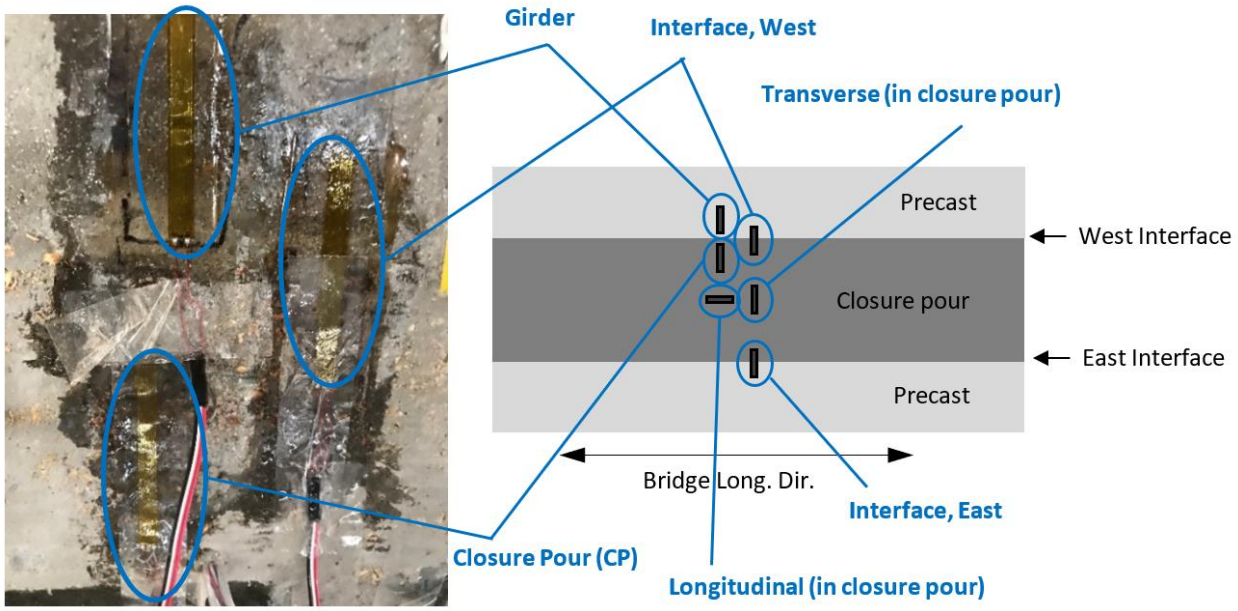

Figure 15. Concrete strain gages from bottom view of the deck.

In addition to the closure pour strain gages, the girders were also instrumented on each side of the bulbs on the interior girders. In Figure 16 the blue circles indicate the bulbs which were instrumented with strain gages. The red indicates the approximate location for each strain gage. These gages were placed to calibrate and verify the Finite Element model which was created to replicate the actual conditions occurring at the bridge.

The process of instrumenting a concrete surface is similar to a steel surface but has a few differences. The installation of concrete gages was also different since they had to be installed upside down underneath the bridge. The first step involved marking the concrete surfaces at the locations where strain gages were to be installed. Then an electric grinder was used to remove any surface irregularities. To clean the surface, degreaser was sprayed onto the concrete and wiped off with gauze pads. For final cleaning, the conditioner and neutralizer from Micro-Measurements were used to clean the surface. For installation of concrete gages an extra step of preparation is needed to ensure the strain gage completely bonds to the concrete surface. The two-part epoxy which is used to attach the strain gages is used to fill in the pores on the surface of the concrete. This was done by creating a large patch of gage installation tape and putting the epoxy over the sticky side of the tape and taping the large patch over the areas to be instrumented. The tape was strong enough to keep the epoxy held up on the concrete surface until it was fully cured. This procedure is shown in Figure 17.

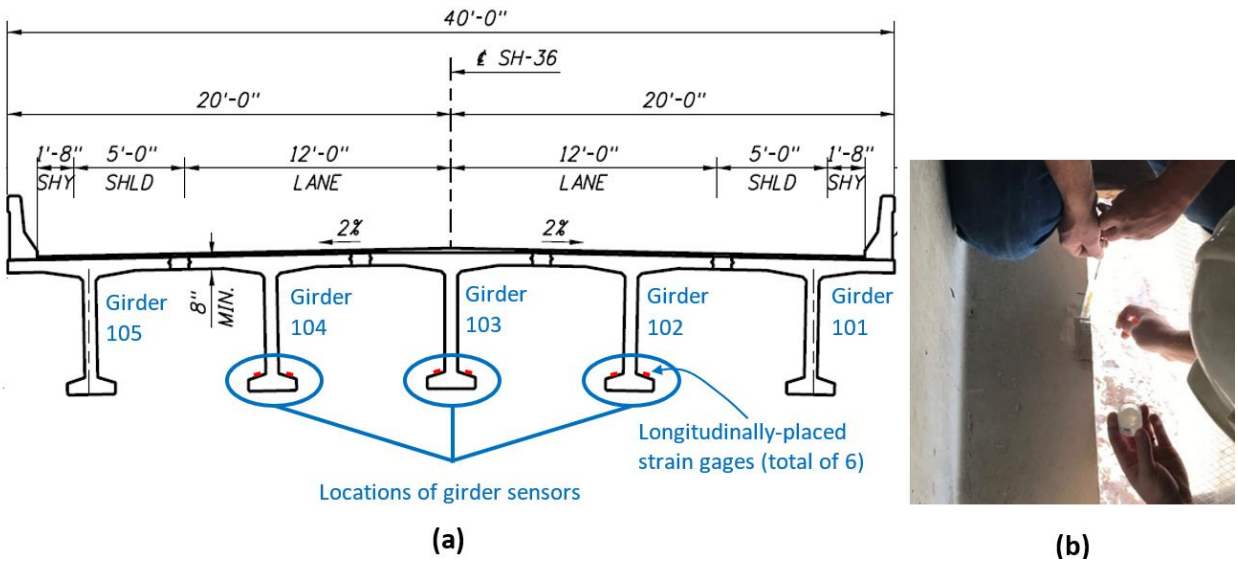

Figure 16. (a) Longitudinally-placed girder strain gages; and (b) placement of a girder strain gage.

Figure 17. Filling pores on concrete surface with epoxy.

After the epoxy cured the tape was removed and the surface was ground down to the concrete surface, so the final bonding surface was the concrete with the pores filled in with epoxy. The surface was again cleaned with conditioner and neutralizer in preparation for gage installation. The next step involved placing strain gages on the surfaces using the gage installation tape. Once the gages were all placed, a two-part epoxy was prepared and placed underneath the gages and the gages were taped back onto the concrete surface for clamping.

The clamping of the strain gages was difficult due to the inverted surface the gages were being installed on and the lack of another surface to use for leverage. In order to overcome this challenge a device was designed to apply the proper amount of pressure on the strain gages. The clamping devices consisted of a threaded rod approximately 4 inches in length with a spring epoxied to one end. The other end of the spring had a small metal plate epoxied to it which was slightly larger than the size of the strain gages. On

top of the plate was a piece of rubber used to distribute the pressure evenly to the strain gages. The threaded rod was then run down through plywood at the locations of the strain gages and the plywood was secured to 2 by 4's (which were epoxied to the girders) with screws. Nuts were used to force the threaded rods upwards thus applying force through the springs and onto the strain gages. The springs were necessary to make sure all six gages had pressure applied to them. Figure 18 shows one of the spring devices used in a typical clamping mechanism. The circular steel plate in Figure 18 represents the plywood and the rod can be forced upwards by turning the nut at the steel plate clockwise. The spring clamps were left in place for a minimum of 24 hours to ensure proper curing of the epoxy. Once the appropriate amount of time passed, the spring devices were removed, and the gages were checked for proper bonding to the concrete and a multi-meter was used to confirm each gage maintained a resistance of 350 ohms. Once all gages were checked, the plywood was reinstalled without the clamps for protection of the strain gages. Figure 19 shows the concrete strain gage clamping mechanism.

Figure 18. Spring clamping device.

(a) **(b)**

Figure 19. Concrete gage clamping mechanism: (a) 2 by 4 Supports, and (b) the plywood supporting the six spring loaded clamps.

Wiring and Protection

Wiring of strain gages was done in November and December to complete the instrumentation of the bridge. Figure 20 shows the wiring of the strain gages in this project. The process involved splicing the strain gage wires with longer wires, running the wires through pipes into lagers junction boxes and attaching them to a computer that was placed in a tent next to the bridge. Specific details will be provided in the following.

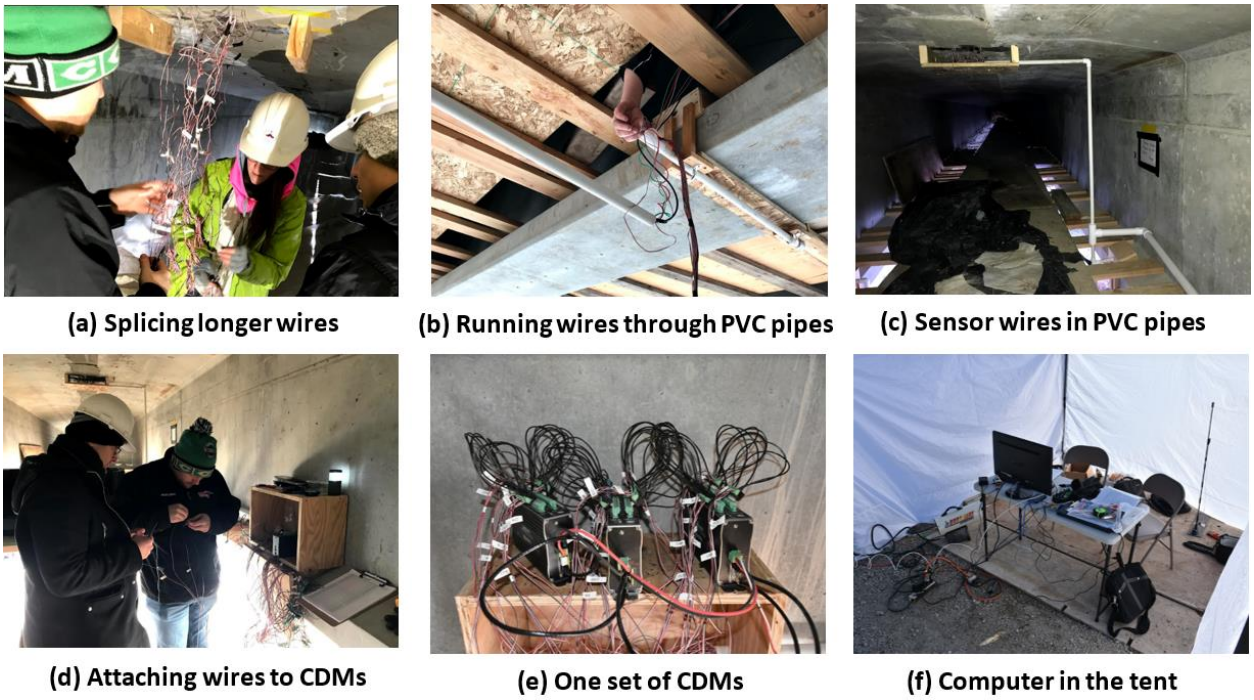

(a) Splicing longer wires (b) Running wires through PVC pipes (c) Sensor wires in PVC pipes

(d) Attaching wires to CDMs (e) One set of CDMs (f) Computer in the tent

Figure 20. Wiring of the strain gages and attaching them to the data acquisition system.

Each strain gage came with ten feet of pre-attached wire, so no soldering was needed. For ease of access in the future, two large junction boxes were placed ten feet away from the southwest abutment in the two interior girders (see Figure 20(d)). The first step was to extend all wires from the strain gages to the junction boxes. The amount of wire needed to extend all wires to the junction boxes was measured and proper lengths of wire were cut and spliced into the existing wires. Each strain gage comes with three lead wires color coded red, black, and white which are used to record strain. Each splice consisted of individual splicing of each of the three color-coded wires. The protection from the strain gage lead wire and the wire to be spliced to it was stripped down by roughly one inch. The color corresponding leads were then twisted together and taped using electrical tape. Once the three color-coded wires were spliced together, all three wires were taped back together to keep the connections from getting caught on other wires while running them through the protective PVC conduit system. Once the wires were spliced, a multi-meter was used to test all strain gages for a resistance of 350 ohms. This ensures all splices and connections of wires to the gages are still reliable. After all wires were tested, each one was relabeled at the end of the spliced wire using a label maker so they could be

identified in the junction box. The next step was to bundle the sets of wires coming from each closure pour using electrical tape to prevent wires from getting caught on others while running them through the PVC conduit. Figure 21 shows part of the PVC conduit system used in this project.

Figure 21. PVC conduit protection for strain gage wires.

The PVC conduit system used consisted of ¾ and 1 ½ inch PVC pipe. The ¾ inch PVC pipe was used for conduit where only one set of closure pour wires were run. The 1 ½ inch PVC pipe was used in locations where multiple bundles of closure pour gages were run. Figure 22 shows a diagram of the PVC conduit system used to protect strain gage wires. All strain gage wires were run through the PVC conduit to the locations marked by red circles. At these two locations the wires were run an additional 10 feet closer to the southwest abutment so the wires could be accessed in the junction boxes (see Figure 20(d)).

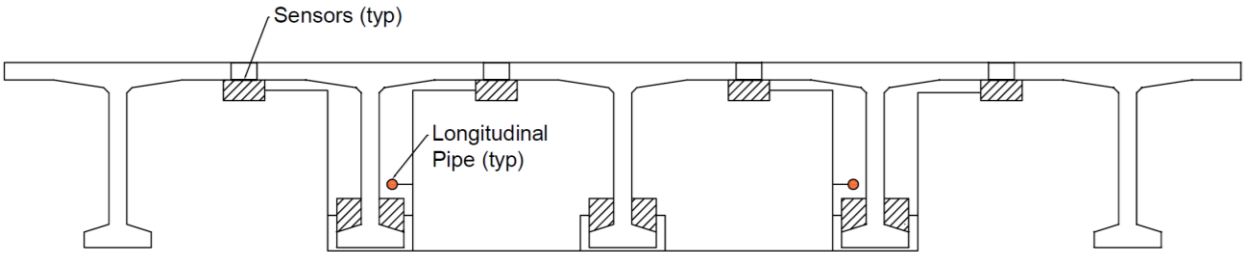

Figure 22. Instrumentation protection system.

Another important aspect of the wiring was knowing which wires was connected to which strain gage. For this reason, one set of labeling was used for all rebar strain gages and another was used for the concrete strain gages. The bridge girders which were instrumented were labeled 101 through 105 from North to South on the West span. The closure pours which were instrumented were labeled 1 through 4 starting from the downstream side. The bulb strain gages (see Figure 16) were located only on the interior girders and were labeled 1 through 6 starting on the downstream side. The labeling system which was used is shown in Tables 1 and 2.

Table 1. Rebar strain gage labeling system.

Girder Number	East or West	North or South	Interface or Head	Top or Bottom
101 to 105	E = East	N = North	I = Interface	T = Top
	W = West	S = South	H = Head	B = Bottom

Table 2. Concrete strain gage labeling system.

Label	Description
Longitudinal	Located in the middle of the closure pour material in the longitudinal direction
Transverse	Located in the middle of the closure pour in the transverse direction
CP (Closure Pour)	Located completely on the closure pour material right next to the interface in the transverse direction
Girder	Located completely on the girder right next to the interface in the transverse direction
Interface East	Located directly on the East interface in the transverse direction
Interface West	Located directly on the West interface in the transverse direction

Figures 23 and 24 show the labeling system for bar strain gages and concrete strain gages, respectively.

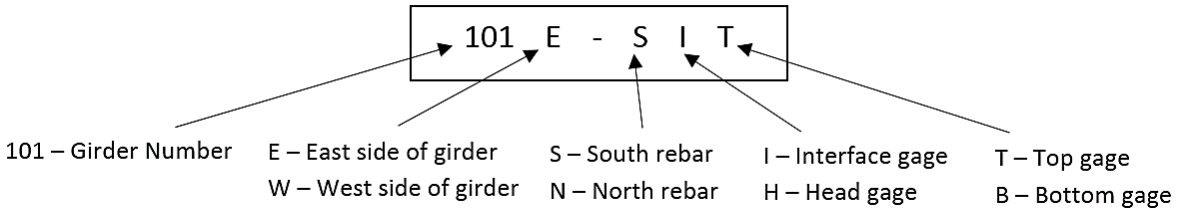

Figure 23. Key for labeling rebar gages.

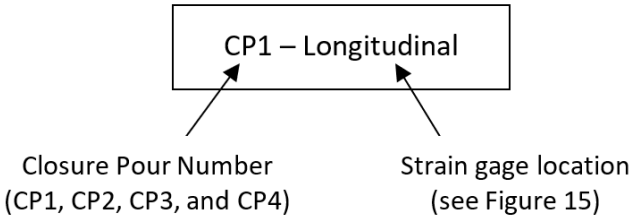

Figure 24. Key for labeling concrete gages.

Chapter 4
Bridge Loading

Introduction

Load testing of the SH-36 Bridge was conducted from December 2018 through March 2019. The loading consisted of both static and dynamic loading. The static loading was done with known truck loads provided by the Idaho Transportation Department and the dynamic loading was done by both known and unknown loads. The unknown loads consisted of commercial vehicle traffic with three or more axles.

Static Loading

Static loading of the bridge was done using trucks with known axle weights placed in various positions on the bridge. The trucks are bridge inspection trucks known as “Under Bridge Inspection Trucks” (UBIT). Two separate UBITs were provided on separate days for the purpose of testing the bridge under the known loads. The purpose of using two trucks to conduct testing was to obtain more than one set of data for determining the response of each directly loaded closure pour and for use in refining the computer model of the bridge. Having two separate loads to compare with the computer model ensures that the model is behaving similar to the actual bridge under various loads. Figure 25 shows pictures of the UBITs used in this project.

(a) Small UBIT **(b) Large UBIT**

Figure 25. Pictures of the small and large UBITs.

The first truck provided was the smaller of the two trucks and the load testing took place on January 29th, 2019. The loading consisted of 12 different truck locations for static testing. Figure 26 shows a diagram of the smaller UBIT with the approximate axle weights for the vehicle. The truck was weighed at

a nearby weigh station before testing and the axle weights were close to the values provided in the diagram.

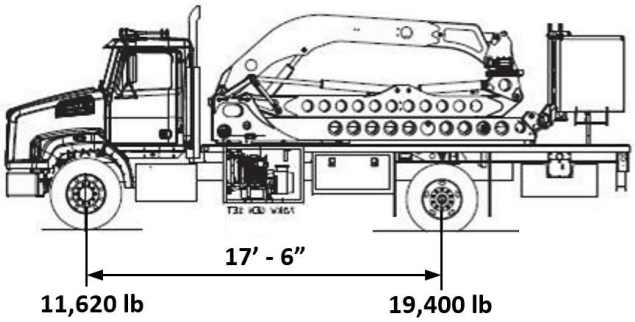

Figure 26. Small UBIT dimensions and axle weights.

The static loading arrangements can be easily described by dividing the 12 load positions into two groups of six positions. The first group of positions (Load Case 1) consisted of placing a front tire directly on top of the closure pours at the location where the closure pours were instrumented. The interior closure pours were loaded with both the driver and passenger tires. The exterior closure pours were only able to be loaded by one of the two tires due to size restrictions. Figure 27 shows the UBIT with the front driver side tire directly loaded on Closure Pour 2. Figure 28 shows the top view of the same loading position.

The loading process consisted of the truck slowly driving onto the bridge and parking directly over the instrumentation for approximately 15 seconds to allow any dynamic effects to settle out. After 15 seconds the truck backed off the bridge in order to zero the data acquisition system before the next loading position. The positioning of the static UBIT loads can be seen in Figure 29.

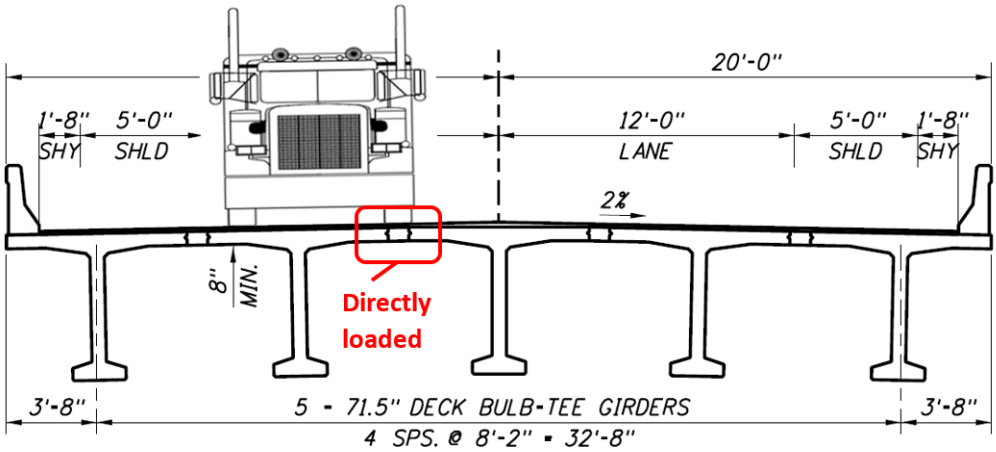

Figure 27. Loading of Closure Pour 2 with the driver side front tire.

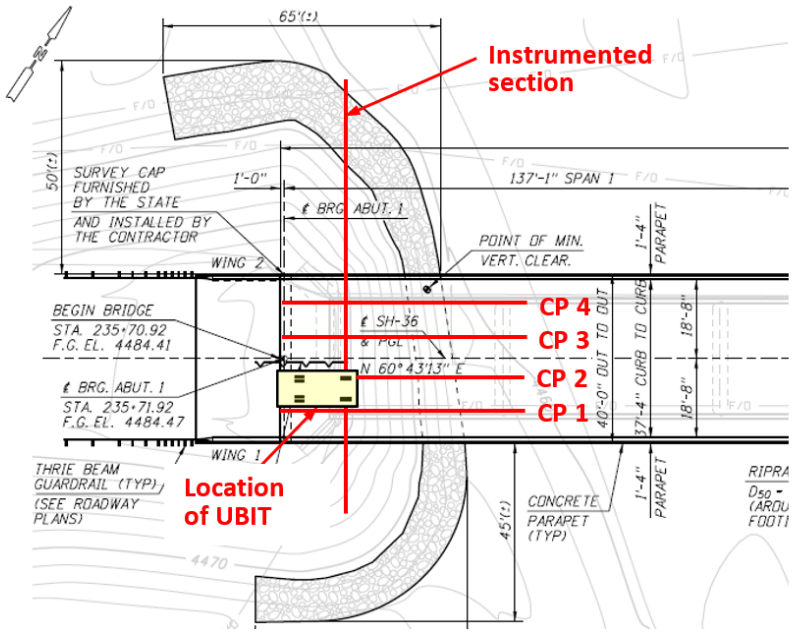

Figure 28. Top view of driver side tire of small UBIT over Closure Pour 2.

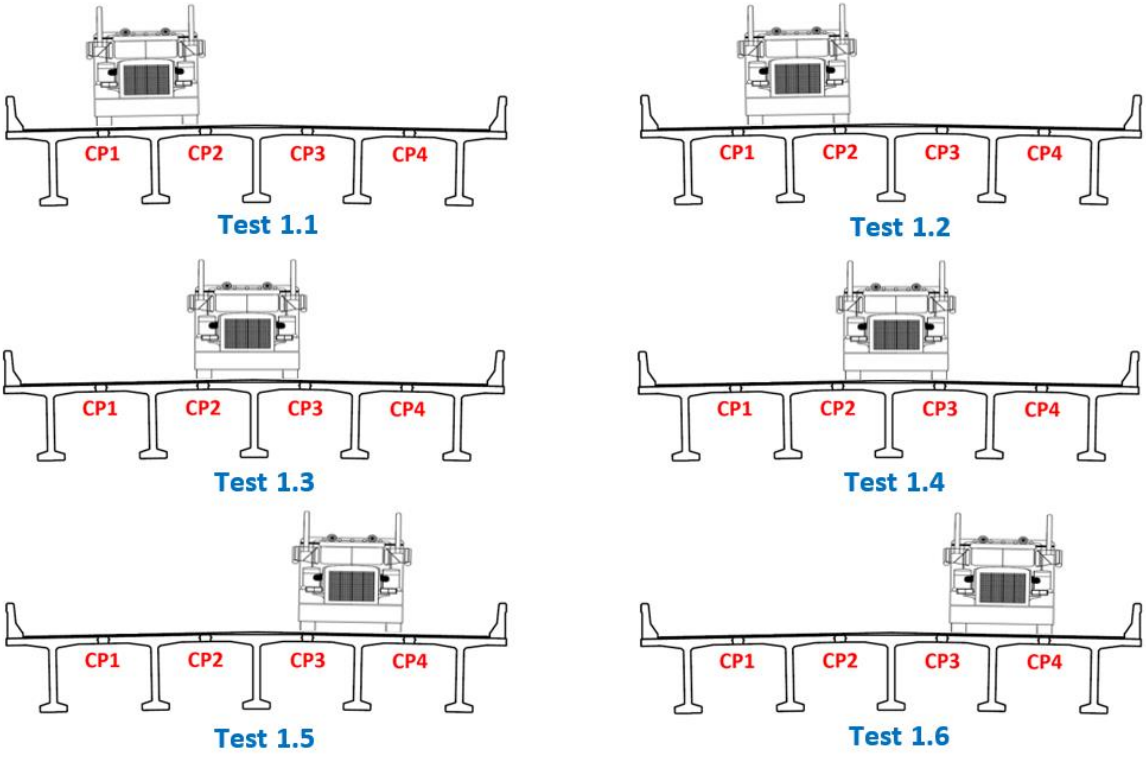

Figure 29. Static Load Case 1 loading positions.

The second set of six static loading positions (Load Case 2) consisted of parking the truck with the front wheel at the ¼, ½, and ¾ span locations on the instrumented span of the bridge. First, the truck was parked with the driver tires directly over the center line of the bridge in the transverse direction. These three tests were labeled Tests 2.1, 2.2, and 2.3, respectively. The second set of three tests were in the same longitudinal positions as the first set except the passenger side tires were placed on the centerline. These three tests were labeled Tests 2.4, 2.5, and 2.6, respectively. Figure 30 shows the loading position where the truck is at the ½ span location and the driver side wheels are located on the centerline of the bridge. All loading positions for Static Load Case 2 are shown in Figure 31.

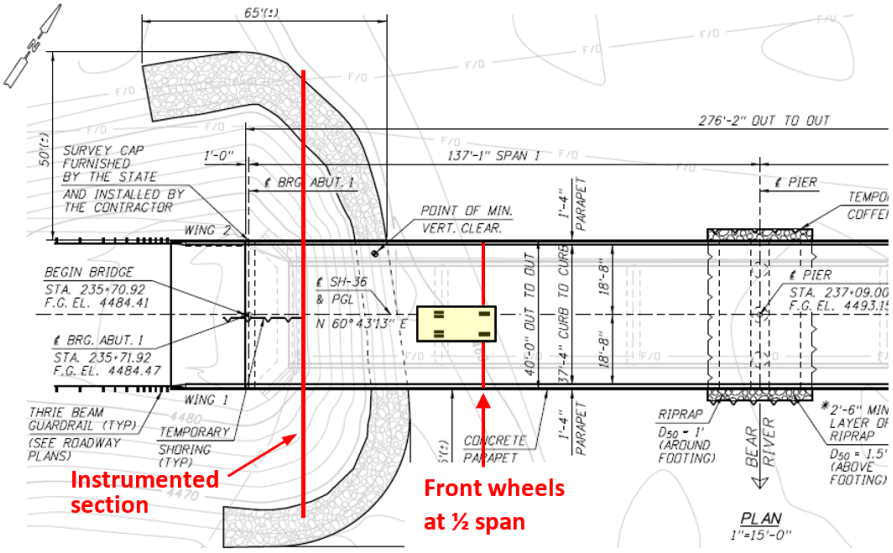

Figure 30. UBIT at center of the instrumented span with the driver side tires on the centerline.

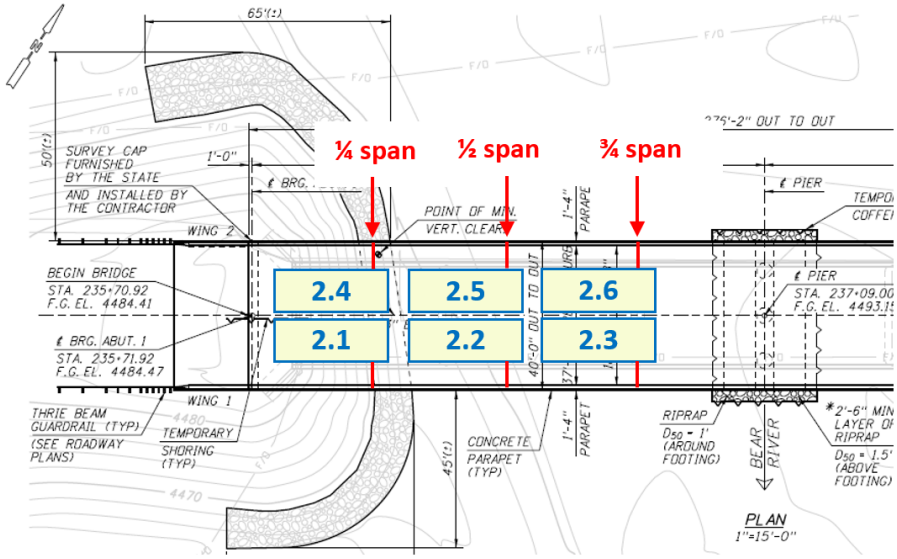

Figure 31. Static Load Case 2: UBIT loading positions for tests 2.1 to 2.6.

The Load Case 2 six positions were performed the same way as the closure pour direct loading where the truck slowly moved onto the bridge and parked in the proper position for approximately 15 seconds.

Static loading for the larger UBIT took place on March 12th, 2019 and the same static loading positions were used. The only difference between the small and large UBIT loadings was the static loadings for the large UBIT were performed twice for repeatability. Figure 32 is a diagram of the large UBIT and includes the axle weights for each axle. The drop axle was down during all tests performed with the large UBIT.

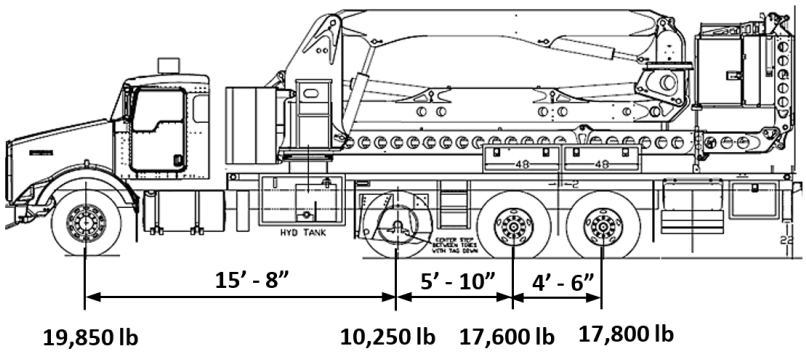

Figure 32. Large UBIT dimensions and axle weights.

Dynamic Loading

Dynamic loading of the bridge consisted of loading the bridge with both known and unknown loads. Dynamic loading was included in this research to observe the strain gage responses in the closure pour material during normal traffic conditions.

Dynamic loading with the known loads was performed with the small and large UBITs. Four dynamic tests were performed with each of the UBITs. The first test consisted of the UBIT traveling over the bridge at a crawl speed (approximately 3 mph) with the driver side tires on the centerline of the bridge. The next test involved the truck traveling the same speed and in the same direction with the passenger side tires on the centerline of the bridge. The final two tests were performed in the same manner as the previous two but at a speed of 10 mph. Figure 33 shows the large UBIT performing a dynamic test with the driver side tires on the centerline of the bridge.

Dynamic tests involving unknown loads were performed over multiple days and on various days of the week to obtain an average sample of traffic. A total of 20 hours of truck traffic data was obtained to analyze the strains seen in the bridge. Individual events where a vehicle consisting of three or more axles were recorded during this time. For each event, the time, type of vehicle, number of axles, direction of travel, and any pertinent notes were taken. Pictures for most of the events were also taken from the end of the bridge to determine where the vehicle passed over the instrumentation in the transverse direction. Figure 34 shows an example of a data sheet used to record the individual events. Figure 35 shows a three-axle truck traveling over the bridge.

Figure 33. Large UBIT dynamic test.

Time (hour, minute)	Type of Vehicle	No. of axles	Direction of travel		Picture of vehicle	Notes
			East	West		
11:04	Pickup & trailer	4	✓		✓	Horse trailer
11:09	Pickup & trailer	4		✓	✓	Empty trailer
…	…	…	…	…	…	…
12:03	Dump truck	3	✓		✓	
12:11	Pickup & trailer	4	✓		✓	Trailer carrying hay bales
…	…	…	…	…	…	…
15:15	Pickup & trailer	3		✓	✓	Trailer carrying 4-wheeler

Figure 34. Partial traffic data collected January 26, 2019.

Figure 35. A three-axle truck traveling over the bridge.

Chapter 5
Data Collection

Introduction

Data collection for this project consisted of collecting data from 94 strain gage sensors at a rate of 33 samples per second. The data collection system used is a product of Campbell Scientific, Inc. and consisted of a CR6 Datalogger, six analog input modules (CDMs; the acronym "CDMs" refers to "Campbell Distributed Modules"), and 94 Terminal Input Modules (TIMs). The system was required to operate at its upper limit due to the sampling rate and number of sensors required in this project.

Data Collection Hardware

The data collection system consisted of four main hardware components: strain gages, TIMs, CDMs, and a CR6. Each of these components will be discussed in this section. A schematic of how the hardware components were arranged in the data acquisition system can be seen in Figure 36.

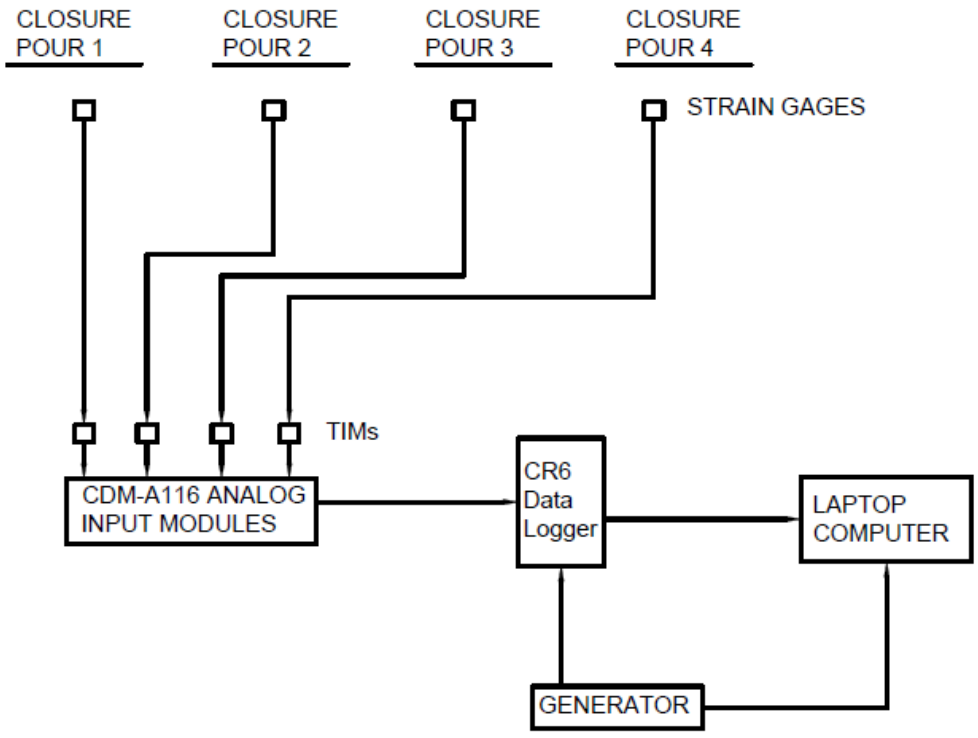

Figure 36. Data Collection Schematic.

The strain gages are the sensors which are attached to the steel and concrete surfaces on the bridge and record strain by means of a change in voltage. A specified voltage is sent through the strain gage and the

change which is observed across the strain gage is recorded and used to determine the amount of strain the gage and material it is attached to is experiencing. For more information on the specific strain gages used in this project please refer to Chapter 3 and Appendix A of the thesis by Clauson, C. (2019).[20]

The strain gages were connected to the Terminal Input Modules (TIMs) using three wires which were color coded red, white, and black. The red wire is used for excitation where the voltage enters the strain gage. The other two wires are used to measure the voltage that leaves the strain gages. Figure 37 shows the wires for four strain gages correctly connected to the TIMs. All strain gages used in this project were 350 ohm gages and the TIMs used in this project were specific to 350 ohm strain gages.

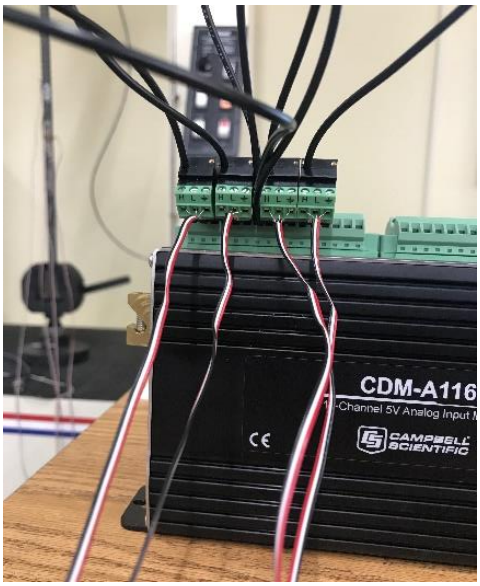

Figure 37. Strain gage wires connected to four TIMs.

The TIMs used were supplied by Campbell Scientific and were used to complete the Wheatstone bridge for accurate strain measurements. The data sheet for the TIMs (4WFBS350) can be found in Appendix A of the thesis by Clauson, C. (2019).[20] A typical TIM used in this project can be seen in Figure 38 which also shows proper installation of a TIM on a CDM terminal block. The high, low, and ground prongs on the TIMs each inserted into the port corresponding to the same symbol on the CDMs terminal block. The black wire which comes out of the TIM is connected to the port labeled X which stands for excitation. For this project, four TIMs were required to share one excitation port since each CDM only has four total excitation ports.

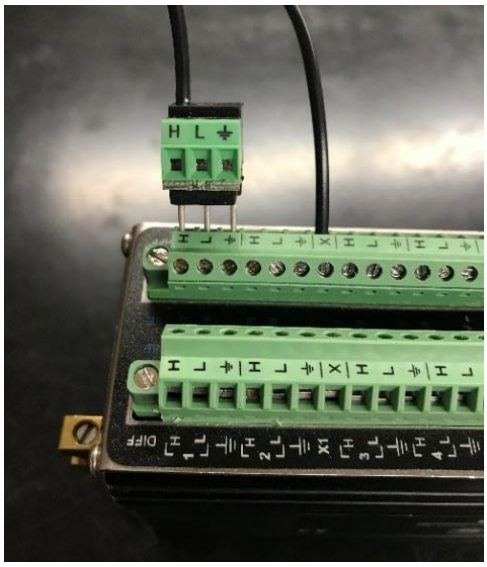

Figure 38. Terminal Input Module (TIM).

The CDMs were also provided by Campbell Scientific and are analog input modules that increase the number of channels in the data acquisition system. The CDMs used in this project were each able to add an additional 16 channels to the data collection system. A total of six CDMs were used in order to record data from all 94 strain gages at one time. The CDMs also work as an analog to digital converter. Converting the data from an analog signal to a digital signal prevents outside sources from interfering with the data. For this reason, it was decided to locate the CDMs closer to the strain gages to limit the length of wire that an analog signal would be transmitting through. A typical CDM used in this project is shown in Figure 39.

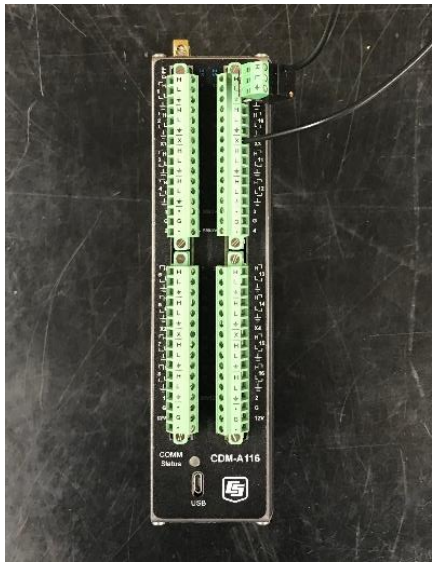

Figure 39. Analog measurement module (CDM-A116).

All six CDMs were connected to a CR6 by means of Ethernet cables. The data which was converted from analog to digital was sent to the CR6 where it was then written to a file on a connected computer. The CR6 was the central location of the data collection system where all data was sent to be recorded. The data sheets for all hardware components of the data collection system can be found in Appendix A of the thesis by Clauson, C. (2019).[20] A picture of the CR6 used in this project is shown in Figure 40.

Figure 40. CR6 datalogger.

Data Collection Software

The software used in this project is a product of Campbell Scientific called Loggernet. Loggernet uses a programming language called CRBasic to manipulate the data collection system. Campbell Scientific also provides a user-friendly way to create a CRBasic program through their shortcut application. Shortcut allows for a new user to easily step through the process of creating a program without having to know the commands associated within it. For this project, the shortcut application was used to build an initial program which provided the large majority of the program that was needed. Once the initial program was built using shortcut, it was opened in Campbell Scientifics CRBasic program editor for further refining. Due to the large number of strain gages (94) and the sampling rate (33 Hz), the data collection system was operating at its upper limit. Therefore, many of the generic battery voltage and temperature measurements that are typically used to monitor the CDMs and CR6 were removed from the program to allow for a sampling rate of 33 Hertz. A step by step tutorial of how to build the program and the final code used for this project can be found in Appendix C of the thesis by Clauson, C. (2019).[20]

The data collection system needed to continuously write data to a file on a laptop. The file was written in a binary data format during the testing to allow the system to keep pace with the speed of the strain gage sampling rate. Once testing was completed, an application in the Campbell Scientific software called Card Convert was used to convert the binary file into an ASCII file which could then be imported into Microsoft Excel for post processing.

Chapter 6
Experimental Results

Introduction

This chapter presents the results from load testing of the SH-36 Bridge over Bear River. There are two main sections: static loading results and dynamic loading results. Graphs and tables are produced to summarize and simplify the results.

Static Loading Results

Static loading consisted of using ITD Under Bridge Inspection Trucks (UBIT) of known weight in various positions on the bridge. Further information on the load positions used in this project can be found in Chapter 4. For each load position the data collection system was zeroed, the vehicle would then drive onto the bridge and park in one or more locations. The truck would remain parked for about 15 seconds in each location to allow any dynamic effects to subside. Then, the truck would leave the bridge to complete the test. For the duration of each loading, traffic would be stopped so that only strain caused by the UBIT vehicles would be observed. Figure 41 shows a typical UBIT static loading.

Figure 41. UBIT static loading.

Results of Load Case 1 (Directly Loaded Closure Pours)

A total of 12 different static load tests were conducted to directly load each closure pour with a front tire. Six tests were for the small UBIT and six tests for the large UBIT. For each test, all 94 strain gages recorded at a rate of 33 samples per second. Once the data was imported into Excel, the strains from the rebar gages which are located on top and bottom of the rebar at the same location along the length of the rebar were averaged to obtain an average strain at that location (see Figures 7 and 8 in Chapter 3). This reduced the number of rebar strain data from 16 to eight for each closure pour. For each test,

eight graphs were made to show the rebar and concrete strain results in all the closure pours. For each closure pour, two graphs were made; one was made for the eight rebar average strain data and one for the six concrete strain data. The following section shows some of the typical closure pour strain graphs. More graphs of the closure pour rebar and concrete strain for Load Case 1 are presented in the thesis by Caluson, C. (2019).[20]

Figures 42 and 43 show the graphs for Closure Pour 1 for the small UBIT Load Test 1.1. Note that, as shown in Figure 29, this test corresponds to Closure Pour 1 being directly loaded with the passenger side front wheel. As seen in Figures 42 and 43, for this particular test the strain gages were zeroed at record number 500, then the small UBIT traveled onto the bridge and parked on the designated location from approximately record number 2000 to 2500, and then the truck backed off the bridge to complete the Load Test 1.1.

Figures 44 and 45 show the steel and concrete strains in Closure Pour 2 due to Load Test 1.1 Note that in Test 1.1, the driver side front wheel is very close to Closure Pour 2. Figures 46 and 47 show the Closure Pour 2 strains under Load Test 1.2 (i.e., Closure Pour 2 being directly loaded by the driver side front wheel). As it can be seen from Figures 44 to 47, Closure Pour 2 concrete has the largest strain at the east interface and the two rebars above the same interface take on more strains.

Figures 48 and 49 show the strain reversal (negative strains) in Closure Pour 3 due to Test 1.2. These two graphs clearly show that the strain reversal is negligible.

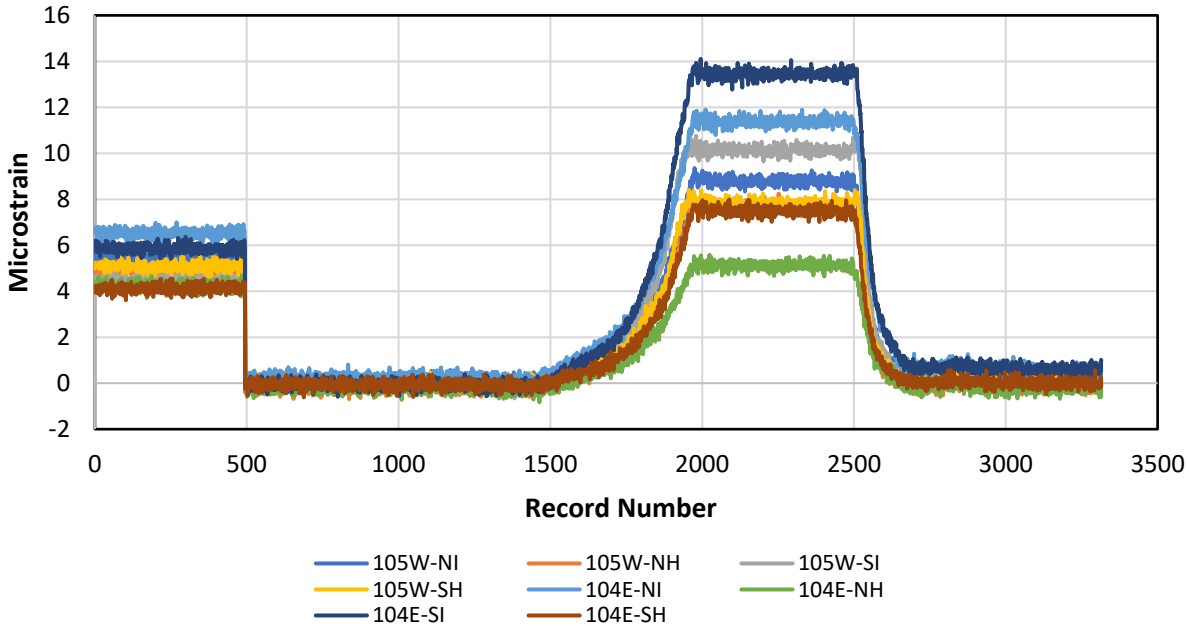

Figure 42. Small UBIT Test 1.1 CP 1 (rebar gages).

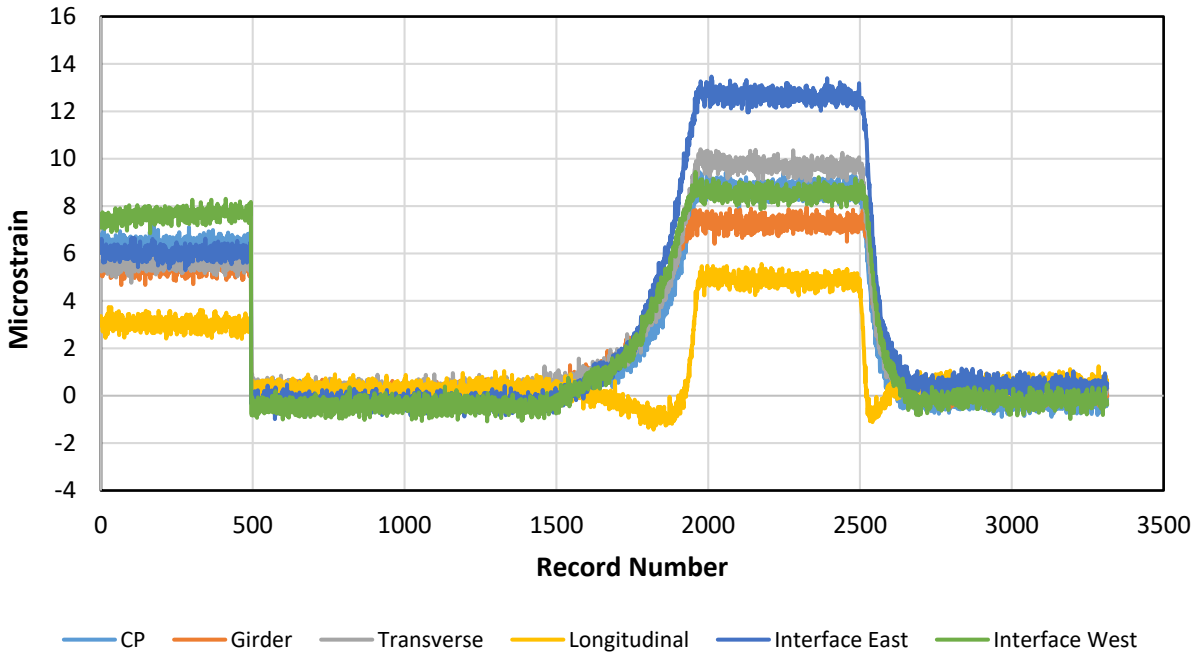

Figure 43. Small UBIT Test 1.1 CP 1 (concrete gages).

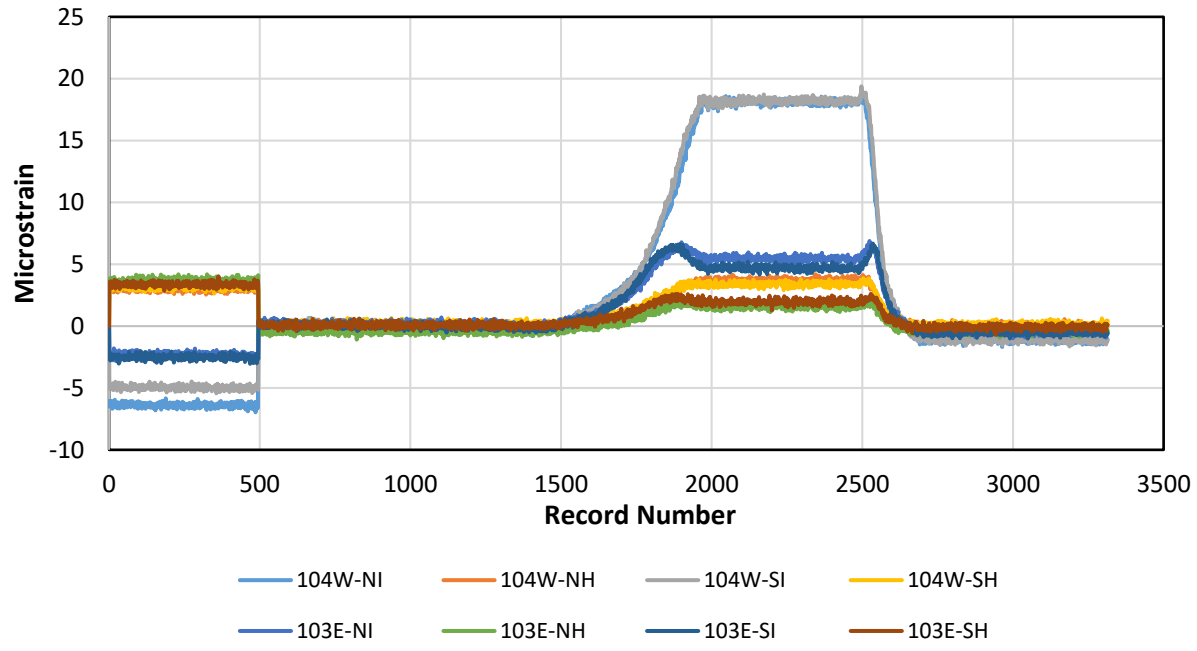

Figure 44. Small UBIT Test 1.1 CP 2 (rebar gages).

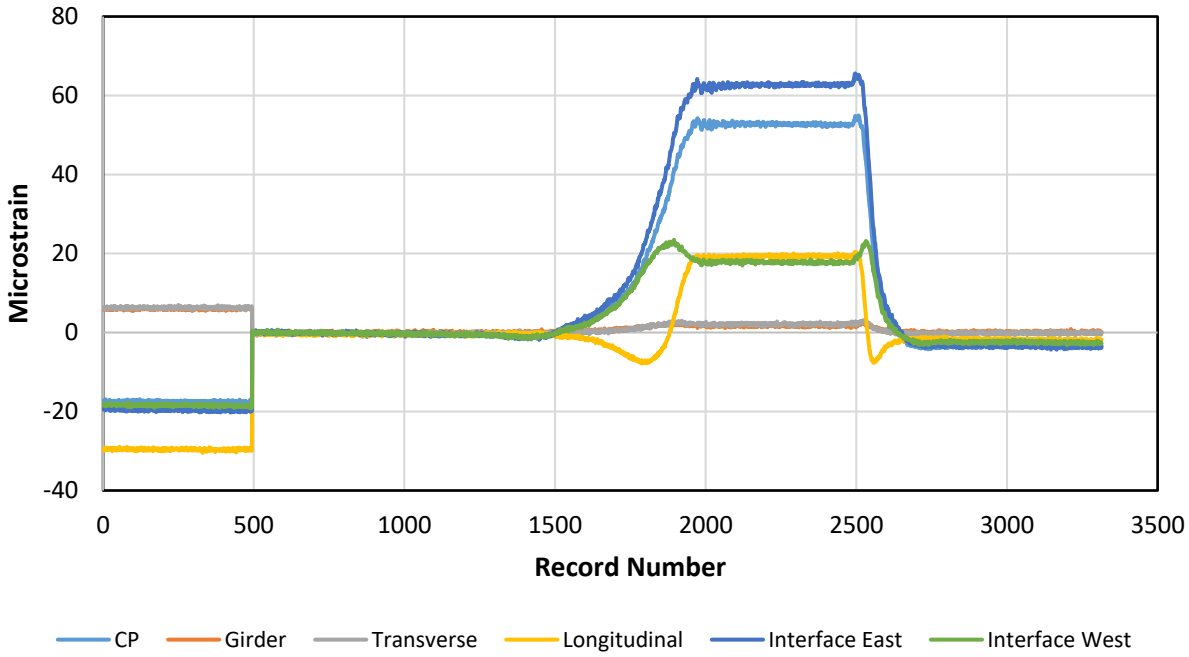

Figure 45. Small UBIT Test 1.1 CP 2 (concrete gages).

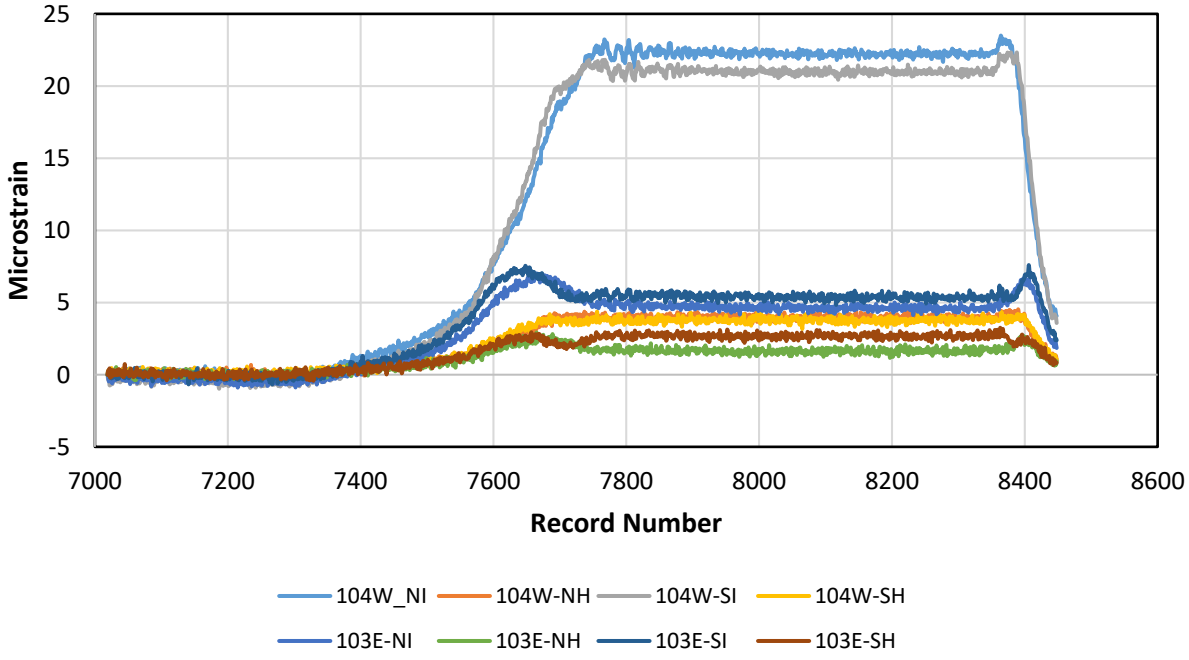

Figure 46. Small UBIT Test 1.2 CP 2 (rebar gages).

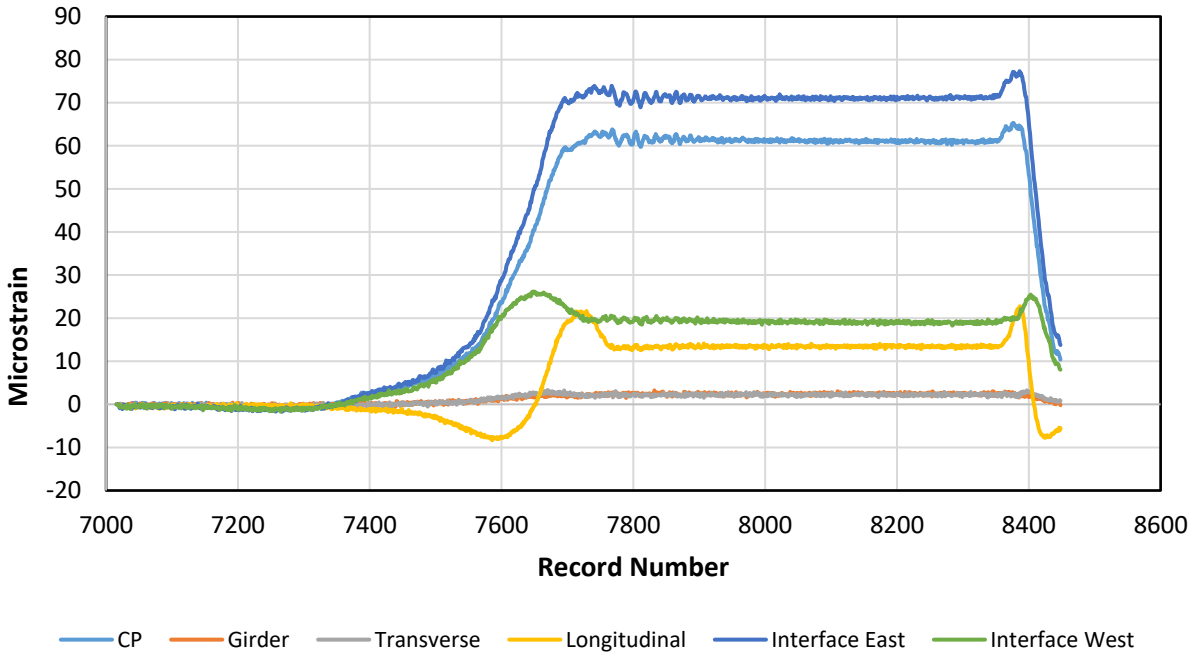

Figure 47. Small UBIT Test 1.2 CP 2 (concrete gages).

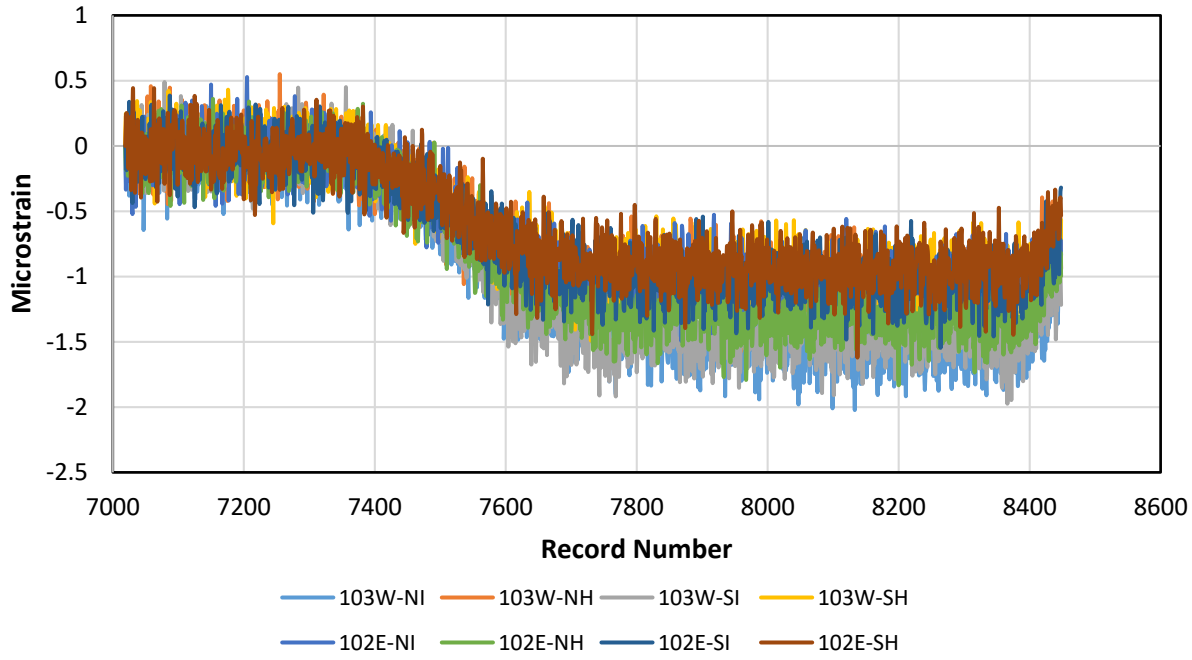

Figure 48. Small UBIT Test 1.2 CP 3 (rebar gages).

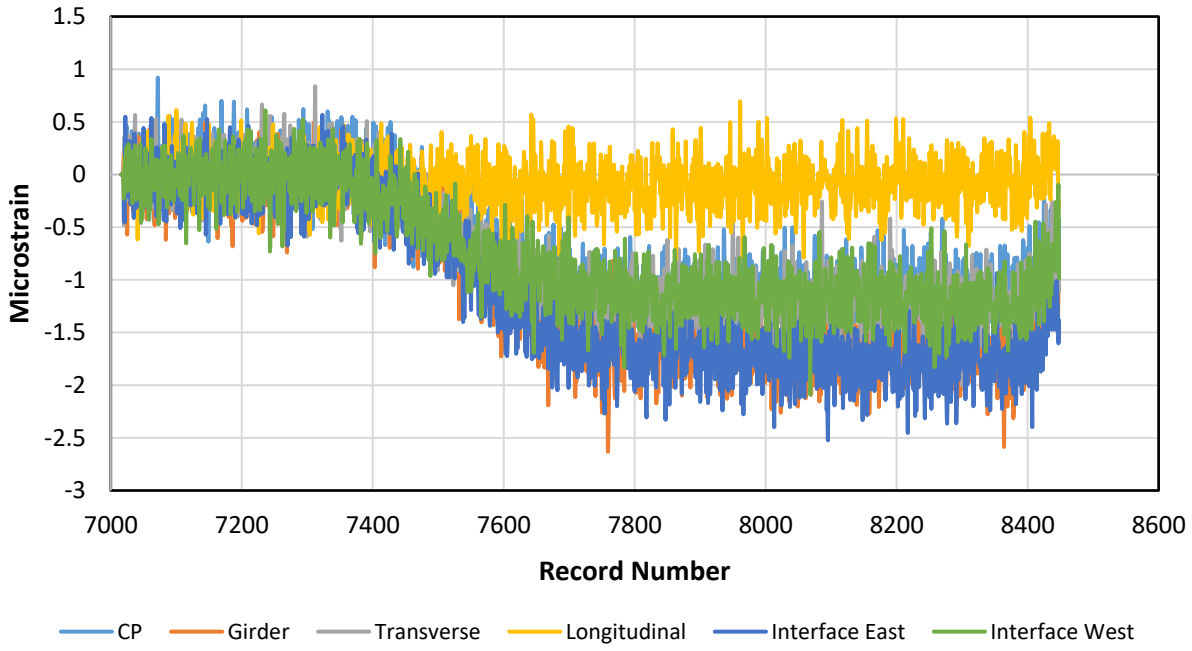

Figure 49. Small UBIT Test 1.2 CP 3 (concrete gages).

Tables 3 and 4 summarize the Load Case 1 strain data for small and large UBITs, respectively. The tables also show the locations where these maximum strains occur. From Tables 3 and 4 it can be observed that strain in Closure Pour 2 is much larger than the other closure pour connections. This trend was observed throughout the project for both static and dynamic loads.

Table 3. Small UBIT maximum values under Load Case 1 tests.

Load Test	Max. concrete strain, $\mu\varepsilon$				Location of the largest maximum concrete strain	Max. rebar strain, $\mu\varepsilon$	Max. rebar stress, psi	Location of bar with largest stress
	CP1	CP2	CP3	CP4				
1.1	13	**62**	-	-	Interface, CP2	19	570	Interface, CP2
1.2	11	**71**	-	-	Interface, CP2	22	638	Interface, CP2
1.3	-	**104**	7	-	Interface, CP2	36	1,044	Interface, CP2
1.4	-	**60**	14	-	Interface, CP2	17	493	Interface, CP2
1.5	-	-	7	19	Closure pour conc. next to interface, CP4	14	406	Interface, CP4
1.6	-	-	7	18	Closure pour conc. next to interface, CP4	16	464	Interface, CP4

Table 4. Large UBIT maximum values under Load Case 1 tests.

Load Test	Max. concrete strain, $\mu\varepsilon$				Location of the largest maximum concrete strain	Max. rebar strain, $\mu\varepsilon$	Max. rebar stress, psi	Location of bar with largest stress
	CP1	CP2	CP3	CP4				
1.1	27	**138**	-	-	Interface, CP2	38	1,102	Interface, CP2
1.2	10	**200**	-	-	Interface, CP2	60	1,740	Interface, CP2
1.3	-	**180**	24	-	Interface, CP2	50	1,450	Interface, CP2
1.4	-	**225**	60	-	Interface, CP2	68	1,972	Interface, CP2
1.5	-	-	35	9	Closure pour conc. next to interface, CP3	20	580	Interface, CP3
1.6	-	-	9	26	Interface, CP4	22	638	Interface, CP4

It can be observed that Closure Pours 1, 3, and 4 have similar behavior and have smaller strain values, while the strains in Closure Pour 2 are much larger, both in the concrete and in the steel.

For every UBIT static loading, high resolution pictures were taken from under the bridge from the directly loaded closure pours. For example, for large UBIT Test 1.2 where Closure Pour 2 is being directly loaded by the driver side front wheel, pictures were taken before and during the loading. These pictures are shown in Figures 50 and 51. In none of the cases, any visible cracks were observed.

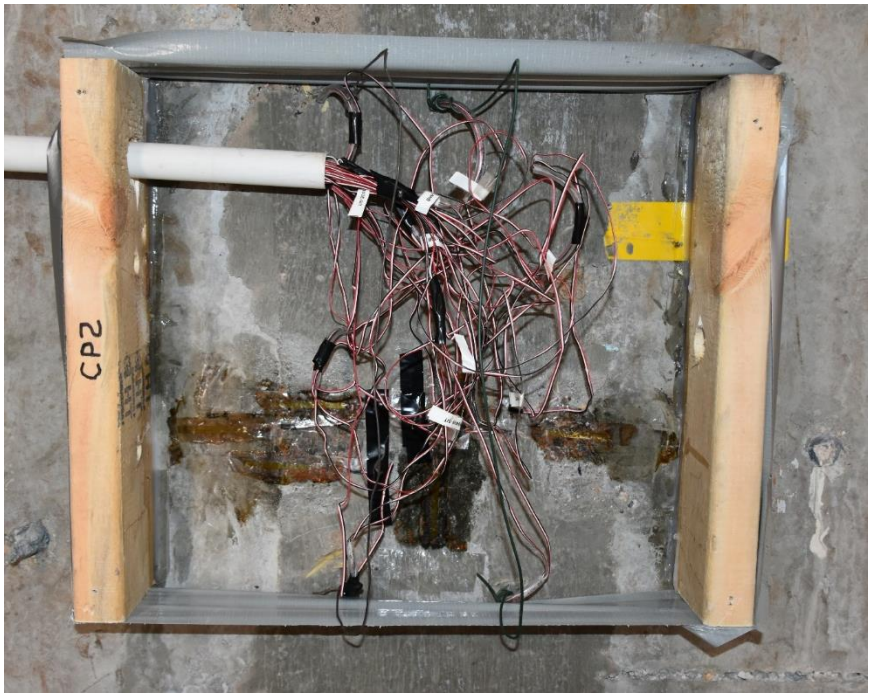

Figure 50. Closure Pour 2 high resolution picture before static loading of Load Test 1.2.

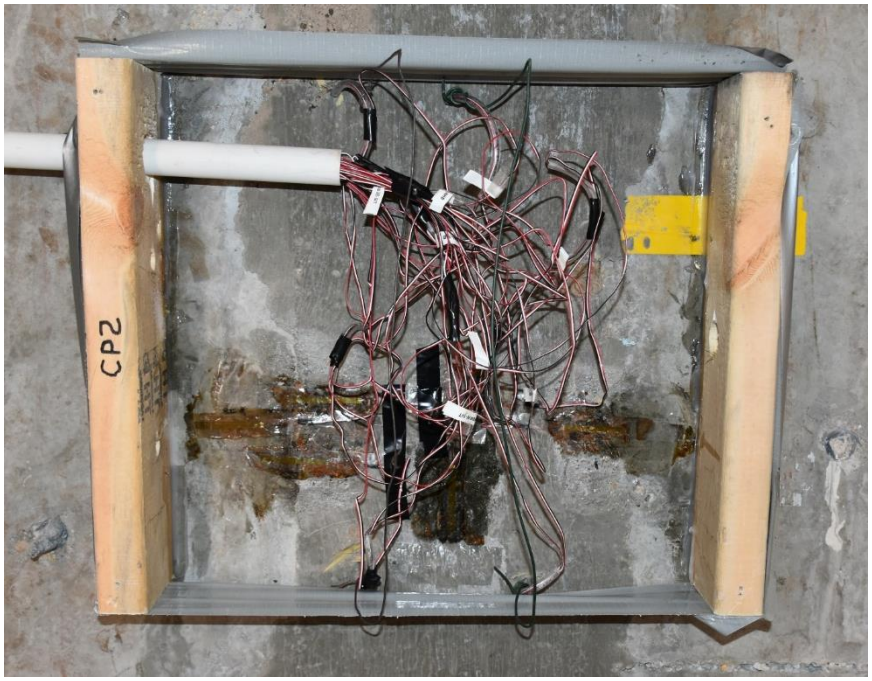

Figure 51. Closure Pour 2 high resolution picture during static loading of Load Test 1.2.

In order to examine the relation between the force (weight of one front wheel) and strain in a directly loaded closure pour at the interface, Figures 52 and 53 were produced. These figures show the UBIT front wheel force as a function of the average of the largest interface strains in concrete and steel in the directly-loaded closure pours. The small UBIT front wheel is approximately 5,810 lb and the large UBIT front wheel is approximately 9,925 lb. In both Figures 52 and 53, the data for Closure Pours 1, 3, and 4 are averaged, while the average of data for Closure Pour 2 is shown separately. As noted earlier, the tests under large UBIT were repeated. Therefore, we had twice the number of data for large UBIT tests. Error bars represent one population standard deviation on each side of a data point. Note that for proper comparison, Figures 52 and 53 have the same horizontal axis range of 0 to 250 microstrain.

After reviewing the figures and tables in this section, the following observations can be made regarding the Load Case 1 data:

1. The strain in Closure Pour 2 concrete exceeds the strain corresponding to the interface bond strength (modulus of rupture) under the large UBIT. In the Phase 1 laboratory experiments, the average bond strength was 612 psi. Assuming a concrete strength of 8,000 psi, the modulus of concrete is approximately 5,300 ksi which results in a limiting strain of approximately 120 microstrain (i.e., $\varepsilon_c = f_r/E_{conc.}$ = (0.612 ksi)/(5,300 ksi) = 0.00012 or 120 microstrain). This threshold strain value is shown by a vertical red line in Figure 52. However, no visible cracks appeared in Closure Pour 2 or any other closure pours during the controlled load testing.
2. The maximum strain in the steel was much lower than the strain corresponding to the specified yield strength (i.e., $\varepsilon_y = F_y/E_{steel}$ = (60 ksi)/(29,000 ksi) = 0.002069 or 2,069 microstrain).

3. Concrete's behavior is not linear. In Figure 52 two bilinear relations are used. Whereas, in all closure pours the steel strain at the interface is linear as a function of the applied wheel force.

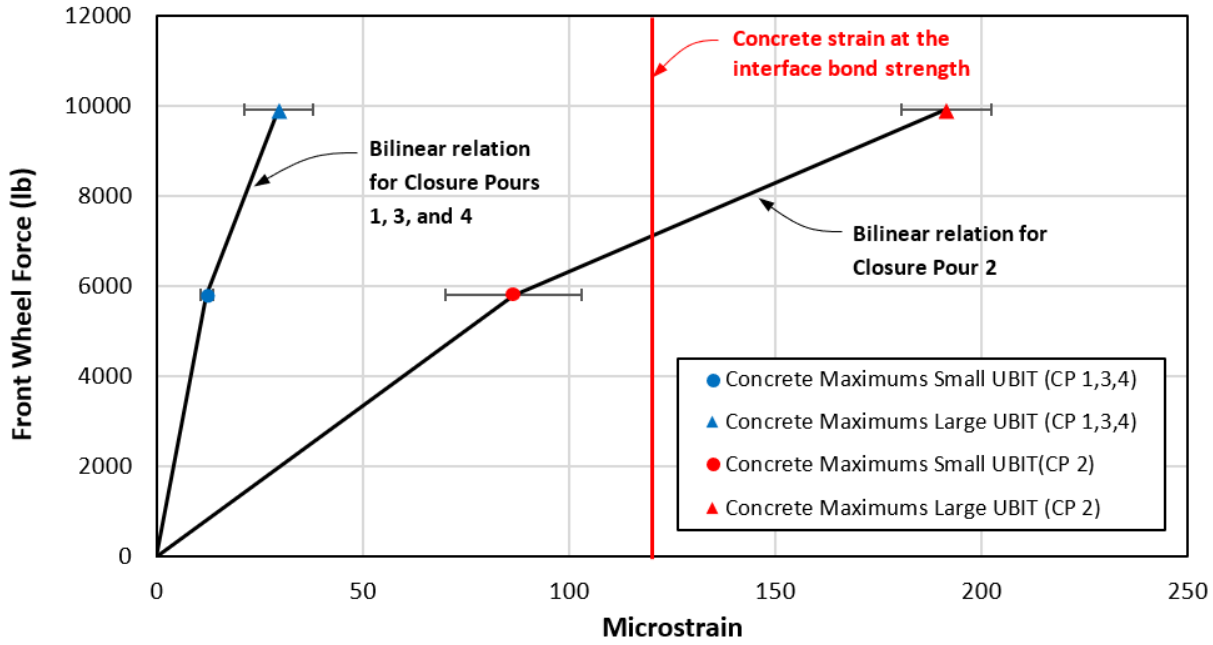

Figure 52. Front wheel force vs. concrete strain for UBIT loading (strain gages at the interface).

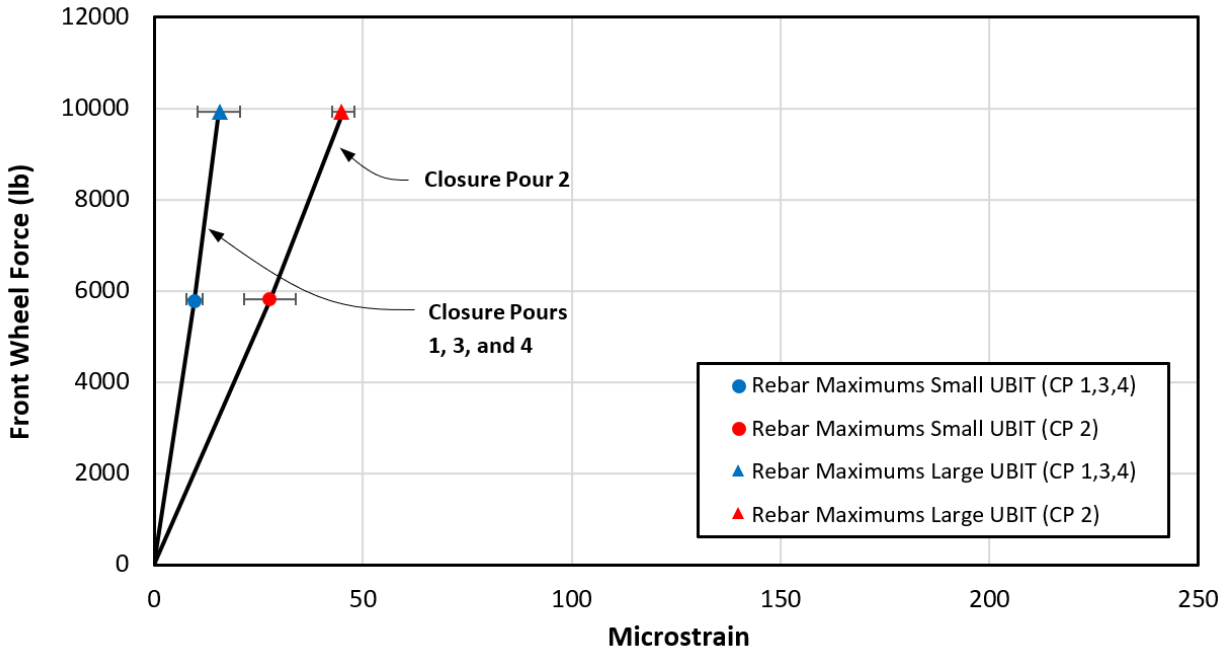

Figure 53. Front wheel force vs. steel strain for UBIT loading (rebar strain gages at the interface).

Results of Load Case 2

As noted in Chapter 4, Load Case 2 consisted of placing UBITs at ¼, ½, and ¾ span on the instrumented span of the bridge. See Figures 30 and 31 in Chapter 4. The data from these tests will be used in next chapter in order to refine the FE model of the bridge. Figures 54 and 55 show the girder bulb strains in Girders 102, 102, and 104 under small UBIT for Tests 2.1 to 2.6. The strain on the horizontal axis represents average of the two strain gages attached on each side of the girder bulb (see Figure 16 in Chapter 4). The data within each box in the figures represent the bulb strain when the truck is at a specified location. For example, in Figure 54, where the truck is on the right (downstream) side of the center line, the driver was instructed to stop with front wheels at ¼ span, then stop at ½ span, and finally stop at ¾ span. The flat regions within each of the three boxes, represent the average bulb strains at each location. The remaining graphs for the large UBIT tests are given in Appendix D of the thesis by Clauson, C. (2019). The tabulated strain results for Load Case 2 will be presented in Chapter 7 and will be compared to the corresponding FE model strains.

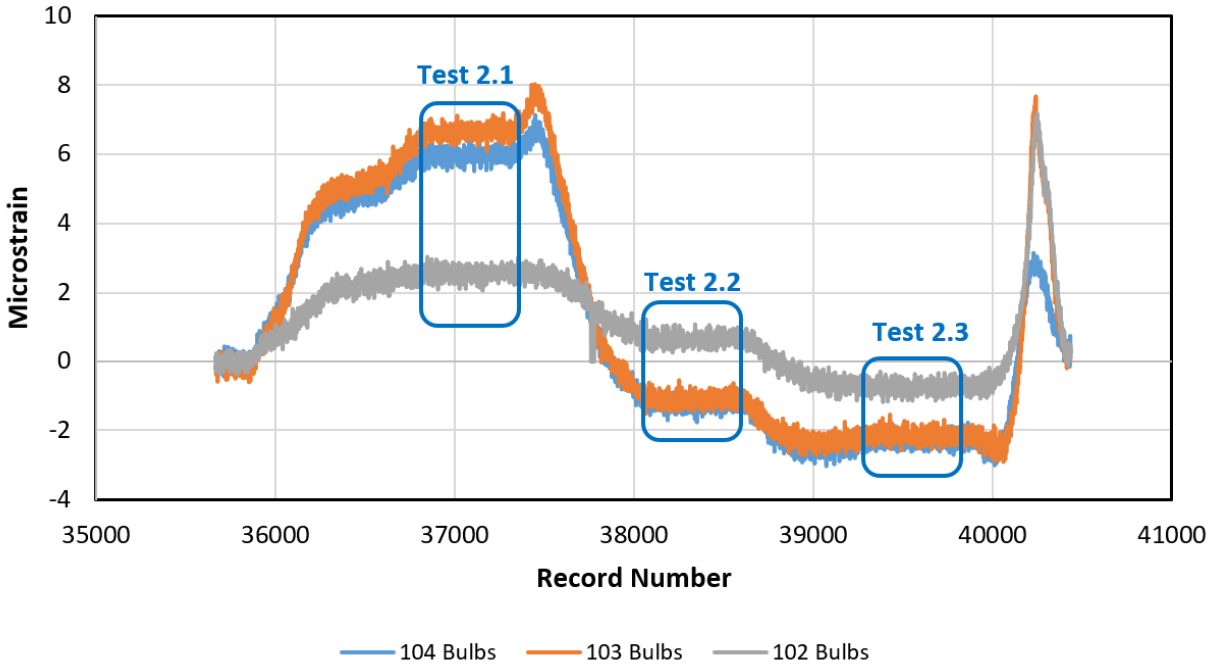

Figure 54. Girder bulb gage strains under small UBIT Tests 2.1, 2.2, and 2.3.

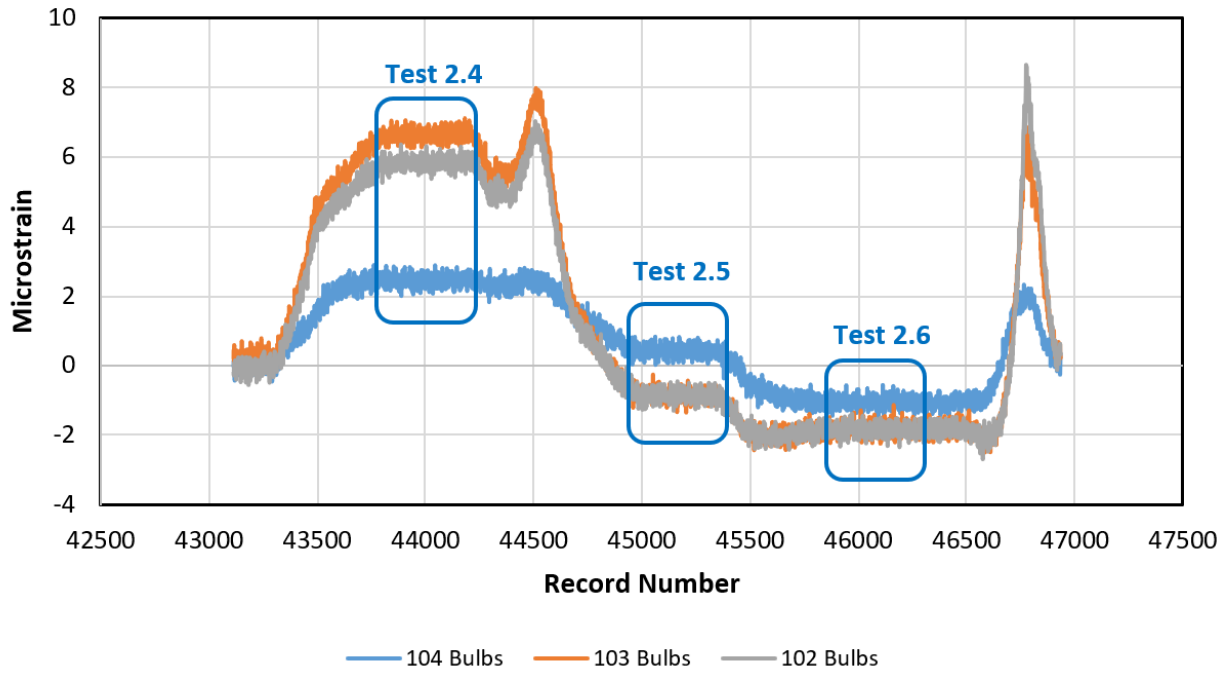

Figure 55. Girder bulb gage strains under small UBIT Tests 2.4, 2.5, and 2.6.

Dynamic Loading Results

Dynamic loading of the bridge consisted of both UBIT vehicles and commercial truck traffic. For the UBIT vehicles, the dynamic load tests consisted of a 10 mph and a crawl speed (approximately 3 mph) test. Commercial traffic loading consisted of 20 hours of data collection where vehicles with three or more axles were recorded. The purpose of the commercial loading is to observe strain in the bridge during normal vehicle traffic.

Dynamic Loads under UBITs

Figures 56 to 59 show dynamic loading strain data for the small and large UBITs with the driver side tires on the bridge centerline. Figures 56 and 57 show data for Closure Pour 2, whereas Figures 58 and 59 show strain data for Closure Pour 3. The concrete strain data is the strain from the larger of the two concrete interface strain gages. The rebar strain data is the data from the rebar that corresponds to the larger concrete interface. It can be seen in these figures that there is not much of a difference in strain between the different travel speeds in this project. The results show that the concrete strain values were all within the concrete strain at the interface bond strength of 120 microstrain except for Closure Pour 2. Also, the rebar strain data was all within the yield strain of 2,069 microstrain for the steel reinforcement. More graphs of the closure pour strains under UBIT moving loads are presented in Appendix D of the thesis by Clauson, C. (2019).[20]

Although the results of the UBIT dynamic load tests at low speeds are interesting, these data were not used. It may have been more useful if the UBITs could travel at normal traffic speeds of about 60 mph, but this was not possible because the traffic on both sides of the bridge was stopped.

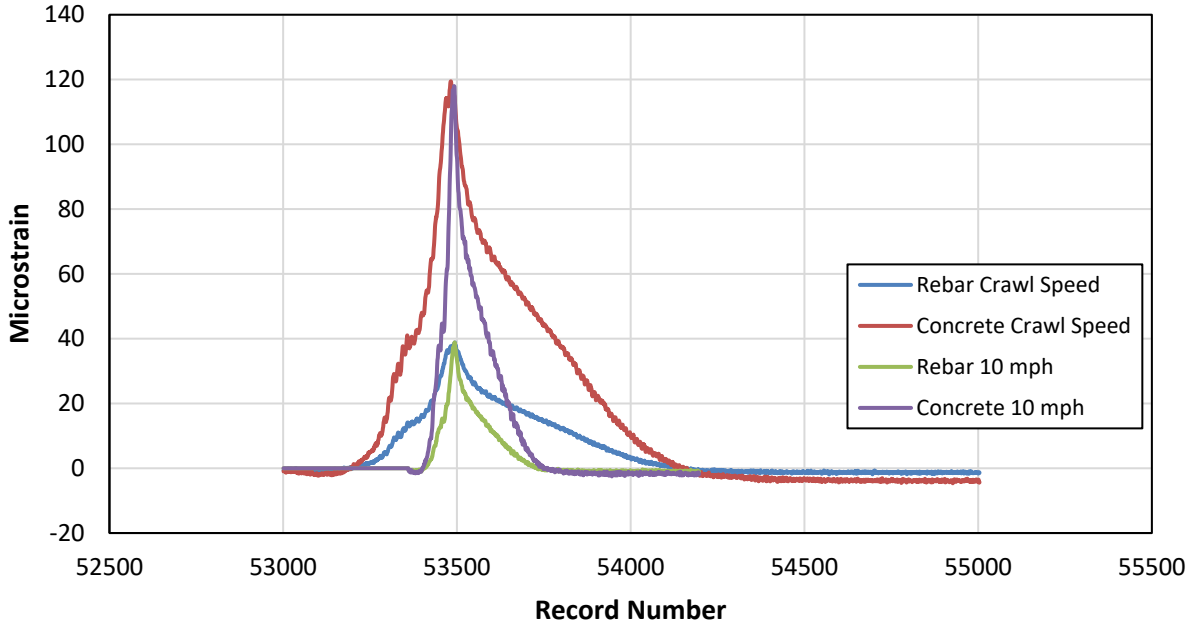

Figure 56. Dynamic interface maximum strain data in Closure Pour 2 for the small UBIT.

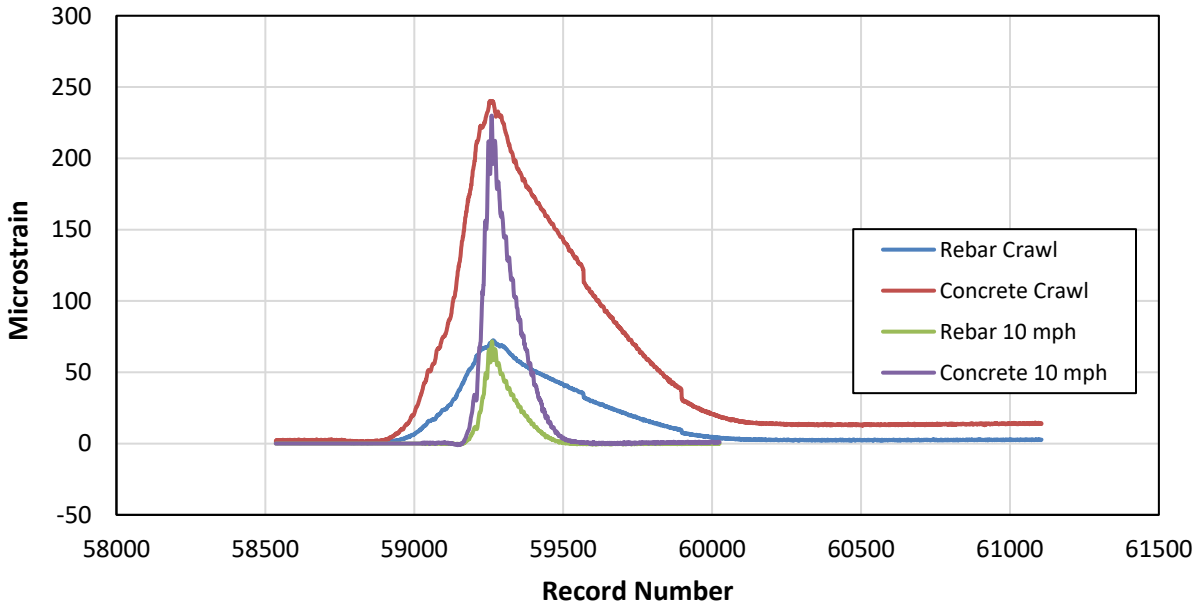

Figure 57. Dynamic interface maximum strain data in Closure Pour 2 for the Large UBIT.

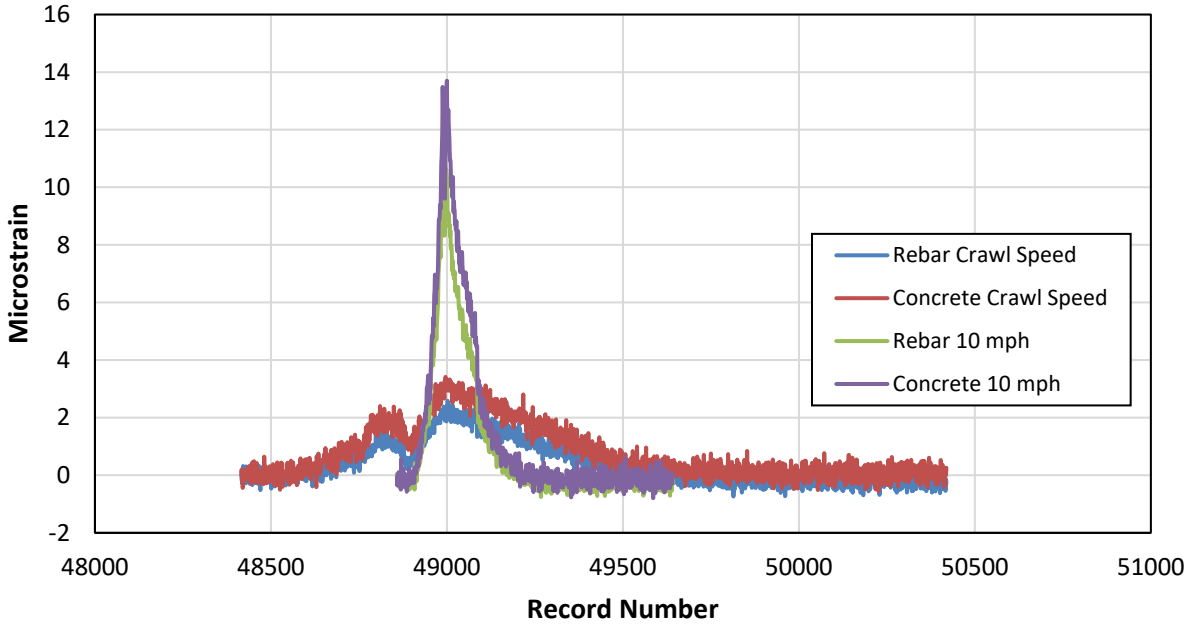

Figure 58. Dynamic interface maximum strain data in Closure Pour 3 for the small UBIT.

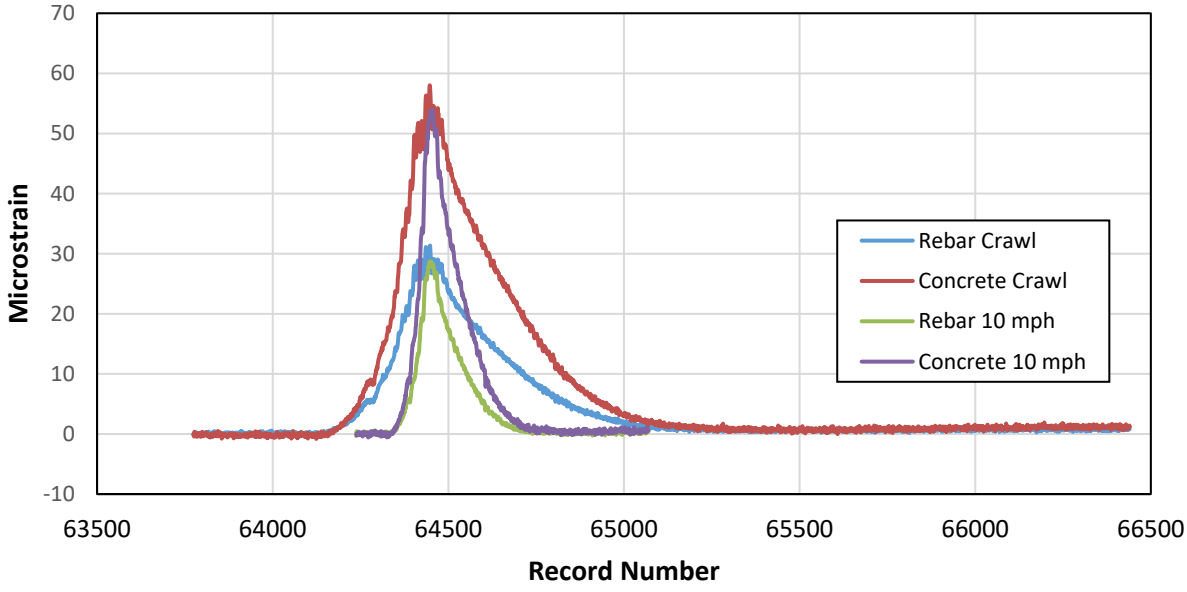

Figure 59. Dynamic interface maximum strain data in Closure Pour 3 for the large UBIT.

Dynamic Loads under Truck Traffic

Commercial traffic loading consisted of 20 hours of data collection where vehicles with three or more axles were recorded. The purpose of the commercial loading was to observe strain in the bridge during normal vehicle traffic. Once data was collected for each day, it was imported into Excel where the rebar strain data could be averaged in the same way as was done for the static loading data. After the averaging, the data could then be separated so the data for each event was analyzed separately. Once the data was separated into individual events, two graphs were made for each closure pour; one for rebar gages and one for concrete strain gages. This gave a total of eight graphs for each individual event. After all graphs were made, the maximum value of strain for the concrete strain gages for each closure pour was recorded into a table along with the location of the largest concrete strain observed throughout all the concrete strain gages. The maximum rebar strain which was observed and the location where it was recorded at was also noted in the table along with the corresponding stress in the rebar. This information can be found in Appendix D of thesis by Clauson, C. (2019).[20]

For this report, the maximum strain data is presented in a graphical form as shown in Figures 60 to 67. These graphs show the maximum concrete and steel strain data under the traveling vehicles for each closure pour. Each dot on Figures 60-67 represents the maximum strain due to one or more vehicles. On the vertical axis the vehicles are identified by the number of axles. Two different symbols are used to represent the vehicle traveling Eastbound (toward Preston) or Westbound. For example, in Figure 60 the furthest blue dot to the right corresponding to a 4-axle vehicle shows the vehicle was traveling Eastbound and it produced a maximum concrete strain of 50 microstrain in Closure Pour 1. The majority of the maximum strains occurred at the interface between closure pour concrete and precast concrete.

Observations on the maximum strain data due to larger vehicles are as follows:

1. As shown in Figure 62, the concrete strain in Closure Pour 2 exceeds the strain corresponding to the interface bond strength (modulus of rupture) for some of the vehicles. This strain threshold is again shown by a vertical red line in Figure 62.
2. The maximum strain values in the rebars were much lower than the strain corresponding to the steel specified yield strength (i.e., 2,069 microstrain).
3. From Observations 1 and 2, it can be concluded that out of eight sets of strain data (four sets for concrete and four sets for steel), only one set of strain data (i.e., concrete strain data in Closure Pour 2) have large values. All other strain values are low.
4. Compared to the rest of the closure pours, Closure Pour 4 showed much lower strains, both in concrete and steel. This may be due to the fact that there were traffic barrels near the upstream parapet (see Figure 35). This parapet was constructed last. Perhaps because of the traffic barrels, which were present during the 20 hours of the traffic strain measurements, the vehicles avoided getting close to Closure Pour 4.

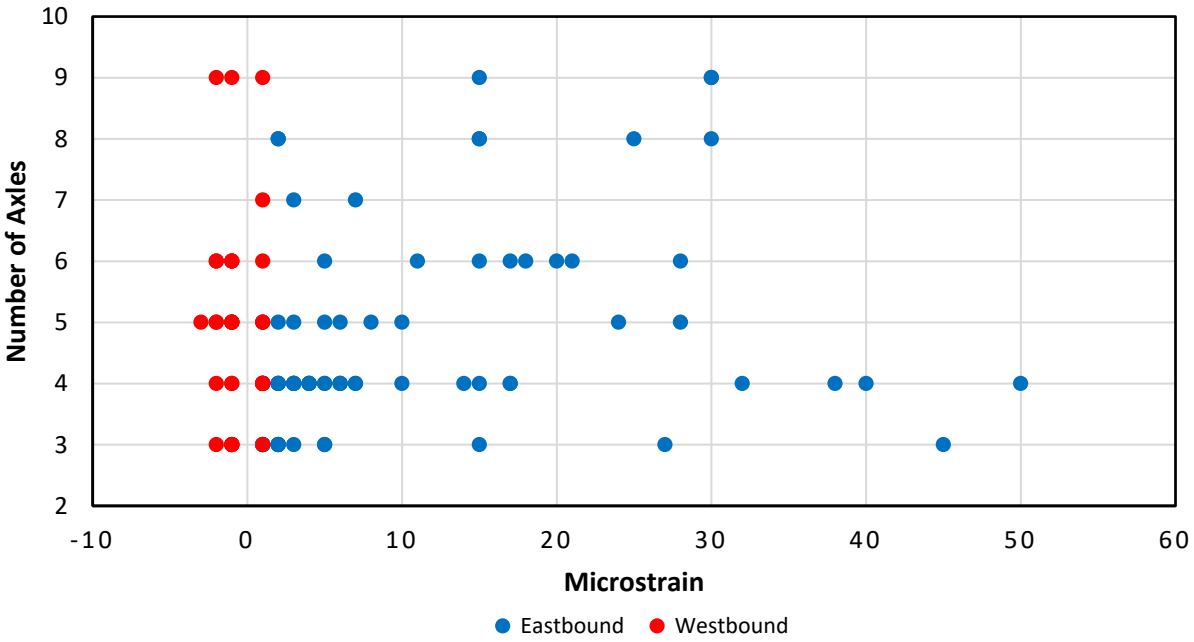

Figure 60. Maximum concrete strain in Closure Pour 1 versus number of axles for larger vehicles.

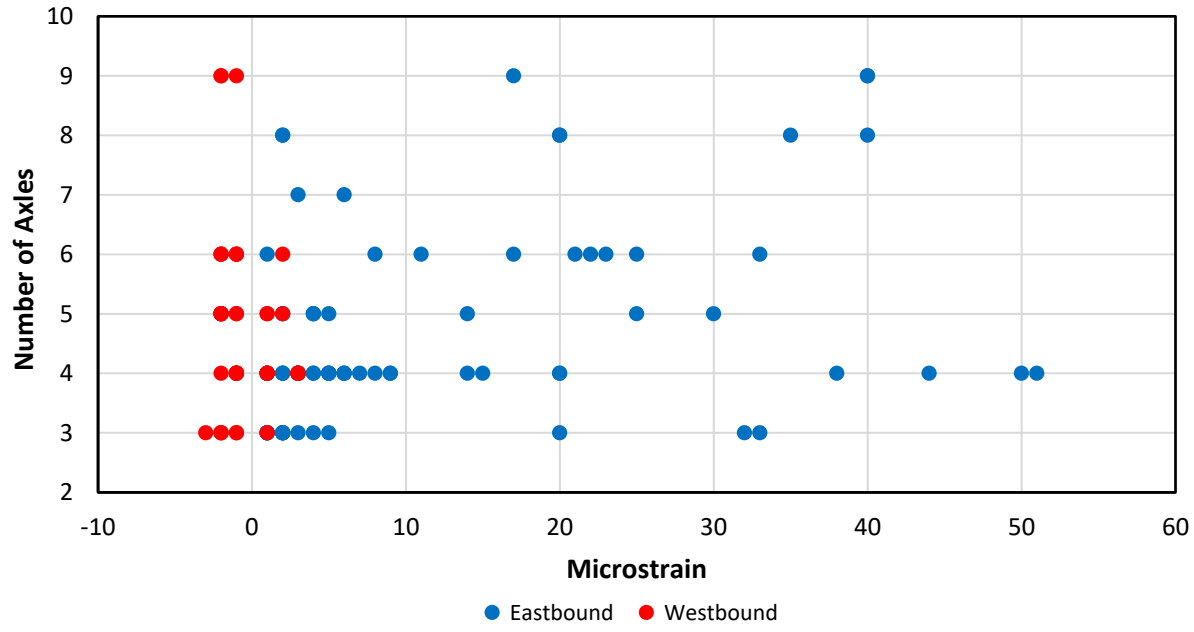

Figure 61. Maximum rebar strain in Closure Pour 1 versus number of axles for larger vehicles.

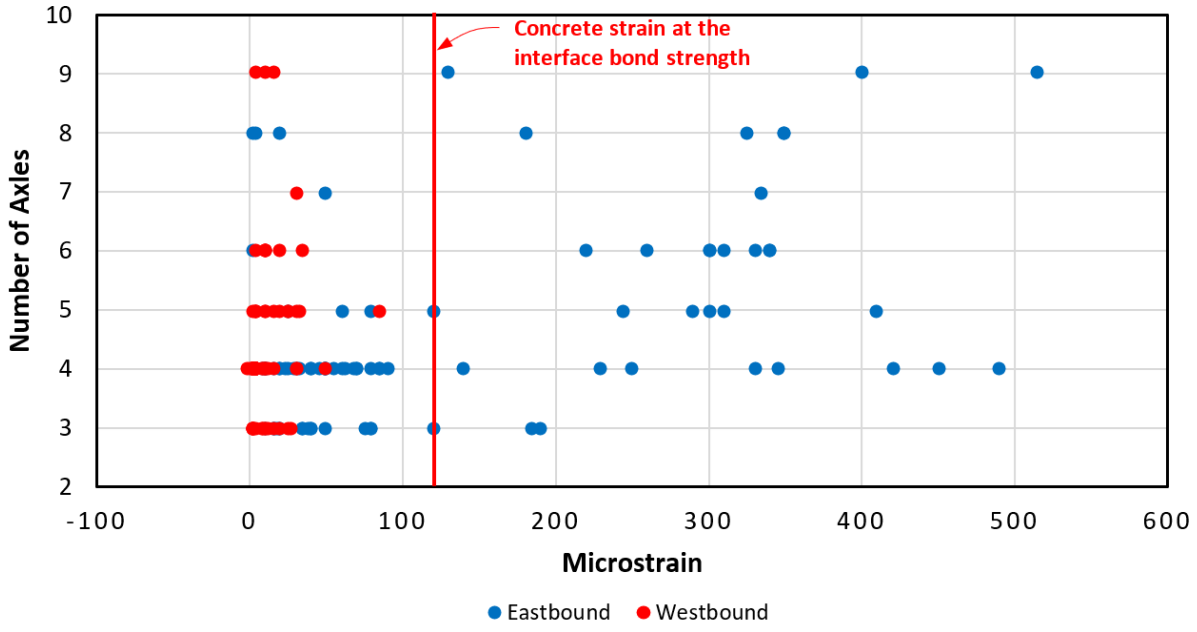

Figure 62. Maximum concrete strain in Closure Pour 2 versus number of axles for larger vehicles.

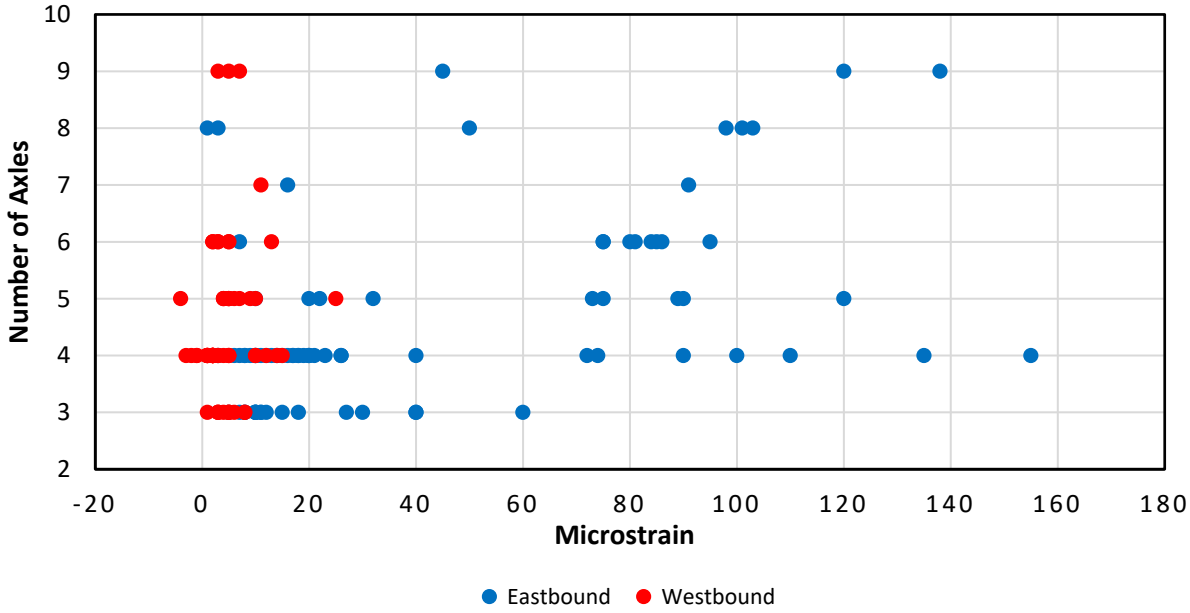

Figure 63. Maximum rebar strain in Closure Pour 2 versus number of axles for larger vehicles.

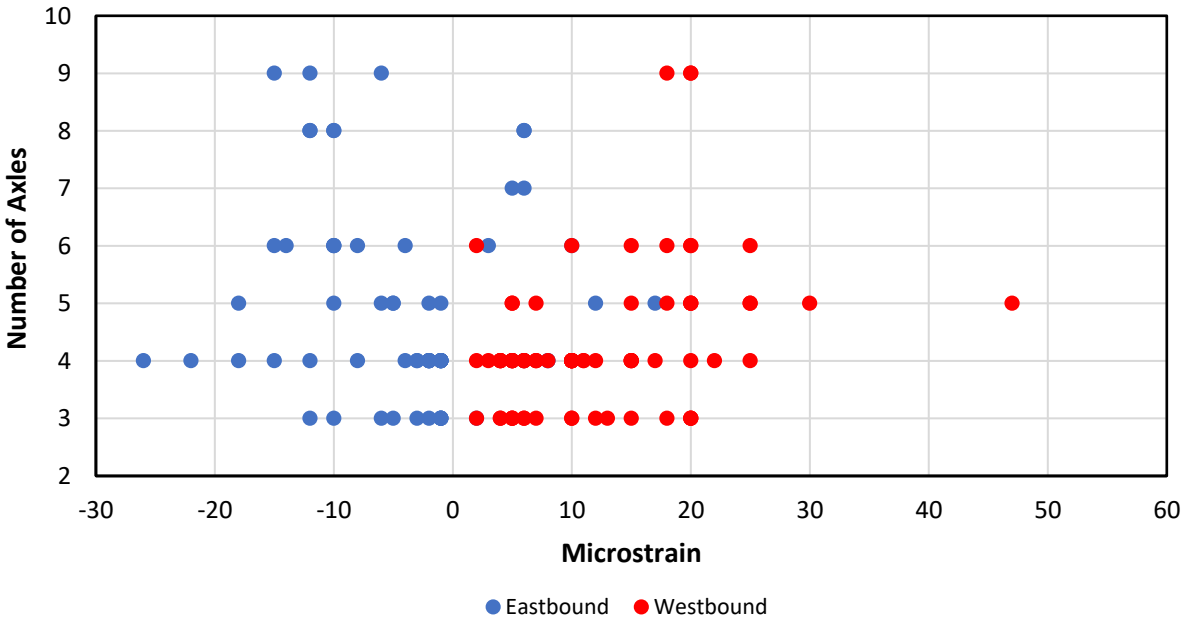

Figure 64. Maximum concrete strain in Closure Pour 3 versus number of axles for larger vehicles.

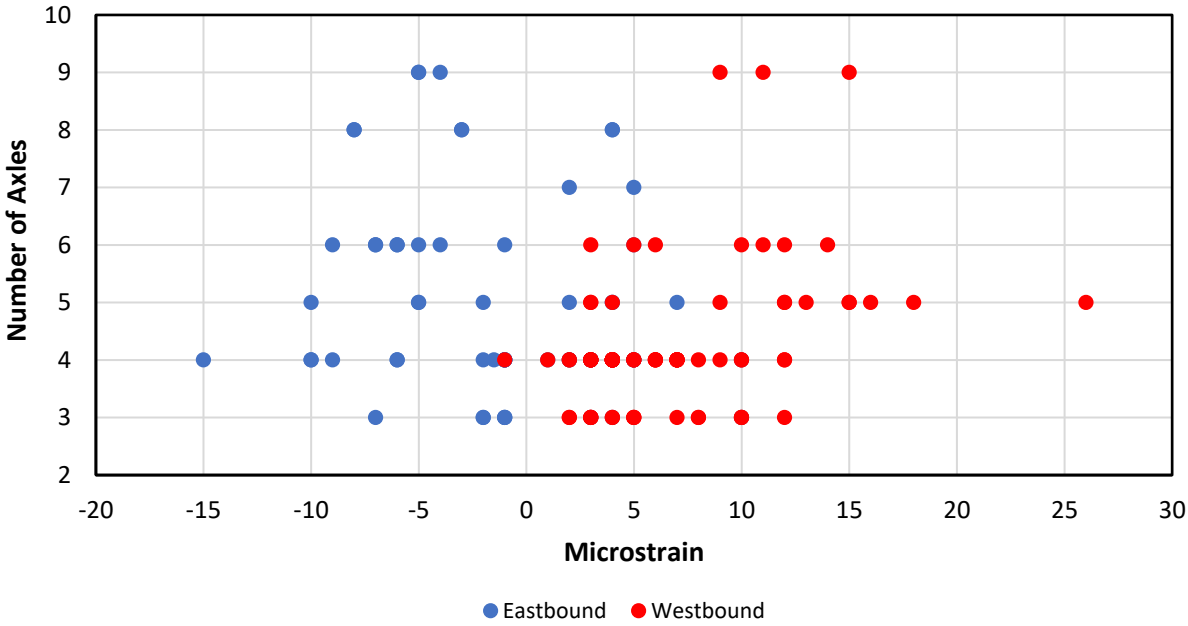

Figure 65. Maximum rebar strain in Closure Pour 3 versus number of axles for larger vehicles.

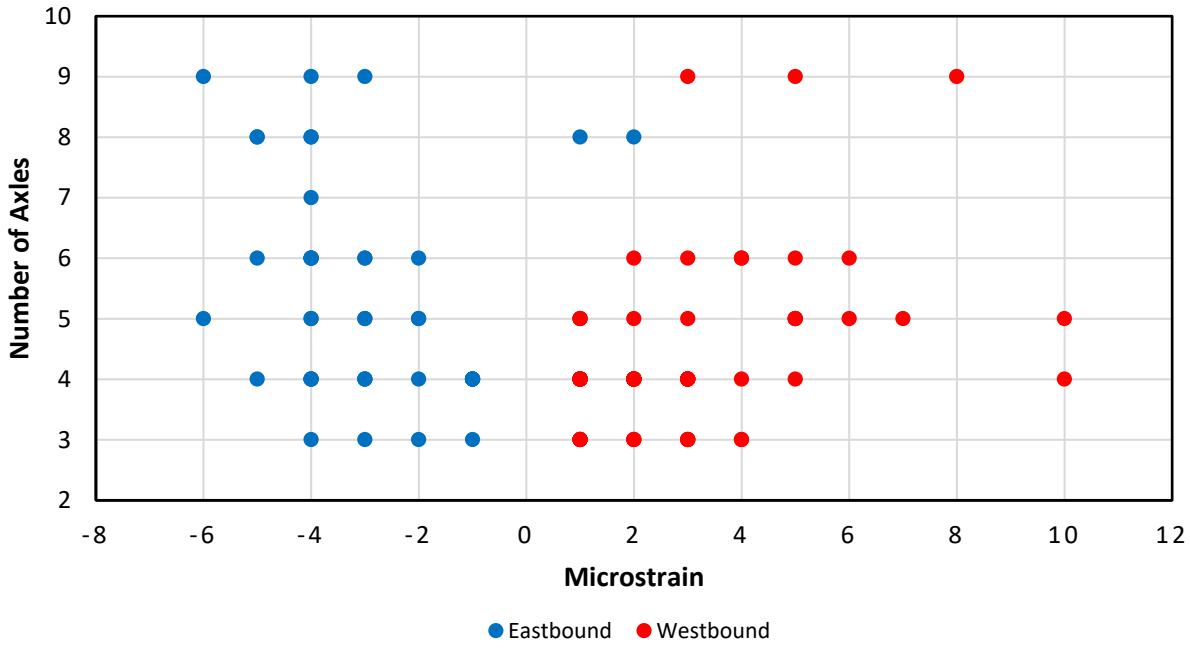

Figure 66. Maximum concrete strain in Closure Pour 4 versus number of axles for larger vehicles.

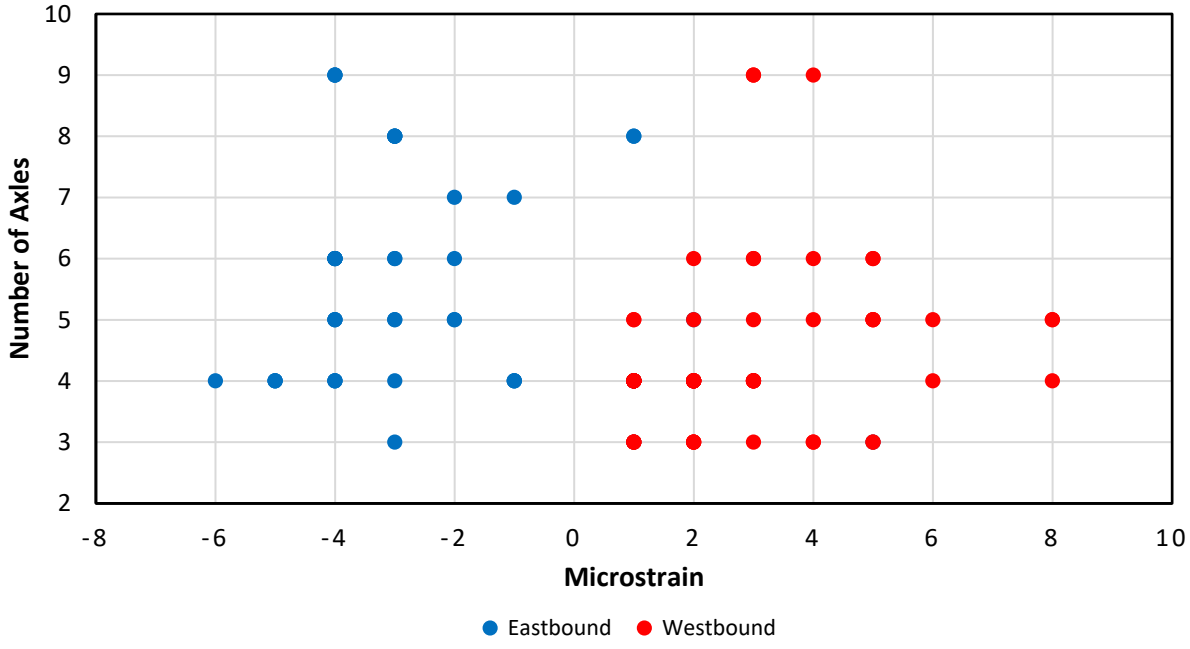

Figure 67. Maximum rebar strain in Closure Pour 4 versus number of axles for larger vehicles.

Discussion

Both static and dynamic loading revealed that two concrete gages in the instrumented location of Closure Pour 2 showed excessive amount of strain. There may be a few reasons for why concrete at Closure Pour 2 may not have performed as well as the other closure pours. Closure Pour 2 was the last one to be placed sometime in the first two weeks of November 2018, so the cold weather could have influenced the bond between the two concrete surfaces. When the bridge deck overlay was poured later in November, heaters were used underneath the bridge to help provide warmth to cure the concrete properly. No heaters were present for the closure pour connections. It was also observed during construction that the exposed aggregate surfaces were not wetted before placement of new concrete against the surface. Research done by Casanova et al. (2018) found that wetting the exposed aggregate surface before placement of new concrete makes a significant difference in the bond strength between the two surfaces.[6] Also, Idaho Transportation Department (ITD) Standard Specification for Highway Construction, Subsection 501.03 G states that the contractor should clean the construction joint surface and saturate it with water immediately prior to concrete placement (Idaho Transportation Department 2018).[21] Despite these deviations from the standard construction practices, the strain data in seven out of eight sets of gages (four sets of concrete and four sets of steel gages) showed low strain values.

Chapter 7
Finite Element Modeling

Introduction

This chapter presents the revised finite element model of the bridge and the calibration of the model using the experimental data from the Load Case 2 static loading with the UBIT at ¼, ½, and ¾ span locations over the instrumented bridge span. The second part of the chapter presents the closure pour stresses under the AASHTO design truck loading.

Finite Element Modeling

Similar to the first phase of the project, the bridge was modeled in the ANSYS finite element (FE) modeling software with beam and shell elements (Ebrahimpour, et al., 2018).[22, 1] However, unlike the first phase, the revised model includes both spans, the cap beam, and three columns at the center pier. Figures 68 and 69 show two views of the bridge in ANSYS. The bridge deck is composed of two layers of shell elements. The shell elements are 6 in. in the longitudinal direction and 4 in. in the transverse direction. Also, the shell elements have two parts, the lower portion (representing the upper flange of the girder and varying in thickness in the transverse direction) and the upper portion (representing the overlay and varying in thickness in the longitudinal direction every 15 ft). The boundary between the two parts of the shell segments (i.e., the reference) is a flat horizontal plane. Beam elements were used for the lower portion of the girders (shown in darker color in Figure 68), the cap beam, and the columns.

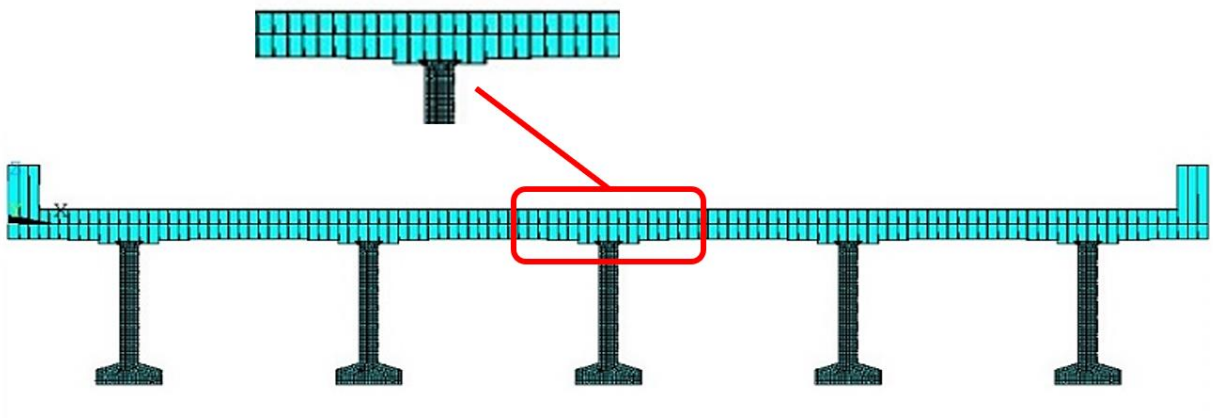

Figure 68. Cross section of modeled deck and girders.

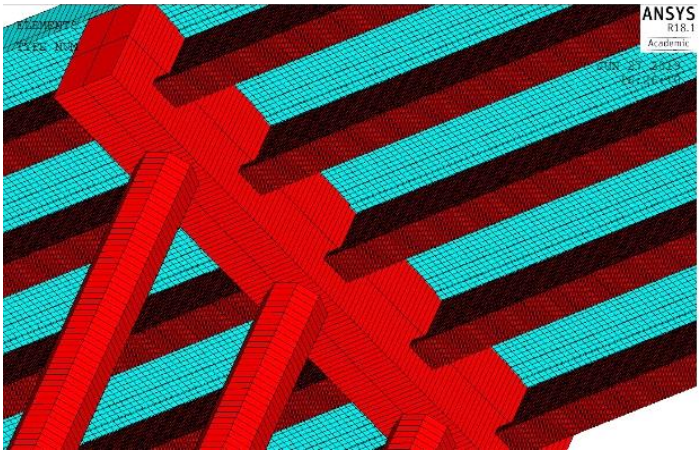

Figure 69. Bridge columns and cap beam in ANSYS.

Optimizing Abutment Stiffness using Load Case 2 Experimental Results

Initially, as shown in Figure 70 (a) and (b), it was assumed that the girder ends over the abutments are either pinned or fixed. But, later as recommended by the ITD Technical Advisory Committee (TAC), the stiffness of the girder ends at both abutments was revised to better match the rotational stiffness of the girder support over the abutments. This boundary condition is depicted in Figure 70 (c). The pier columns were, however, kept as fixed at the bottom. This assumption seems appropriate for two reasons: (1) there are many more piles at the bottom of the pier footing (i.e., the footing is stiffer compared to abutments), and (2) it would be difficult to adjust two boundary conditions at the same time and obtain optimum stiffness values for both.

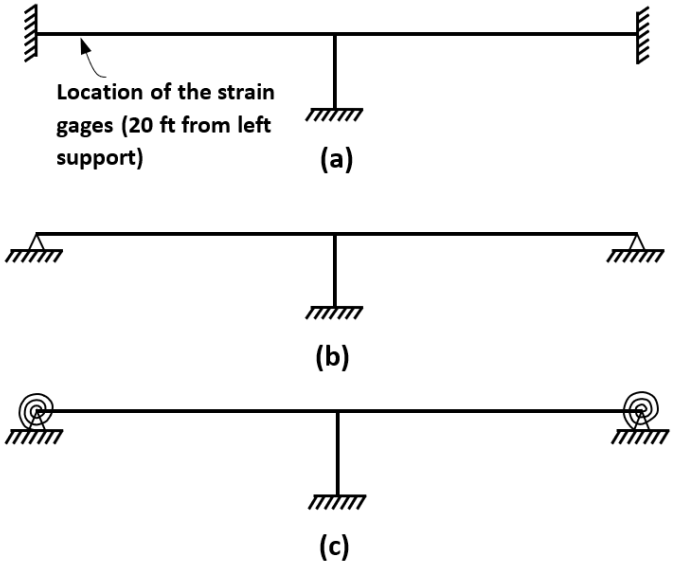

Figure 70. FE model boundary conditions.

In order to estimate the stiffness of the spring supports in Figure 70 (c), the modeling process started with the assumption that each of the eight 14-in. diameter with ½ in. thickness abutment piles can be assumed to have a length of 9.5 ft with bottom end fixed and the top end rigidly connected to the girder. Since there are five girders, five columns were used with $(EI)_{column} = [8(EI)_{one\ pile}]/5$. Figure 71 shows this arrangement for the column-to-girder set-up.

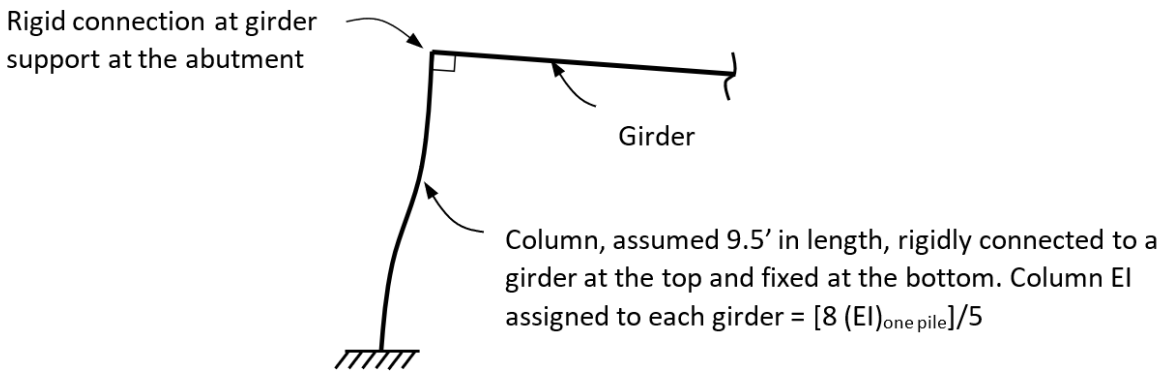

Figure 71. First trial of the pile support at the abutment for a single girder.

Steel modulus of elasticity $E = 29 \times 10^3\ ksi$ is used and moment of inertia of a single pile is calculated as $I = \frac{\pi}{4}(\mathrm{r}_o^4 - \mathrm{r}_i^4) = \frac{\pi}{4}(7^4 - 6.5^4) = 483.76\ in^4$. The column bending stiffness is determined as $(EI)_{col} = \left(29{,}000\frac{k}{in^2}\right)(8 \times 483.78\ in^4)/5 = 2.245 \times 10^7 k - in^2$.

In order to find the optimum rotational stiffness of the girder end at the abutment, the square root of the sum of the squares of the differences (SSSD) of the FE results and the measured girder bulb strains for Load Case 2 under the large UBIT was used. The SSSD is described by the following equation:

$$SSSD = \sqrt{\sum_{i=1}^{3}\sum_{j=1}^{6}\left(\varepsilon_{FE\,ij} - \varepsilon_{measured\,ij}\right)^2}$$

Where,

$\varepsilon_{FE\,ij}$= FE strain for the *i*th girder at the location of the instrumented bottom flange, *i* = 1, 2, 3, and *j*th UBIT location, *j* = 1, 2, …, 6.

$\varepsilon_{measured\,ij}$= measured strain for the *i*th girder at the instrumented bottom flange, and *j*th UBIT location.

In the equation, *i* = 1, 2, and 3 correspond to Girders 102, 103, and 104, respectively. Also, it should be noted that the unit for SSSD is the same as the unit for strain (i.e., microstrain). The smaller SSSD means

a better match between the FE and measured strain values at the girder bottom flanges at the instrumented locations.

Table 5 shows the SSSD values for the initial abutment pile support length of 9.5 ft as well as other lengths. The Table 5 column labeled (4*EI/L)* corresponds to the total abutment rotational stiffness of $4\left(29{,}000\,\frac{k}{in^2}\right)(8 \times 483.78\ in^4)/L$ for a column with the far end fixed, where *L* is in inch.

Table 5. SSSD values for different abutment pile lengths and the corresponding total abutment *(4EI/L)*.

Abutment pile length (ft) or boundary condition of the girder end at the abutment	Total abutment rotational stiffness *(4EI/L)* (k-in./rad)	SSSD (microstrain)
Pinned	0	53.8
12	3.12E+06	36.9
9.5	3.94E+06	35.9
6	6.24E+06	32.7
4	9.35E+06	18.8
3	1.25E+07	16.8
2	1.87E+07	16.7
1	3.74E+07	14.5
0.5	7.48E+07	6.6
0.4	9.35E+07	12.6
0.25	1.50E+08	16.0
Fixed	Large	45.1

As it can be seen from Table 5, the length *L* had to be decreased in order to reduce the SSSD value. The lowest SSSD value of 6.6 microstrain corresponds to the optimum rotational stiffness of 7.48E+07 (k-in./rad).

Tables 6 and 7 show the experimental and FE girder bottom flange strain results for Load Case 2 for the large and small UBITs, respectively. Both tables show the experimental strain values as well as numerical results for (a) all supports fixed; (b) girder ends pinned over the abutments; (c) average of the two boundary conditions in (a) and (b); and (d) optimum abutment stiffness. The bottom rows of each table give the SSSD values for each boundary condition considered. As it can be seen, the optimum abutment stiffness for the large UBIT data also gave the lowest SSSD value for the small UBIT. It is also interesting to note that the calculated average responses of the girder being pinned and fixed over the abutments gave almost the same response as the optimum abutment stiffness.

Table 6. Experimental and FE girder bulb strain results for Load Case 2 under Large UBIT.

Load Case	**Experimental** (microstrain)			**Numerical Results for all Supports Fixed** (microstrain)			**Numerical Results for Girder Ends Pinned over Abutments** (microstrain)			**Numerical Results for the Average of two Boundary Conditions** (microstrain)			**Numerical Results for the Optimum Abutment Stiffness** (microstrain)		
	Girder 102	Girder 103	Girder 104	Girder 102	Girder 103	Girder 104	Girder 102	Girder 103	Girder 104	Girder 102	Girder 103	Girder 104	Girder 102	Girder 103	Girder 104
2.1	5	13	12.5	0.5	3.3	2.5	17.0	23.0	23.2	8.7	13.1	12.9	8.3	12.8	12.5
2.2	2.5	-1.5	-1.5	-10.9	-15.2	-15.4	15.4	14.6	16.4	2.3	-0.3	0.5	1.7	-0.7	1.1
2.3	-2	-5	-5	-11.2	-13.3	-14.0	6.8	6.5	7.2	-2.2	-3.4	-3.4	-2.1	-3.3	-3.1
2.4	12	12	5	2.5	3.3	0.5	23.2	23.0	17.0	12.9	13.1	8.7	12.5	12.8	8.3
2.5	0	-1.5	2	-15.4	-15.2	-10.9	16.4	14.6	15.4	0.5	-0.3	2.3	1.1	-0.7	1.7
2.6	-4.5	-5	-1.5	-14.0	-13.3	-11.2	7.2	6.5	6.8	-3.4	-3.4	-2.2	-3.1	-3.3	-2.1
SSSD for each case → (microstrain)				45.1			53.8			6.9			6.6		

Table 7. Experimental and FE girder bulb strain results for Load Case 2 under Small UBIT.

Load Case	**Experimental** (microstrain)			**Numerical Results for all Supports Fixed** (microstrain)			**Numerical Results for Girder Ends Pinned over Abutments** (microstrain)			**Numerical Results for the Average of two Boundary Conditions** (microstrain)			**Numerical Results for the Optimum Abutment Stiffness** (microstrain)		
	Girder 102	Girder 103	Girder 104	Girder 102	Girder 103	Girder 104	Girder 102	Girder 103	Girder 104	Girder 102	Girder 103	Girder 104	Girder 102	Girder 103	Girder 104
2.1	3	6.5	6	0.3	2.6	2.1	9.5	13.6	13.5	4.9	8.1	7.8	4.5	7.7	7.4
2.2	1	-1	-1	-5.7	-7.6	-7.8	6.5	6.1	6.8	0.4	-0.8	-0.5	0.1	-1.0	-0.6
2.3	-1	-2	-2	-4.9	-5.7	-6.0	2.8	2.6	2.9	-1.0	-1.5	-1.5	-0.9	-1.4	-1.4
2.4	6	7	3	2.1	2.6	0.3	13.5	13.6	9.5	7.8	8.1	4.9	7.4	7.7	4.5
2.5	-1	-1	0.5	-7.8	-7.6	-5.7	6.8	6.1	6.5	-0.5	-0.8	0.4	-0.6	-1.0	0.1
2.6	-2	-2	-1	-6.0	-5.7	-4.9	2.9	2.6	2.8	-1.5	-1.5	-1.0	-1.4	-1.4	-0.9
SSSD for each case → (microstrain)				20.8			26.4			4.4			3.6		

Comparison of Experimental Closure Pour Strains in Load Case 1 with the FE Model Results

Based on the optimum abutment rotational stiffness determined under Load Case 2, Table 8 shows a comparison of experimental and FE results for the directly loaded closure pours under UBIT front wheels (i.e., Load Case 1 load tests). Unlike the results presented in Figure 52 in Chapter 6 in which the larger interface concrete strain at each closure pour was used, here the average strain of both sides of each closure pour seems more appropriate and is compared to the FE results. The results show that, except for Closure Pour 2, the FE strains closely match the measured strain values.

With the optimum abutment stiffness used in the FE model and not considering the Closure Pour 2 data (shown with underlined text in Table 8), on the average the FE strain values are about 10% lower than the experimental values.

Table 8. FE and experimental interface concrete strains at the directly-loaded closure pours.

Load Case	Small UBIT		Large UBIT	
	Experimental Average Strain (microstrain)	Numerical Average Strain for Optimum Abutment Stiffness (microstrain)	Experimental Average Strain (microstrain)	Numerical Average Strain for Optimum Abutment Stiffness (microstrain)
1.1	11.0	9.3	18.3	16.1
1.2	45.0	9.7	172.5	16.7
1.3	84.5	10.2	171.3	17.7
1.4	11.5	10.2	19.5	17.7
1.5	11.0	9.7	17.5	16.7
1.6	8.5	9.3	19.0	16.1

Closure Pour Stresses under AASHTO Design Truck Loading

The following sections present the process for determining the maximum stresses and their values in closure pour at the interface concrete and the headed bars using the improved finite element (FE) model of the bridge under AASHTO design truck load. Although in the above section, the structural contribution of the parapets was included in fine-tuning the FE model, in this section the structural contribution of the parapets is ignored. The justification is that not in all cases the composite action of the parapets and the deck can be relied on. However, the weight of the parapets, along with the weight of the concrete overlay, are included in non-composite bridge deck analysis. In the non-composite analysis, the upper part of the shell elements (representing the overlay concrete) was turned off. For the stresses caused by the AASHTO design truck and the future wearing surface, a composite deck action was considered (i.e., the upper portion of the shell elements was turned back on).

Location of the AASHTO Design Truck on the Bridge

In the first phase of the project, one span of the bridge was modeled with simply-supported girder ends. Therefore, it was easy to determine the longitudinal location of the truck using classical method of locating a set of axle loads to obtain the maximum bending moment in the span. In that case, the maximum moment location corresponded to the front axle of the truck at 54 ft from the end of the span. In the revised model, two cases were considered; one was for the truck traveling Westbound and one for the truck traveling Eastbound. For each case, we started with placing the lead axle at d = 54 ft from the end of girders at the abutment (for Westbound) or at d = 54 ft from the end of the girders at the pier (for Eastbound) and moved the truck 2 ft at a time back and forth and determined the maximum bending stress in ANSYS. Note that it was more convenient to determine the maximum span

bending stresses than the maximum bending moments, but they both serve the same purpose. For the Westbound, d = 48 ft gave us the largest bending stresses (i.e., normal stresses, σ_y, where *y* is the axis along the bridge longitudinal direction). In the Eastbound direction, d = 60 ft gave the largest bending stresses. Figure 72 shows the truck traveling Westbound with the location of the lead axle measured from the girder end at the abutment.

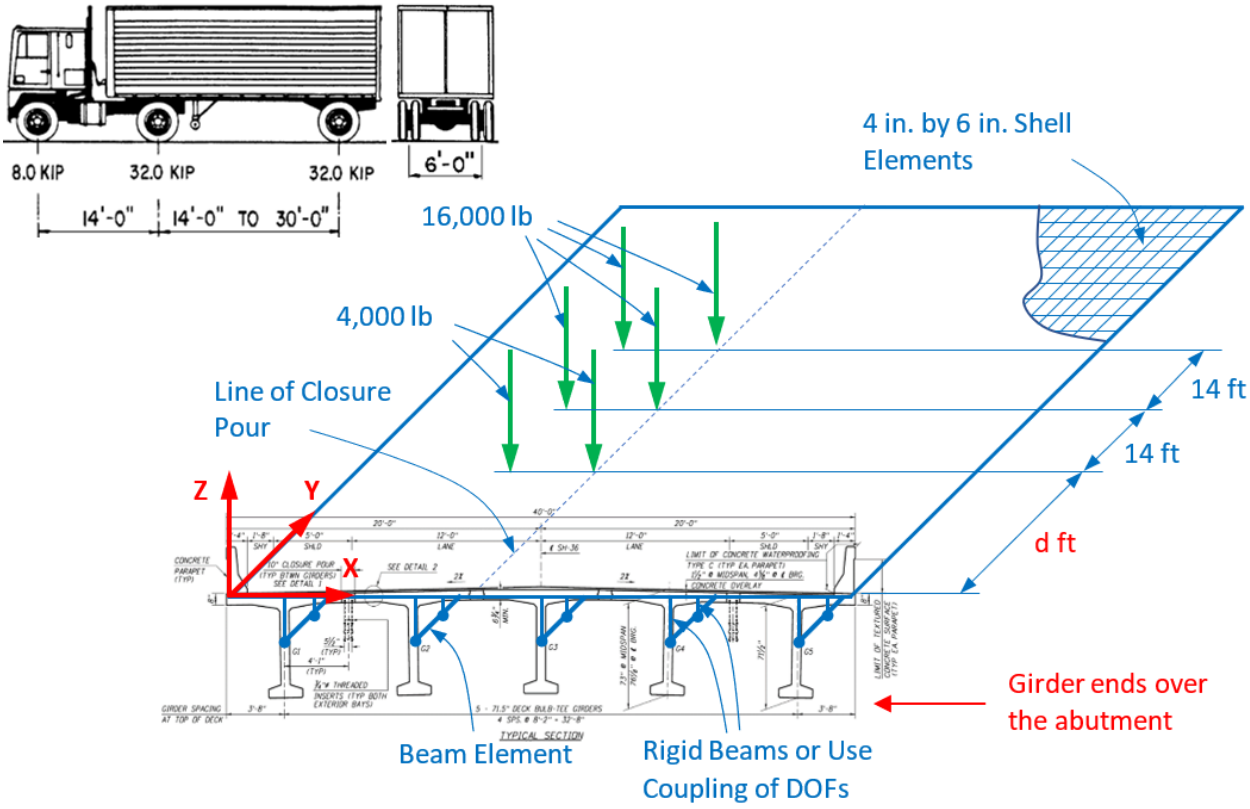

Figure 72. AASHTO design truck traveling Westbound on the instrumented span (not to scale and only portion of the deck shown).

Figure 73 shows the stresses in the FE model for when the truck is traveling Westbound with the lead axle at 48 ft from the end of the girders at the abutment. Note that here the maximum compressive stresses (in blue) are shown under the truck wheels. The same locations will result in maximum tensile stresses (not shown in the figure) at the bottom of the girders.

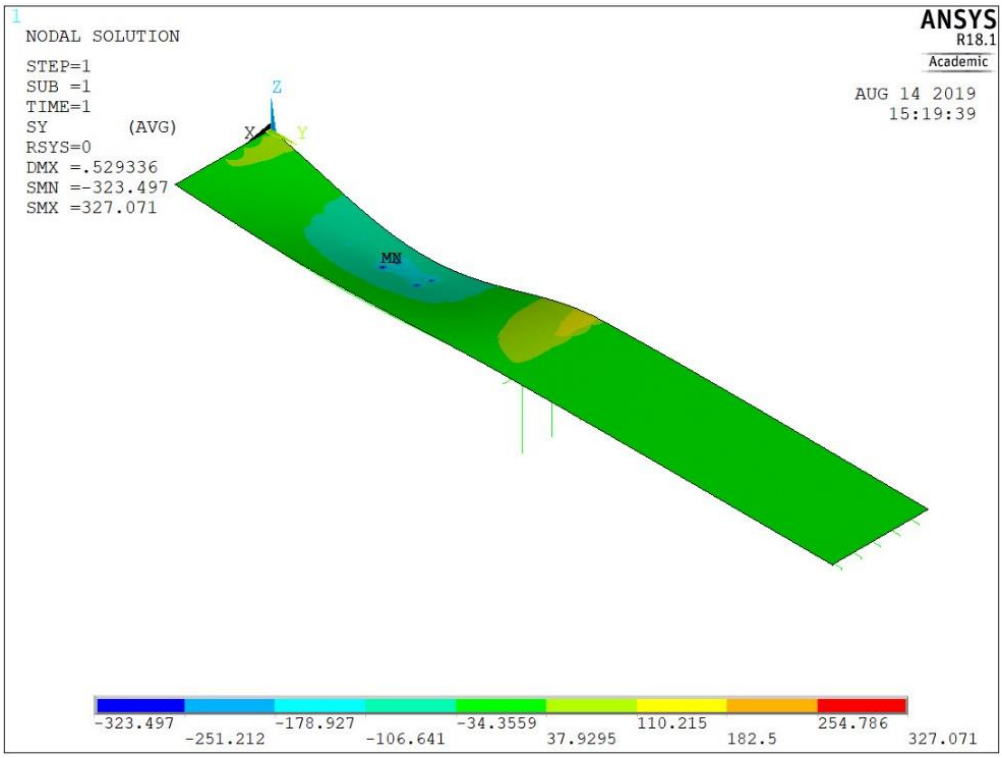

Figure 73. The normal stress in y direction based on the AASHTO design truck traveling Westbound with the lead axle at 48 ft from the end of the girders at the abutment.

Concrete Stresses under AASHTO Design Truck Load and the Added Dead Loads

In this section the stresses in the concrete are determined at the closure pours under both AASHTO design truck and the dead load of the overlay concrete, parapets, and the future wearing surface of 28 psf. In the ANSYS model, a smeared material model is used for the deck reinforced concrete with an effective material modulus representing the concrete and reinforcing steel. Because of the smeared model, the stresses in the "concrete" will be on the conservative side since in reality the concrete has a lower modulus of elasticity than the effective modulus used in ANSYS.

In the Phase 1 of the project, the bridge deck was modeled using 12" x 12" shell elements and for the AASHTO design truck, the deck stresses were found in two shell elements with the controlling 16-kip load distributed over them. The remaining truck loads were treated as concentrated forces. Therefore, the patch area was 24"x12". In the current revised model, the deck shell elements are 6" in the longitudinal direction by 4" in the transverse direction. As shown in Figure 74, the patch area under the controlling 16-kip load is composed of 10 elements (or total area of 20"x12"). This area is slightly larger than AASHTO's 20"x10" patch area. The stresses at the interface locations are determined by interpolation.

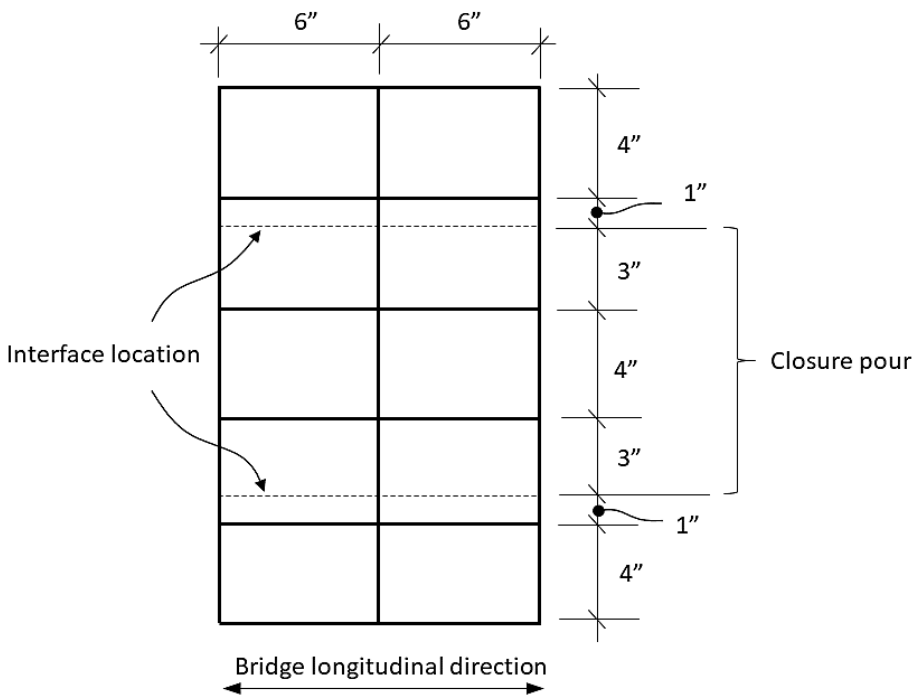

Figure 74. The patch area used under the 16-kip load.

Four probable AASHTO truck load cases were considered in the ANSYS analysis. These cases and the corresponding lead axle positions, as determined in the previous section, are shown in Figure 75. Since the bridge has two equal length spans, the cases are shown for this project's instrumented span. As an example, Figure 76 shows the truck loading for Westbound, Case 2.

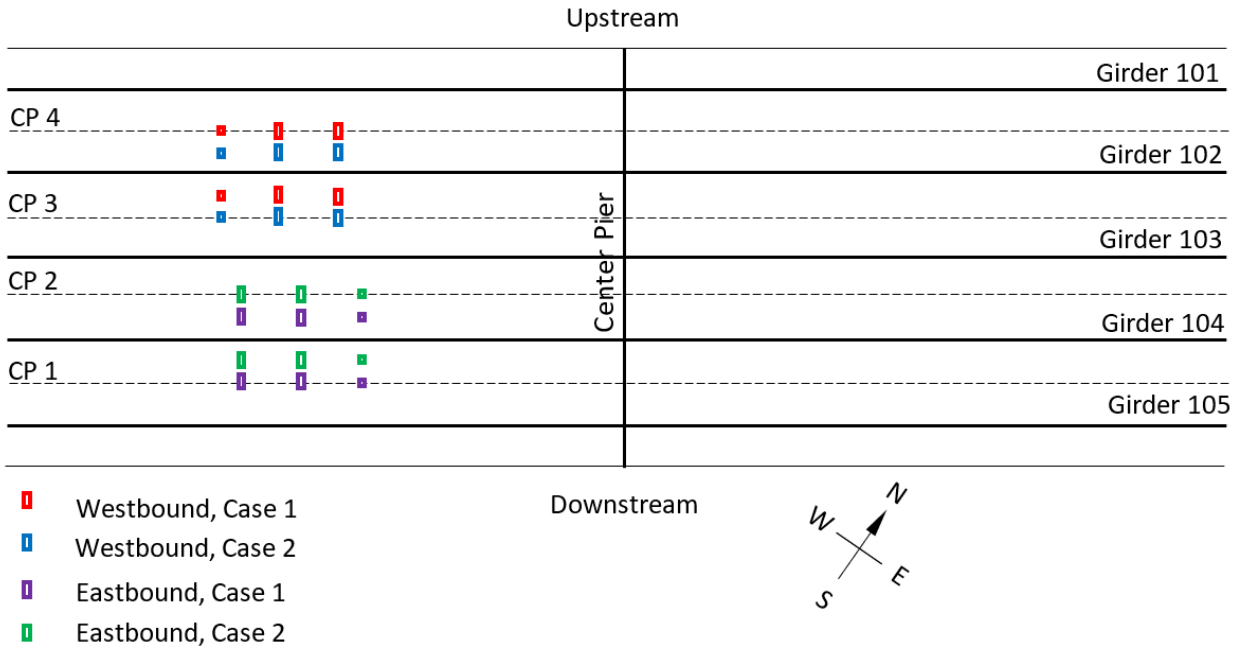

Figure 75. Plan view of the bridge showing probable AASHTO design truck load cases (not to scale).

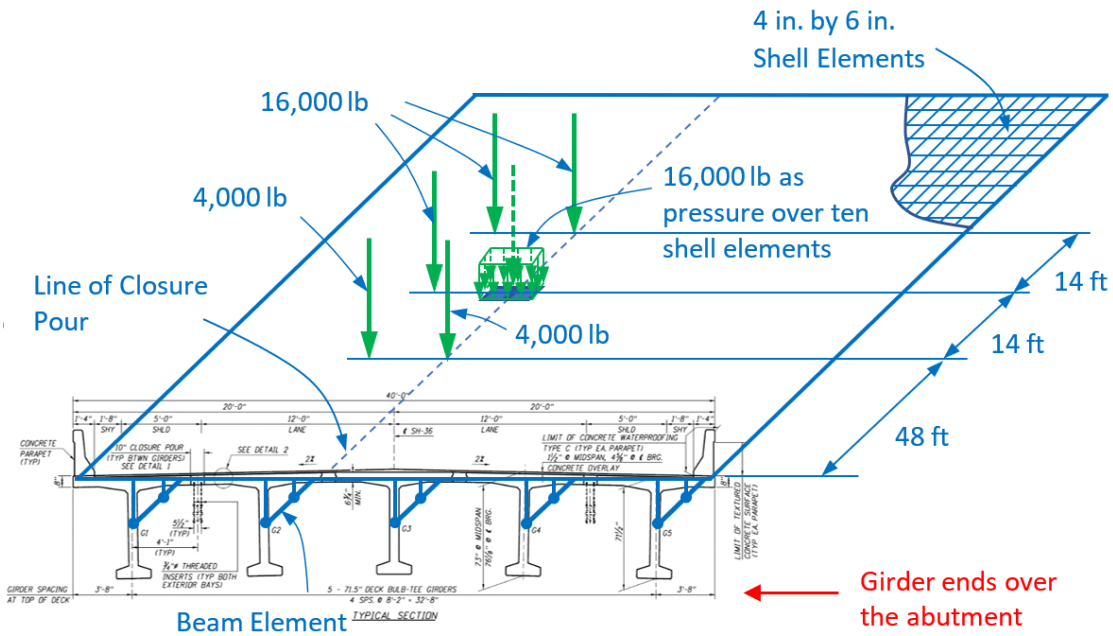

Figure 76. AASHTO design truck load for Westbound, Case 2 (not to scale, portion of the deck shown).

Table 9 shows the maximum concrete stresses at the bottom of the deck at the interface under the pressure patch load of the AASHTO design truck middle 16-kip wheel load over the closure pour (see Figures 74 and 75) and the dead load stresses of (a) the added concrete overlay and the parapet loads under the non-composite deck action (i.e., deck shell elements of 6.5 in. thick); and (b) the future wearing surface under the deck composite action, both at the same location as the maximum stress due to the truck load. Although in the ANSYS model the overlay concrete has a varying thickness (lower in the middle and larger at the ends of the span), an average weight was used as pressure everywhere on top of the deck. This approach is a little more conservative (i.e., will give larger stresses). The dead load due to parapets was also assumed as a uniform pressure over the deck. From Table 9, it can be seen that the Westbound, Case 2 loading stresses control.

Table 9. Maximum concrete stresses at the bottom of the deck at the interface.

Load Case	Maximum Concrete Stress due to AASHTO Design Truck Load (psi)	Concrete Stress Due to the added Dead Load of Overlay and Parapets at the Location of Max. Conc. Stress due to Truck (psi)	Concrete Stress Due to the added Dead Load of Future Wearing Surface at the Location of Max. Conc. Stress due to Truck (psi)	Concrete Stress Due to the Total added Dead Loads (psi)
Westbound, Case 1	288.2	9.3	4.6	13.9
Westbound, Case 2	325.3	17.7	7.5	25.2
Eastbound, Case 1	287.7	9.3	4.6	13.9
Eastbound, Case 2	325.9	16.3	7.1	23.4

The AASHTO Service I Limit State for controlling flexural cracking requires the following:

$$1.0\,DW\ +\ 1.0\,LL\,(1+IM)$$

Where, DW = added dead load due to concrete overlay, parapets, and future wearing surface; LL = live load (AASHTO design truck); and IM = impact factor = 0.33. Again, as noted above, two separate analyses were performed to combine the added dead load effects; one for non-composite and one composite deck action.

From the Phase 1 laboratory experiments on interface bond strength between closure pour (Mix D) and precast concrete using the ASTM C78, a modulus of rupture f_r = 612 psi was obtained. From the FE analysis for the controlling case, the deck maximum concrete bending stress under the added dead load and AASHTO design truck live load is:

$$f_{concrete} = 1.0(25.2) + 1.0(325.3)(1+0.33) = 458\,psi < f_r = 612\,psi \quad \textbf{O.K.}$$

As noted in the previous section, the FE model underestimates the closure pour strains by about 10%. If the above concrete stress is increased by 10%, a value of 504 psi is obtained which is still less than the modulus of rupture.

Headed Bar Stresses under AASHTO Design Truck Load and the Added Dead Loads

As shown in Figure 77, the maximum steel bar stress is to be calculated at the location of lower bars using interpolation. The location of the headed bar of 1.375 in. from the bottom of the deck is an approximate depth to the center of the bar and it is based on a bottom cover of 1 in. as shown in the bridge shop drawings. When interpolating, the shell nodes to be used will be the same nodes that were used for calculating the maximum concrete stresses. Also, this process was done only for the controlling AASHTO design truck loading (not all four cases), since stresses will be proportional and the load case for the maximum steel stress will be the same as the maximum concrete stress. Since for the concrete stress, the Westbound, Case 2 controlled, we considered this load case to find the lower bar stresses.

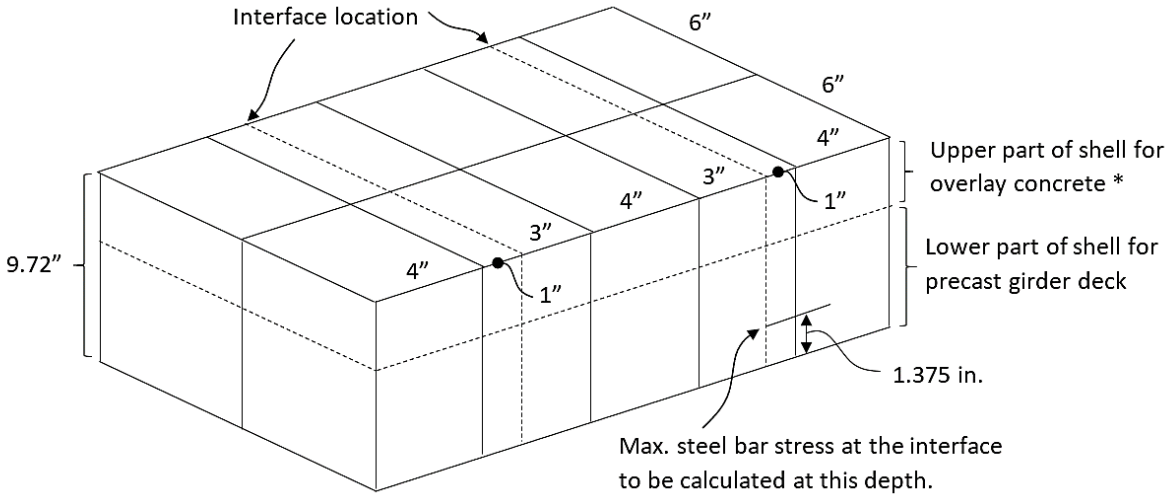

* Note the upper part of shell elements was removed for determining the stresses under the added dead load of overlay and parapets.

Figure 77. View of the shells representing the deck under pressure from the controlling 16-kip load of the design truck.

To estimate the maximum headed bar stresses, the following two methods were used:

Method 1: In this method, by interpolation of the deck concrete stresses at the top and bottom, we obtained the concrete stresses at the location of the headed bars (i.e., at the assumed location of 1.375 in. from the bottom). Then, we multiplied these stress values by the ratio of the modulus of elasticity of steel to the modulus of elasticity of concrete (or, $n = E_s/E_c$). The following stresses were obtained:

$$(f_{steel})_{AASHTO\ design\ truck} = 1{,}015\ psi$$

$$(f_{steel})_{Added\ dead\ load\ of\ overlay\ and\ parapets} = 44.8\ psi$$

$$(f_{steel})_{Added\ dead\ load\ of\ future\ wearing\ surface} = 23.3\ psi$$

$$(f_{steel})_{Total\ added\ dead\ loads} = 44.8 + 23.3 \cong 68\ psi$$

Method 2: In this method, we assumed that the state of the stress toward the bottom of the deck is approximately plane stress. For the smeared concrete material in ANSYS, which is assumed to be linear-elastic, homogeneous and isotropic, the transverse stress in concrete at the location of steel bar is:

$$\sigma_{x_{conc.}} = E_c\varepsilon_x + \nu\sigma_{y_{conc.}}$$

Where, x is the bridge's transverse direction, y is the bridge's longitudinal direction, σ is the normal (bending) stress, E_c= modulus of elasticity the concrete, ε_x is the transverse strain, and ν is the Poisson's ratio of the smeared concrete (assumed to be approximately equal to 0.2). Here, it is assumed that the strain in concrete and steel are the same at the location of steel. At the location of bottom steel bars, the transverse steel stress becomes:

$$\sigma_{x_{steel}} = E_s\varepsilon_x + \nu(\sigma_{y_{conc.}})n = f_{steel}$$

Using the above approach, the following steel stresses were obtained:

$$(f_{steel})_{AASHTO\ design\ truck} = 1{,}018\ psi$$

$$(f_{steel})_{Added\ dead\ load\ of\ overlay\ and\ parapets} = 45.4\ psi$$

$$(f_{steel})_{Added\ dead\ load\ of\ future\ wearing\ surface} = 23.4\ psi$$

$$(f_{steel})_{Total\ added\ dead\ loads} = 45.4 + 23.4 \cong 69\ psi$$

As it can be seen from the above results, both methods give essentially the same results and the differences can be attributed to roundoff errors. Also, as it can be seen from the above low steel stress values, and considering the steel has a specified yield of 60,000 psi, no matter what format is used (LRFD or ASD), the stresses are well within acceptable range. In fact, one can conclude that the headed bars are not necessary for the bottom rebars in the closure pour.

Another limit state that is considered is the steel bar Fatigue I Limit State (infinite fatigue life) under the AASHTO design truck, but with 30 ft between the 32 kip axles, instead of the 14 ft used above. For a conservative fatigue analysis, the steel stresses under the AASHTO design truck (i.e., with 14 ft between the 32-kip axles) are used. Fatigue I Limit State for infinite load-induced fatigue life uses the following relation:

$$1.75\ LL\ (1 + IM)$$

Where, LL = live load due to AASHTO fatigue truck, IM = 0.15.

Using the above relation, the steel stress due to live load is calculated as 1.75× 1,018 × 1.15 = 2,049 psi or 2.05 ksi. For the stress range, the effect is doubled which can be very conservative. This will give:

$$\gamma(\Delta f_s) = 4.1\ ksi$$

Where, $\gamma(\Delta f_s)$ = factored live load stress <u>range</u> in the steel bar.

The constant-amplitude fatigue threshold, $(\Delta F)_{TH}$, for reinforcement is:

$$(\Delta F)_{TH} = 26 - \frac{22 f_{min}}{f_y} \qquad \text{AASHTO Eq. (5.5.3.2-1)}$$

Where, f_{min}= minimum live-load stress resulting from the Fatigue I load combination, combined with the more severe stress from either the permanent loads or the permanent loads, shrinkage, and creep-induced external loads; positive if tension, negative if compression (ksi). Assume $f_{min} = 0$. Therefore,

$$(\Delta F)_{TH} = 26\ ksi$$

$$\gamma(\Delta f_s) \ll (\Delta F)_{TH} \quad \textbf{<u>O.K.</u>} \qquad \text{AASHTO Eq. (5.5.3.1-1)}$$

Chapter 8
Summary, Conclusions, and Future Work

The objectives of this research project were to (1) assess the performance of a closure pour mix similar to the ISU's optimum closure pour mix in the field; and (2) improve the bridge FE model and refine it based on the observed field data. To accomplish these objectives, several tasks were performed. In the following paragraphs, summary of each section is provided, followed by conclusions. At the end, the future work (i.e., Phase 3 of this project) is briefly noted.

Summary and Conclusions

Literature Review

In the literature review, four areas were reviewed: (1) instrumentation of bridges to measure response to traffic or environmental loads, (2) static and dynamic loading on bridges, (3) data acquisition system, and (4) finite element modeling of the bridges. When it comes to instrumentation using strain gages, the material in the technical data sheets by Measurements Group, referred to as "Tech Tips", was the most useful source of information.

Instrumentation, Loading, and Data Acquisition

The SH-36 Bridge over Bear River was instrumented with 94 strain gages. The instrumentation is located along a section approximately 20 ft from the west end of the bridge. Each of the four closure pours were instrumented with 16 rebar gages and six concrete gages under the deck. In addition, six gages were installed on the bulbs of the interior three girders; these gages were to be used in refining the FE model of the bridge.

In collaboration with ITD TAC, both static and dynamic load tests were developed. The static loading involved the known loads from the UBITs provided by the ITD and the dynamic loading was by both UBITs and truck traffic.

The data acquisition system used is a product of Campbell Scientific, Inc. In all tests, a sampling rate of 33 Hz proved adequate to capture the data without having too much information for data processing.

Experimental Results

Several graphs and tables were produced to summarize the collected data. While the dynamic versus time graphs provide an overall signature of the loading, the tables summarize the maximum strains and locations where these strains occurred. Key conclusions in this section are: (1) the concrete strain in Closure Pour 2 exceeds the strain corresponding to the interface bond strength (i.e., approximately 120 microstrain) for some of the static and dynamic loads, and (2) the maximum strain values in the rebars were much lower than the strain corresponding to the steel specified yield strength (i.e., 2,069 microstrain).

Computer Modeling and Stress Analysis under AASHTO Design Truck

A detailed finite element model of the bridge was developed in ANSYS software consisting of both spans, the cap beam, and three columns at the center pier. The deck shell elements have two parts, the lower portion (representing the upper flange of the girder and varying in thickness in the transverse direction) and the upper portion (representing the overlay and varying in thickness in the longitudinal direction every 15 ft). Beam elements were used for the remaining elements. In the FE model, the rotational stiffness of the two abutments was calibrated using the experimental UBIT loads at ¼, ½, and ¾ span locations over the instrumented bridge span. Using the calibrated model, when comparing the FE and measured strains under the directly loaded closure pours (Load Case 1), as expected, the results did not closely match for Closure Pour 2. However, the FE estimated concrete strain values at the interface were very close to the experimental results. On the average, the FE strain values are about 10% lower than the experimental values.

Finally, the bridge model was analyzed under the AASHTO design truck. The concrete stresses at the interface of closure pour concrete and precast met the AASHTO Service I Limit State for controlling flexural cracking. The stresses in the headed bars were significantly lower than the bar yield stress. Although not required by AASHTO LRFD Bridge Design Specifications, the stresses in the bars also met the Fatigue I Limit State for infinite load-induced fatigue life. From the FE analysis it can be concluded that, if properly installed, the High-Early Strength Class 50AF concrete with Polypropylene fibers in the ITD's 10-in. closure pours should perform well under AASHTO design truck loading.

Future Work

The third phase of this project was approved by ITD in Summer 2019. Phase 3 involves the long-term monitoring of the performance of the closure pours under both UBIT loading and commercial truck traffic. The tasks in this phase are: (1) replacing/preparing concrete strain gages for long-term moisture protection, (2) periodic measurements of the bridge under UBIT loading, (3) more data under commercial traffic, and (4) periodic closure pour inspection.

References

1. **Ebrahimpour, A., Mashal, M., Casanova, M., Rashique, U., Clauson, C. and Shokrgozar, A.** *Effectiveness of High-early Strength Concrete Class 50AF with Polypropylene Fibers as a Cost-effective Alternative for Field-cast Connections of Precast Elements in Accelerated Bridge Construction*. Washington, D.C.: Federal Highway Administration. Rep. No. FHWA-ID-18-265, 2018.

2. **Hedegaard, B. D., French, C. E. W., Shield, C. K., Stolarski, H. K., and Jilk, B. J.** "Instrumentation and Modeling of I35W St. Anthony Falls Bridge." *Journal of Bridge Engineering*, Vol. 18, No. 6 (June 2013): 476–485.

3. **Micro-Measurements.** "Strain Gage Selection: Criteria, Procedures, Recommendations." 2018. http://www.vishaypg.com/docs/11055/tn505.pdf Accessed October 10, 2019.

4. **Micro-Measurements.** "Strain Gage Installations for Concrete Structures." 2015. http://www.vishaypg.com/docs/11091/tt611.pdf Accessed October 10, 2019.

5. **Micro-Measurements.** "Strain Gage Clamping Techniques." 2015. http://www.vishaypg.com/docs/11090/tt610.pdf Accessed October 10, 2019.

6. **Casanova, M.** "Mechanical Properties of High Early Strength Concrete with Polypropylene Fibers for Field-cast Connections of Bridge Precast Elements." Master's Thesis, Idaho State University, Pocatello, ID, 2018.

7. **Micro-Measurements.** "M-Coat F Application Instructions." 2018. http://www.vishaypg.com/docs/11134/11134B134.pdf Accessed October 10, 2019.

8. **Campbell Scientific.** "Preventing and Attacking Measurement Noise Problems." 2001. https://s.campbellsci.com/documents/us/technical-papers/mnoise.pdf Accessed Oct. 10, 2019.

9. **Micro-Measurements.** "Leadwire Selection." 2010. http://www.vishaypg.com/docs/11174/VMM-11.pdf Accessed October 10, 2019.

10. **Micro-Measurements.** "Noise Control in Strain Gage Measurements." 2013. http://www.vishaypg.com/docs/11051/tn501.pdf Accessed October 10, 2019.

11. **Provines, J. T., Connor, R. J., and Sherman, R. J.** "Development of Load Rating Procedure for Railroad Flatcar Bridges through Use of Field Instrumentation. I: Data Collection and Analysis." *Journal of Bridge Engineering*, Vol. 19, No. 5 (2014).

12. **Sanayei, M., Phelps, J. E., Sipple, J. D., and Bell, E. S.** "Instrumentation, Nondestructive Testing, and Finite-element Model Updating for Bridge Evaluation using Strain Measurements." *Journal of Bridge Engineering*, Vol. 17, No. 1 (January 2012): 130–138.

13. **Chajes, M. J., and Shenton, H. W.** "Using Diagnostic Load Tests for Accurate Load Rating of Typical Bridges." *Bridge Structures*, Vol. 2, No. 1 (August 2006): 13–23.

14. **Barr, P. J., Woodward, C. B., Najera, B., and Amin, M. N.** "Long-term Structural Health Monitoring of the San Ysidro Bridge." *Journal of Performance of Constructed Facilities*, Vol. 20, No. 1 (February 2006): 14–20.

15. **Rutz, F. R., and Rens, K. L.** "Wind Pressure and Strain Measurements on Bridges. I: Instrumentation/Data Collection System." *Journal of Performance of Constructed Facilities*, Vol. 22, No. 1 (February 2008): 2–11.

16. **Campbell Scientific.** "4WFBS120, 4WFBS350, 4WFBS1K 4-Wire Full-Bridge Terminal Input Modules (TIMs)." 2017. https://s.campbellsci.com/documents/us/manuals/4wfbs.pdf. Accessed October 10, 2019.

17. **Jáuregui, D. V., and Barr, P. J.** "Nondestructive Evaluation of the I-40 Bridge over the Rio Grande River." *Journal of Performance of Constructed Facilities*, Vol. 18, No. 4 (November 2004): 195–204.

18. **Cardini, A. J., and DeWolf, J. T.** "Long-term Structural Health Monitoring of a Multi-girder Steel Composite Bridge using Strain Data." *Structural Health Monitoring*, Vol. 8, No. 1 (April 2008): 47–58.

19. **Bell, E. S., Lefebvre, P. J., Sanayei, M., Brenner, B., Sipple, J. D., and Peddle, J.** "Objective Load Rating of a Steel-Girder Bridge Using Structural Modeling and Health Monitoring." *Journal of Structural Engineering*, Vol. 139, No. 10 (October 2013): 1771-1779.

20. **Clauson, C.** "Field Performance of HES Class 50AF Concrete with Fibers as Field-Cast Connection between Deck Bulb-T Girders in Accelerated Bridge Construction Applications." M.S. thesis, Dept. of Civil and Environmental Engineering, Idaho State Univ., Pocatello, ID, 2019.

21. **Idaho Transportation Department.** *Standard Specifications for Highway Construction*. Boise, ID, 2018.

22. **ANSYS Inc.** "ANSYS User Manual (Version 18)." Cannonsburg, PA: ANSYS Inc., 2016.